Improvement of PWR (LOCA) safety analysis based on PKL experimental data

Zur Erlangung des akademischen Grades

Doktor der Ingenieurwissenschaften

von der KIT-Fakultät für Maschinenbau des

Karlsruher Instituts für Technologie (KIT)

genehmigte

DISSERTATION

von

M. Sc. Hong XU

Tag der mündlichen Prüfung: 03. November 2020

Hauptreferent: Prof. Dr.-Ing. Xu Cheng

Korreferent: Prof. Dr.-Ing Thomas Schulenberg

I declare that I have developed and written the enclosed thesis completely by myself, and have not used sources or means without declaration in the text.

Karlsruhe, 11.11.2020

. . . . . .

(Hong XU)

Acknowledgements

I would like to express my gratitude to all those who helped me during the period of my Ph.D. study.

Firstly, I am very grateful to Prof. Dr.-Ing. Xu Cheng, the leader of the IATF, for his support, deep academic knowledge and invaluable guidance. During my Ph.D. study in IATF, he improved my research skills and also broaden my vision. Without his patient instruction, insightful criticism, and expert vision in this research, the present work and dissertation would not have been possible to be completed.

Secondly, I would like to thank Prof. Dr.-Ing. Thomas Schulenberg, the second supervisor of my Ph.D. work, for his kind review and valuable suggestion of the dissertation. I was very impressed by the width and depth of his knowledge in the thermal-hydraulic area.

I would like to thank all my colleagues at the IATF for the good cooperation, the pleasant atmosphere. Especially, I would like to thank Dr. Aurelian Florin Badea for the helpful regular discussion of my Ph.D. work and the patience in the modification of the journal papers and dissertation. I would like to thank Fangnian Wang, Meiqi Song, and already graduated Dr. Xi Wang and Dr. Dali Yu for the fruitful discussion about the thermal-hydraulic topic and PKL simulation. I want to thank Moritz Schenk and Ludwig Köckert for the help in my daily life because of my poor German language. The only regret for me during these years is that I did not have lunch every workday with my colleagues.

Moreover, I would like to thank GRS for providing ATHLET code and the corresponding training and Framatome for offering the PKL related documents and data. Besides, I am grateful to the helpful discussion with Dr. Philipp Schöffel, Dr. Henrique Austregesilo and Dr. Tomasz Skorek from GRS and Mr. Simon Philipp Schollenberger from Framatome.

Last but not least, I want to acknowledge my parents because of the support and encouragement. The missing for them became a huge motivation for me to complete my studies. My wife and son deserve special thanks for their unconditional support and patience. My wife gave up her good job in Beijing and my son had to leave his favorite kindergarten and his friends. As foreigners, they faced different kinds of problems in Germany but they tried their best to support me. They are the sunshine in my heart throughout my studies, especially when I was in trouble with the research.

Hong XU

Karlsruhe, 11.11.2020

Abstract

Nuclear safety analysis is always the fundamental item for nuclear power development. Within the safety analysis, the most important aspect is the thermal hydraulic analysis of operation conditions and accidents (including design-basis accident (DBA) and beyond-design-basis accident (BDBA)). The loss-of-coolant accident (LOCA) is the most concerned DBA for nuclear thermal hydraulic safety analysis. After the development of around half a century, the concerned issue in thermal hydraulic safety analysis has switched in the recent decade from large-break LOCA (LBLOCA) and small-break LOCA (SBLOCA) to intermediate-break LOCA (IBLOCA) scenario. IBLOCA scenario has been the focus of experimental studies in Rig-of-Safety assessment/large scale test facility (ROSA/LSTF), advanced thermal-hydraulic test loop for accident simulation (ATLAS), and most recently the PKL (German abbreviation for "Primärkreislauf", "primary loop" in English) facility. Based on the IBLOCA test scenario of the LSTF facility, it was found that the phenomena of core heat up and peak cladding temperatures (PCTs) are very sensitive to the break size and the operation of safety injections. Unfortunately, most of the system thermal-hydraulic (STH) codes could not reproduce these processes in different IBLOCA scenarios. In order to confirm and to solve this problem, the PKL I2.2 IBLOCA benchmark was resorted to, as a counterpart test similar to the IBLOCA scenario in LSTF. Some typical STH codes should be evaluated by the test data of PKL I2.2 IBLOCA benchmark.

ATHLET (short for Analyses of THermal-hydraulics for LEaks and Transients) was used for the simulation of PKL I2.2 IBLOCA benchmark and the model assessment/modification of ATHLET was focused on. The main steps for ATHLET input deck preparation, the simulation results - including steady state and transient - were described in details in this work. In order to make the results convincing, the related state-of-art methodology was used: a nodalization qualification method was described and applied before the benchmark scenario simulation; a well-known method – Fast Fourier Transform Based Method (FFTBM) was introduced for the evaluation of the effectiveness of ATHLET on PKL I2.2 IBLOCA simulation. Based on the analysis of the transient results and the FFTBM results, one may come to the conclusion that most of the variables in PKL I2.2 IBLOCA benchmark were predicted very well by ATHLET, which confirmed its effectiveness on IBLOCA simulation. But unfortunately the PCT was not reproduced in the simulation. According to the average amplitude (AA) values from the FFTBM method and the results of the sensitivity study which - based on new developed methodology (two-layer FFTBM – MSM coupling sensitivity study method, MSM here means Morris screening method), this failure is most likely related to the break mass flow modelling.

Consequently, a new two-phase model (non-equilibrium and non-homogeneous two phase critical flow model (NNTPCM)) for the analysis of two-phase critical discharge was developed as a potential critical flow model (CFM) in ATHLET. The model allows thermodynamic non-equilibrium and hydrodynamic non-homogeneity between the liquid and vapor phases. It comes out as the solution of the six conservation equations of mass, momentum and energy for separated phases (the present ATHLET CFM - Critical Discharge Rate 1 Dimension model (CDR1D) - is a 4-equation model). The model is able to simulate several flow regimes, from subcooled to annular flows. Closure was

achieved by a set of constitutive relations chosen from an extensive literature review. Two kinds of choking criteria (determinant and pressure gradient) are discussed. For the determinant criterion, a compatibility condition should be considered for the system of ordinary differential equations (ODEs) describing the two-phase flow to have a solution at choking point. In order to confirm the two criteria, they were numerically investigated for long pipe, short pipe and orifice discharge tests. The results obtained by using the two different criteria are consistent as long as the pressure gradient threshold value remains large enough. Simultaneously, according to the results, this value is larger for the case of orifice and short pipe discharges (compared with a long pipe discharge). The model was validated by the experimental data from Al-Sahan tests (long pipe discharge), Celata test (nozzle discharge), Dobran test (long pipe discharge), Sozzi–Wutherland tests (short pipe discharge) and Henry tests (which comprises 9 subcooled and 10 saturated upstream conditions). The comparison of results showed excellent agreement with measured critical mass fluxes (but also with pressure profiles in Al-Sahan and Henry tests). The calculation results were the best ones, compared with other models from literature. A special attention was paid to the understanding of the choking process by analyzing the evolution of the main constitutive parameters, aspect seldom considered in previous studies. According to this analysis of the constitutive parameters, some interesting conclusions are extracted: the interfacial area becomes maximum at the transition point from bubble to slug/churn flow; the virtual mass force becomes important and sometimes decisive for choked flow; for long pipe, the thermodynamic non-equilibrium plays negligible role because of the good heat transfer between the two phases but the hydrodynamic non-homogeneity has to be taken into account since the velocity difference becomes very large at the choked point; on the contrary, the hydrodynamic non-homogeneity may be neglected but the thermodynamic non-equilibrium considered for short pipe or orifice because of the superheated liquid and small velocity difference.

As a potential substitute for CDR1D model in ATHLET, the methodology for the plugin in ATHLET has been described in details. To validate the effectiveness of the model and to verify its ability in replacing the CDR1D model, several Marviken full scale critical flow tests and PKL I2.2 IBLOCA benchmark were chosen for the model validation; the model was compared with both test data and also with the results obtained by the ATHLET built-in CDR1D model. The results showed that NNTPCM could get better or at least comparable results than CDR1D model for the simulation of thermal-hydraulic scenarios in PWRs.

Kurzfassung

Sicherheitsanalysen sind essenziell für die Entwicklung der Kernenergie, dabei ist die thermohydraulische Analyse bei Betriebsbedingungen und Unfällen (inklusive design-basis accident (DBA) und beyond-design-basis accident (BDBA)) der wichtigste Aspekt. Loss-of-coolant Unfälle (LOCA), d.h. Unfälle bei denen es zum Verlust des Kühlmittels kommt, ist der am meisten auftretende und damit der wichtigste DBA für die nuklearthermische und hydraulische Sicherheitsanalyse. Nach rund einem halben Jahrhundert der Entwicklung hat sich dieses wichtige Forschungsgebiet der thermohydraulischen Sicherheitsanalyse in den letzten zehn Jahren von großen (Large-Break LOCA (LBLOCA)) und kleinen (Small-Break LOCA (LBLOCA)) Leckagen hin zu mittleren Leckagen (intermediate-break LOCA (IBLOCA)) gewandelt. IBLOCA-Szenarios standen im Mittelpunkt experimenteller Studien in der Rig-of-Safety Assessment/Large Scale Test Anlage (ROSA/LSTF), Advanced Thermal-hydraulic Test Loop for Accident simulation (ATLAS) und zuletzt in der PKL (PrimärKreisLauf) Anlage. Anhand des IBLOCA-Testszenarios der LSTF-Anlage wurde festgestellt, dass die Kernerwärmung und maximale Hüllrohrtemperatur (peak cladding temperatures (PCTs)) sehr empfindlich auf die Bruchgröße und den Einsatz von Sicherheitsinjektionen reagieren. Leider konnten die meisten thermohydraulischen Systemcodes (System Thermal-Hydraulic (STH) Codes) diese Prozesse in verschiedenen IBLOCA-Szenarien nicht reproduzieren. Um dieses Problem zu verifizieren und zu lösen, wurde auf den PKL I2.2 IBLOCA-Benchmark als entsprechender Test zurückgegriffen, der dem IBLOCA-Szenario in LSTF ähnelt. Einige typische STH-Codes sollten anhand der Testdaten des PKL I2.2 IBLOCA-Benchmarks bewertet werden.

In dieser Arbeit wurde ATHLET (kurz für Analyses of THermal-hydraulics for LEaks and Transients) für die Simulation des PKL I2.2 IBLOCA-Benchmarks verwendet und es wurde sich auf die Modellbewertung / -modifikation von ATHLET konzentriert. Die Hauptschritte für die Vorbereitung des ATHLET-Eingabedecks, die Simulationsergebnisse - einschließlich stationärer und transiente Zustände - wurden in dieser Arbeit ausführlich beschrieben. Um überzeugende Ergebnisse zu bekommen, wurde eine aktuelle Methodik verwendet: Zunächst wird eine Methode beschrieben und angewendet, die die Diskretisierung bewerten kann, danach wird das Benchmark-Szenario simuliert und schließlich wird eine bekannte Methode, basierend auf der schnellen Fourier Transformation (Fast Fourier Transform Based Method (FFTBM)), zur Bewertung der Wirksamkeit von ATHLET in der PKL I2.2 IBLOCA-Simulation eingeführt. Basierend auf der Analyse der transienten und der FFTBM-Ergebnisse könnte man zunächst zu dem Schluss kommen, dass die meisten Werte im PKL I2.2 IBLOCA-Benchmark von ATHLET sehr gut prognostiziert werden können, womit die Leistungsfähigkeit von ATHLET bei der IBLOCA-Simulation bestätigt wäre. Die maximale Hüllrohrtemperaturwird kann jedoch in der Simulation nicht reproduziert. werden. Laut der Durchschnittsamplitude (AA) der FFTBM-Methode und den Ergebnissen der Sensitivitätsstudie, die auf einer neu entwickelten Methodik (zweischichtige FFTBM - MSM-Kopplungssensitivitätsstudienmethode, MSM bedeutet hier Morris Screening Method) basieren, ist dieser Fehler höchstwahrscheinlich auf die Modellierung des Massenstroms aus der Leckage zurückzuführen.

Infolgedessen wurde ein neues Zweiphasenmodell (Non-Equilibrium und Non-Homogeneous Two Phase Critical Flow Model (NNTPCM)) zur Analyse der zweiphasigen kritischen Leckageströmung als potenzielles Critical Flow Model (CFM) in ATHLET entwickelt. Das Modell ermöglicht ein thermodynamisches Nichtgleichgewicht und ein hydrodynamische Inhomogenität zwischen der Flüssigkeits- und der Dampfphase. Die Lösung der sechs Erhaltungsgleichungen von Masse, Impuls und Energie für die getrennten Phasen ermöglicht dieses Modell (das vorhandene ATHLET CFM - Critical Discharge Rate 1 Dimension Model (CDR1D) - ist ein 4-Gleichungsmodell). Das Modell kann die Strömungsformen von unterkühlten bis zu Ring- Strömungen simulieren. Die Schließbedingungen wurden durch eine Reihe von konstitutiven Beziehungen erreicht, die mit Hilfe einer intensiven Literaturrecherche ausgewählt wurden. Zwei Arten von der Durchflussbegrenzung (Determinante und Druckgradient) werden diskutiert. Für das Determinantenkriterium sollte eine Kompatibilitätsbedingung für das System von Gewöhnlichen Differentialgleichungen (ODEs) berücksichtigt werden, die die Zweiphasenströmung beschreiben, um eine Lösung am Drosselpunkt zu erhalten. Um die beiden Kriterien zu testen, wurden sie numerisch für Langrohr-, Kurzrohr- und Düsenentladungen untersucht. Die Ergebnisse, die durch die Verwendung der zwei verschiedenen Kriterien erhalten werden, sind konsistent, solange der Druckgradientenschwellenwert groß genug bleibt. Gleichzeitig ist dieser Wert laut den Ergebnissen für Düsen und kurze Rohre größer, im Vergleich zu langen Rohren. Das Modell wurde durch die experimentellen Daten des Al-Sahan-Tests (Langrohrentladung), Celata-Tests (Düsenentladung), Dobran-Tests (Langrohrentladung), Sozzi-Wutherland-Tests (Kurzrohrentladung) und des Henry-Tests (9 unterkühlte und 10 gesättigte Upstream-Bedingungen) validiert. Im Vergleich zu den gemessenen kritischen Massenflüssen (aber auch mit den Druckprofilen in Al-Sahan- und Henry-Tests) zeigen die Ergebnisse eine hervorragende Übereinstimmung. Verglichen mit anderen Modellen aus der Literatur weisen die hier vorgestellten Ergebnisse die größte Übereinstimmung mit den Versuchsdaten auf. Besonderes Augenmerk wurde auf das Verständnis des Drosselprozesses gelegt, indem die Entwicklung der wichtigsten konstitutiven Parametern analysiert wurden, ein Aspekt, der in früheren Studien selten berücksichtigt wurde. Nach der Analyse der konstitutiven Parameter können einige Schlussfolgerungen gezogen werden: Der Grenzflächenbereich wird am Umschlagspunkt von Blasen- zur Kolbenströmung/Schaumströmung maximal, die virtuelle Massenkraft wird wichtig und manchmal entscheidend für den gedrosselten Fluss, bei langen Rohren spielt das thermodynamische Ungleichgewicht aufgrund der guten Wärmeübertragung zwischen den beiden Phasen eine vernachlässigbare Rolle, jedoch muss die hydrodynamische Inhomogenität berücksichtigt werden, da die Geschwindigkeitsdifferenz am Drosselpunkt sehr groß wird. Umgekehrt dazu kann die hydrodynamische Inhomogenität bei kurzen Rohren vernachlässigt werden und das thermodynamische Ungleichgewicht muss für kurze Rohre oder Düsen, aufgrund der überhitzten Flüssigkeit und der geringen Geschwindigkeitsdifferenz, berücksichtigt werden.

Als möglichen Ersatz für das CDR1D-Modell in ATHLET wurde die Methodik als Plugin für ATHLET ausführlich beschrieben. Um die Wirksamkeit des Modells zu validieren und seine Fähigkeit zu überprüfen das CDR1D-Modells zu ersetzen, wurden mehrere Marviken-Tests für den kritischen Durchfluss in vollem Umfang und der PKL I2.2 IBLOCA-Benchmark für die Modellvalidierung ausgewählt. Das Modell wurde sowohl mit den Testdaten als auch mit den Ergebnissen des in ATHLET integrierten CDR1D-Modells verglichen. Die Ergebnisse zeigten, dass das NNTPCM bessere oder zumindest vergleichbare Ergebnisse als das CDR1D-Modell für die Simulation thermohydraulischer Szenarien in PWRs erzielen kann.

Contents

List of Figures

List of Tables

Table of Acronyms

Latin Symbols

a_i	interfacial area per unit volume, 1/m
A	discharge pipe cross-sectional area, m^2
$\boldsymbol{A}$	ODE matrix
$\boldsymbol{b}$	ODE vector
C	parameter for interfacial heat transfer in bubbly flow
C_c	pressure gradient at critical point, Pa/m
$(C_D)_{1-\alpha}$	drag force coefficient
C_{fi}	interfacial drag coefficient
C_p	specific heat at constant pressure, J/(kg·K)
d_b	average diameter of bubble, m
D	pipe diameter, m
f	frictional coefficient
F_{Gi}	interfacial momentum force due to mass transfer for vapor, N/m^3
F_{LG}	interfacial force, N/m^3
F_{Li}	interfacial momentum force due to mass transfer for liquid, N/m^3
F_{WL}	force from wall to liquid, N/m^3
g	gravitational acceleration, m/s^2
G	mass flux, $kg/(m{\cdot}s^2)$
h	enthalpy, J.
HTP	heat transfer parameter, $W{\cdot}s^2/m$
k	thermal conductivity, W/(m·K)
m	parameter for interpolation of slug/churn flow
n	parameter for interpolation of slug/churn flow
N	bubble density, $1/m^3$
Nu	Nusselt number
P	Pressure, Pa
Pr	Prandtl number
q_i	interfacial heat transfer rate per unit volume, J/m^3
Re	Reynolds number
T	temperature, K
u	fluid velocity, m/s
x	quality, 1/m
$\boldsymbol{X}$	vector for ODE unknown parameters
z	coordinate along the discharge pipe, 1/m

Greek symbols

α	void fraction
α_1	interpolation parameter for virtual mass coefficient
α_2	interpolation parameter for virtual mass coefficient
η	momentum sink proportion

θ	angle of inclination with the horizontal
λ	parameter for a special convective derivative of virtual mass force
π	PI
ρ	density, kg/m^3
ρ_m	mixture density, kg/m^3
τ_W	wall shear stress, N/m^2

Subscripts

0	initial condition
a	annular flow
b	bubbly flow
D	drag force
G	vapor phase
i	interfacial
L	liquid phase
LO	liquid only
sat	saturation
TP	two phase
VM	virtual mass
W	wall

Abbreviations

1M	One momentum equation system
2M	Two momentum equation system
AA	Average Amplitude
ACC	Accumulator
ATHLET	Analyses of THermal-hydraulics for LEaks and Transients
ATLAS	Advanced Thermal-hydraulic Test Loop for Accident Simulation
BC	Boundary Condition
BDBA	Beyond-Design-Basis Accident
BEPU	Best Estimate Plus Uncertainty
BWR	Boiling Water Reactor
CCFL	Counter-current flow limitation
CDR1D	Critical Discharge Rate – 1 Dimension model within ATHLET
CEA	Commissariat à l' énergie atomique
CET	Core Exit Temperature
CFM	Critical Flow Model
CFR	Code of Federal Regulations
CIAU	Code with the capability of Internal Assessment of Uncertainty
CL	Cold Leg
CNSI	Committee on the Safety of Nuclear Installations
CPU	Central Processing Unit
CV	Control Volume
CVO	Control Volume Object
DBA	Design-Basis Accident
DC	Down-Comer

DCV	Down-Comer Vessel
ECCS	Emergency Core Cooling System
FFT	Fast Fourier Transform
FFTBM	Fast Fourier Transform Based Method
GCSM	General Control Simulation Module within ATHLET
GRS	Gesellschaft für Anlagen- und Reaktorsicherheit
HCO	Heat Conduction Object
HCV	Heat Conduction Volume
HECU	Heat transfer and heat conduction
HEM	Homogenous Equilibrium Model
HL	Hot Leg
HPSI	High Pressure Safety Injection
HTC	Heat Transfer Coefficient
IAEA	International Atomic Energy Agency
IBLOCA	Intermediate Break LOCA
IC	Initial Condition
ITF	Integral Test Facility
JAERI	Japan Atomic Energy Research Institute
JRC/EC	Joint Research Center of the Commission of the European Communities
KAERI	Korea Atomic Energy Research Institute
KIT	Karlsruhe Institute of Technology
LBLOCA	Large Break LOCA
LOCA	Loss Of Coolant Accident
LOFT	Loss-Of-Fluid Test
LOOP	Loss Of Off-site Power
LP	Lower Plenum
LPSI	Low Pressure Safety Injection
LSC	Loop Seal Clearing
LSTF	Large Scale Test Facility
MARS	Multi-dimensional Analysis of Reactor Safety
MCP	Main Coolant Pump
MFW	Main Feedwater
MSL	Main Stream Line
MSS	Main Steam System
NEA	Nuclear Energy Agency
NEUKIN	Neutron Kinetics module in ATHLET
NPP	Nuclear Power Plants
ODE	Ordinary Differential Equation
OECD	Organization for Economic Co-operation and Development
PCT	Peak Cladding Temperature
PDF	Probability Distribution Function
PKL	German abbreviation for “Primärkreislauf”
PRZ	Pressurizer
PWR	Pressurized Water Reactor
RCP	Reactor Cooling Pump
RCS	Reactor Cooling System
RELAP	Reactor Excursion and Leak Analysis Program
ROSA	Rig of Safety Assessment

RPV	Reactor Pressure Vessel
SBLOCA	Small Break LOCA
SCRAM	Reactor Trip (emergency shutdown)
SG	Steam Generator
SMR	Small Modular Reactor
SOT	Start Of Test
STF	Separate Test Facility
STH	System Thermal-Hydraulic
TFD	Thermo-Fluid-Dynamics
TMI-2	Three Mile Island Unit 2
TRAC	Transient Reactor Analysis Code
TRACE	TRAC/RELAP Advanced Computational Engine
UH	Upper Head
UMAE	Uncertainty Method based on Accuracy Extrapolation
UP	Upper Plenum
USNRC	United State Nuclear Regulatory Commission
V&V	Verification and Validation
V&V&C	Verification, Validation and Consistency
WCOBRA	Westinghouse COBRA
WL	Water Level

1 Introduction

After the first nuclear power plant (NPP) in the world, finished in Obninsk by Soviet Union around 1955[1], the peaceful usage of nuclear energy has developed more than sixty years. During this period, the NPP technologies have undergone at least three updates of generations and the styles of NPPs become more and more versatile. Nowadays, the NPPs which are under construction are almost all NPPs of the third generation. Simultaneously, the research is focused on Generation-IV nuclear power, as guided by the Generation-IV International Forum (GIF) [2] in the last two decades.

The world's nuclear reactors made a growing contribution to supplying clean and reliable electricity, up to 2563TWh in 2018. This is the sixth successive year that nuclear electricity generation has risen. At the end of 2018 the capacity of the world's 449 operable reactors was 397GWe [3]. In the coming decades, the world will need to produce significant amounts of energy in order to meet the needs of the growing population and raise the living standards in developing countries. The world development scenario predicts a growth of about 2.5 times in demand for global primary energy in the period from 2000 to 2050, and an increment of about 4.7 times in demand for electricity[4]. The criteria for any acceptable energy supply should be reliability, efficiency, low cost, and safety, as well as environmental considerations. At least for the next few decades, there are basically three realistic options for providing energy supply. These include fossil, renewable (such as wind, solar, biomass, and geothermal), and nuclear energy sources. Compared to the first option, nuclear energy has the potential to contribute to a sustainable solution for the world's growing energy needs and environmental problems [5].

Generally speaking, different countries have different attitudes towards nuclear energy development because of different issues, e.g. the energy structure, public attitude, technical level, etc. But from the technical point of view, nuclear safety is basically the fundamental issue for nuclear energy development, which will be introduced next.

1.1 Nuclear safety

For different types of NPPs, the nuclear safety issues have both common points and special requirements because of different technical routes. This study focuses on the Pressurized Water Reactors (PWRs). In this section, some background about PWR and its nuclear safety issue, which is the original motivation for this work, will be presented.

1.1.1 PWR

The current status of nuclear energy, which is dominated by thermal light water reactors (LWRs), shows excellent performance compared to other energy alternatives[6]. About 80% of all operating nuclear power reactors are LWRs. An additional 11% are Heavy Water Reactors (HWRs) and 4% are advanced gas cooled, graphite moderated nuclear power reactors (AGRs) [7]. LWRs use low enriched

uranium fuel, which makes for greater flexibility in the choice of reactor core materials, especially allowing normal (light) water to be used as a coolant and moderator. LWRs could be further divided into predominantly Pressurized Water Reactors (PWRs) and Boiling Water Reactors (BWRs).

In recent two decades, several new generation (i.e., the 3rd generation) of advanced PWR NPPs have been developed, building upon the past success, as well as applying lessons learned from past operating experience. The advanced PWR design features address utility and regulatory requirements. The Generation III PWRs are characterized by several advantages in safety features comparing with PWRs of the 2nd generation [8]:

1) Reduced frequency of core melt accidents (by 10-100 times), the core damage frequency (CDF) currently ~ 10^{-7} -10^{-5}/year;
2) Minimal effect on the environment (practically eliminating the need for emergency planning zone), the large early release frequency (LERF) ~ 10^{-9} -10^{-6}/year;
3) Dedicated systems for mitigation of severe accidents (SAs);
4) Increased period without operator actions during accident, sometimes infinitely;
5) Robust double containment (with annulus venting), increased strength, designed against aircraft crash;
6) Seismic resistance of standard design 0.25-0.3 g.

From the analysis and the classification of off-normal events which may happen in a real system, the following classes of accidents for PWR [9] were selected:

1) Large break Loss-of-coolant Accident (LOCA) (LBLOCA, rupture area greater than 25% of A_{max}, the maximum pipe area connected with the pressure vessel);
2) Small break LOCA (SBLOCA, rupture area less than or equal to 11% of A_{max});
3) Intermediate break LOCA (IBLOCA, rupture area between 11% and 25% of A_{max});
4) Transients, where upset conditions are created by multiple failures of one or more systems in the plant;
5) Transients at shutdown conditions;
6) Accident management for a non-degraded core.

Historically, the emergency core cooling systems (ECCS) against LOCA scenario (items 1-2) was one of the major topics of safety assessment for PWRs established with the publication of the "Acceptance Criteria"[10]. LBLOCAs (item 1), are dominated by inertia effects and characterized by strong but rather homogeneous steam/water flow distribution inside the primary loop, in particular during the depressurization period. For SBLOCAs (item 2), gravity and stratification effects are important phenomena to be simulated. IBLOCAs (item 3) may contain features related to both LBLOCAs and SBLOCAs. The actual sub-division between items 1-3 depends in general upon the size of the plant and the position of the break. It should be noted that the selected boundary of IBLOCA (between 11% and 25% of A_{max}) must be seen as approximate and somehow arbitrary.

1.1.2 Issues of nuclear safety

The development of the world's nuclear industry currently faces economic, environmental and safety concerns. The root of the concerns is the nuclear safety. The commissioning of a nuclear installation requires a rigorous licensing process in order to prove the safety of the facility, comparing with different levels of regulatory in **Figure 1.1** [11].

The fundamental safety objective is to protect people and the environment from harmful effects of ionizing radiation. “Nuclear safety” therefore means the protection of people and the environment against radiation risks [12][13].

For each design of a NPP, the regulatory body establishes a set of design basis accidents. For each of these postulated events, regulatory acceptance criteria that the design needs to fulfill are postulated by the regulatory bodies.

Safety goals can be qualitative or quantitative; the latter ones can either be deterministic or probabilistic and they are often denoted as safety targets. Quantitative deterministic safety goals can also be used to decide whether the results given by deterministic safety analysis (for the specific safety case) are acceptable or not [14].

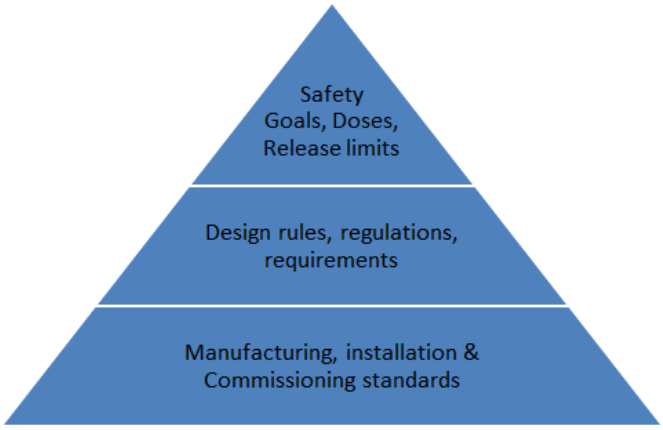

Figure 1.1: Regulatory pyramid

1.1.3 Nuclear safety analysis

Nuclear safety analysis is the basic technical item for nuclear development. It is based on mainly three aspects: NPP, system thermal hydraulic (STH) code and test facilities. Actually, the theories related to these three aspects are very complex, involving thermal hydraulic, statistics, experimental theory, system theory et al. In this respect, Figure 1.2 illustrates briefly their relationship.

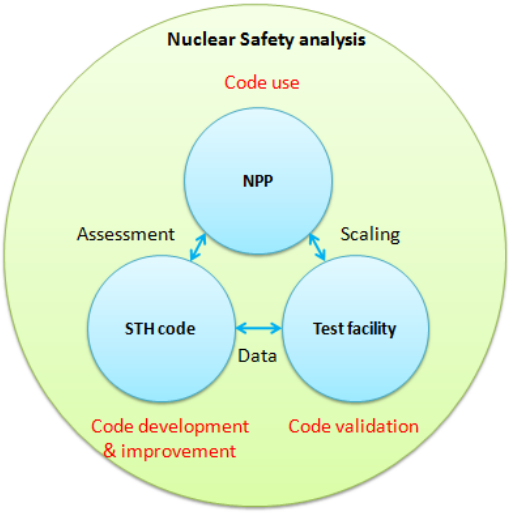

Figure 1.2: Nuclear safety analysis contents

In order to verify the safety issues of NPP, STH codes are developed as a tool for NPP accident scenario simulation and assessment. The most accident scenarios are not allowed to happened or test in NPP because of the huge costs of safety and economy. Consequently, an alternative method is resorted to: test facilities, which are scaled down from NPP, but still keeping the main characteristic/phenomena of the NPP thermal hydraulic behaviors.

Currently, the test facilities are used as the main tool for STH code validation. On one hand, they provide various types of test data in different conditions, to be compared with simulation results. In this way, the capabilities of STH codes are enhanced and they become more and more powerful. On the other hand, test facilities are used for phenomena cognitions for STH code development. Since the phenomena in NPP are very complex, it is impossible to understand or predict them clearly, especially as strong two-phase flow phenomena occur when nuclear thermal hydraulic accident scenarios happen. After the STH code simulates test facilities meeting the requirements of accuracy, it may be used to simulate NPP accident scenarios to some extent (also much work should be done which is not related to the present one and, therefore, not discussed here).

In the following, a review of STH codes and test facilities will be presented. The main idea is to discuss how they promoted each other during the development of nuclear energy.

(1) The STH code

Evaluation of nuclear power plants (NPPs) performances during accident conditions has been the main issue of the research in nuclear fields during the last 50 years. Nuclear technology and especially nuclear safety depend strongly on the development and assessment of numerical simulation tools (e.g. STH or CFD codes). The application of the numerical simulations in the framework of safety and licensing is mainly required by the impracticability of executing full-scale safety related experiments and the absence of simplified scaling criteria for the important physical processes (occurring during the scenarios of interest), which otherwise would allow a direct transfer of results from small scale test facilities to the nuclear power plant.

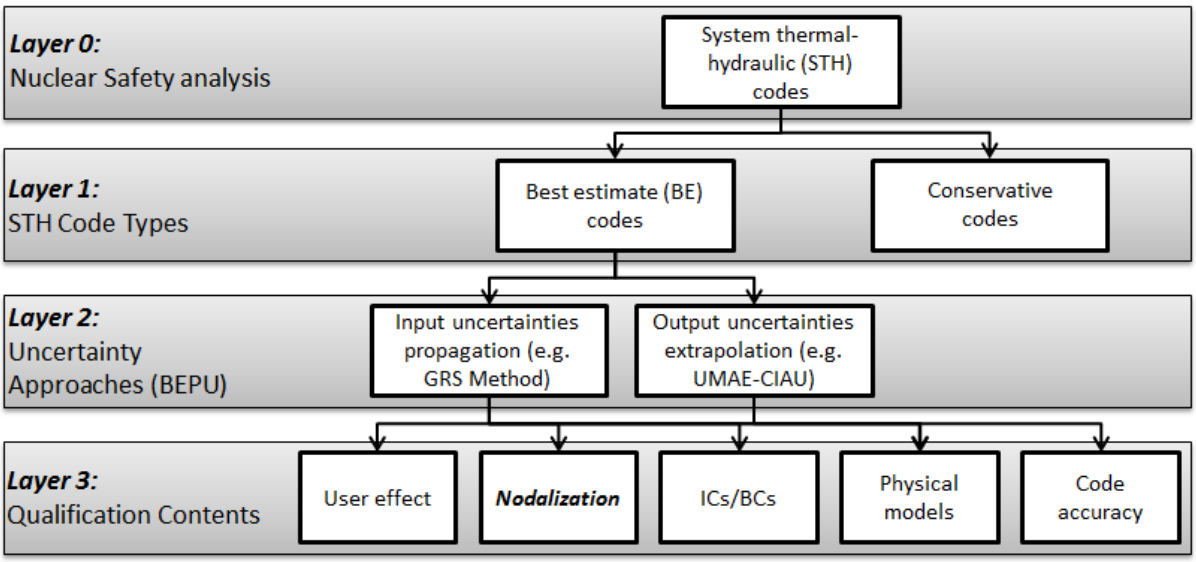

Figure 1.3: Classification of system thermal hydraulic codes and qualification contents

Thermal hydraulic safety assessment represents the most relevant issue in the design and licensing of NPPs ensuring the acceptability of scenario management. The two main branches through which the thermal hydraulic safety process develops, are the deterministic safety analysis (DSA) and the probabilistic safety analysis (PSA) [15]. DSA is an important tool for confirming the adequacy and efficiency of provisions within the defense in depth concept for the safety of NPPs. Two different methodologies have been adopted to assess the deterministic thermal hydraulic safety analysis, namely the conservative approach and the best estimate approach.

For the analyses of transients and LOCAs in LWRs, STH codes have been developed over the last half a century. The concept of conservative methods was introduced in the early days of safety analysis to cover uncertainties that prevailed in the 1970s, due to the limited capability of modeling and the limited knowledge of physical phenomena, and to simplify the thermal hydraulic analysis. It should be noted that the conservative approach does not provide any indications as for the true safety margins nor does it provide a true simulation of a specified scenario [16]. The results obtained by this approach may be misleading (unrealistic behavior predicted, order of events changed) and the level of conservatism is unknown. Therefore, there has been a move away from over-conservatism in safety analysis towards the application of so-called best estimate methodologies. Since the 1988 Appendix K Rulemaking change [17], there has been significant interest in the development of codes and methodologies for "best-estimate" analysis of LOCAs, which was considered more realistic [18].

Best-estimate approach, aimed to provide a detailed realistic description of postulated accident scenarios based on best-available modeling methodologies and numerical solution strategies, is the current strategy and trend adopted in nuclear thermal hydraulic safety analysis[19]. The concept of best-estimate is generally applied to the codes used in the analysis. In the best-estimate analyses, the thermal hydraulic phenomena are simulated as accurately as possible (according to present knowledge) and the obtained safety margins reflect better the real margins in the plant. This type of analyses provides also more realistic simulations of the NPP behavior during the course of the transient scenarios, and can consequently reveal detailed system information that can be relevant for the understanding of thermal hydraulic phenomena interaction. If best estimate analyses are used for licensing purposes, they must be accompanied by uncertainty analyses, to quantify the uncertainty of calculated parameters. The STH codes for nuclear safety analysis could be divided into best estimate codes (e.g. RELAP, TRAC, CATHARE, ATHLET et al.) and conservative codes (e.g. NOTRUMP et al.), see Layers 0 and 1 in Figure 1.3.

Since the best estimate codes used a more realistic technique, the uncertainty issue was inevitable introduced and should be considered in detail. This triggered the idea of best estimate plus uncertainty (BEPU) for accident analysis in NPP technology. Briefly speaking, BEPU [20] constitutes an approach or a procedure aimed at making feasible the application of nuclear thermal hydraulics to the licensing and the safety evaluation processes of Nuclear Power Plants (NPPs). Several methodologies have been proposed to evaluate the uncertainty of best estimate code predictions [21].

The most used two methods at the industrial level (based on the selection of input or output uncertain parameters) are input uncertainties propagation approach and output uncertainties extrapolation approach, respectively, as shown by Layer 2 of Figure 1.3. GRS method [22] is a representative method for the first approach. UMAE/CIAU (acronyms of Uncertainty Method based on Accuracy Extrapolation and Code with the capability of Internal Assessment of Uncertainty) method is a representative method for the second approach [23]. But no matter which BEPU method is chosen, in order to increase the reliability of results, some qualification contents/procedures have been established and the related overall uncertainty items should be qualified before the formal calculation

of codes. These items [24] include the user effect, nodalization, initial conditions and boundary conditions (ICs/BCs), physical models and code output accuracy assessment, which are comprised in Layer 3 of **Figure 1.3**.

Table 1.1 Parameters for typical ITFs

Parameters	Unit	PKL	LOBI	SPES	BETHSY	LSTF	ATLAS
Country and Organization	-	Germany-AREVA NP	Italy-JRC/EC	Italy-SIET	France-CEA	Japan-JAERI	Korea-KAERI
Operating years	-	1977 -	1979 - 1991	1983 -	1993 -	1980 -	2007 -
Reference reactor	-	KWU-PWR-4L	KWU-PWR-4L	W-PWR-3L	F-PWR-3L	W-PWR-3L	APR1400-2L
Power of the reference reactor	MWth	3765	3900	2775	2775	3423	
ITF nominal power	MWth	2.512	5.280	6.490	2.860	10.000	2
Time scale	-	1	1	1	1	1	0.71
Volumetric scale	-	1/145	1/712	1/427	1/100	1/48	1/288
Height scale	-	1	1	1	1	1	0.5
ITF number of loops	-	4	2	3	3	2	2
ITF volume (with PRZ)	m^3	3.282	0.648	0.624	2.88	7.952	0.55
PRZ volume	m^3	0.516	0.087	0.0954	0.407	1.147	
SG secondary side volume	m^3	5.824	0.1648-0.7307	1.163	1.952	4.742-4.842	
Pressurizer nominal pressure	MPa	4.5	15.7	15.5	15.5	15.55	15.5
Secondary side operating pressure	MPa	5.6	6.91-6.94	6.94	6.80-6.84	7.0	-
Primary side fluid total mass	kg	-	436	423	1984	5404	-
Number of simulated rods	-	314	64	97	428	1064+104	396

(2) Test facilities

While in the early 1970's the experiments were focused on large break issues, in the following, up to now, parallel to the advancement in code development, integral tests have been carried out to investigate PWR system behavior during design basis accidents (DBAs) transients, e.g. LOCAs, transients under shutdown conditions, and beyond design basis accidents (BDBAs). Construction of code validation matrices is an attempt to collect together the best sets of test data for code validation

and improvement, from the wide range of experiments that have been carried out worldwide in the field of thermal hydraulics. The first formulation of a validation matrix was proposed by Wolfert and Frisch [25]. Except for the target of thermal-hydraulic facilities to reproduce the fluid phenomenon in operation and accident situation of NPP, another goal is to provide validation data for system thermal-hydraulic (STH) codes, subsequently used in design and evaluation of NPPs.

Nowadays, there are two kinds of experiments for STH code validation: separate effects tests (SETs) and integral test facilities (ITFs) [26]. The overall results of the code calculations are validated mainly by data from ITFs, representing the primary and secondary coolant systems. Comparing with SETs, ITFs have a complicated configuration and are expensive to operate. Compromises, for instance with respect to scaling to real plants, are inevitable. Simultaneously, the instrumentation for measurements of parameters governing different two-phase flow phenomena is limited. This makes the integral tests less suitable for detailed investigations of specific two phase flow phenomena. But in order to study the complex phenomena in the loops of NPP, ITFs are essential and very important tools, which provide data on the overall behavior of a simulated reactor system during a LOCA or transient.

Table 1.1 shows some significant parameters for typical ITFs in the world [27]. This study will concentrate on PKL facility and one benchmark test of it.

1.2 Motivation

This study is focused on thermal hydraulic model improvement for STH code ATHLET. The motivation of the work is based on the background history of STH development and is in line with the actual trends, as shown by Figure 1.4.

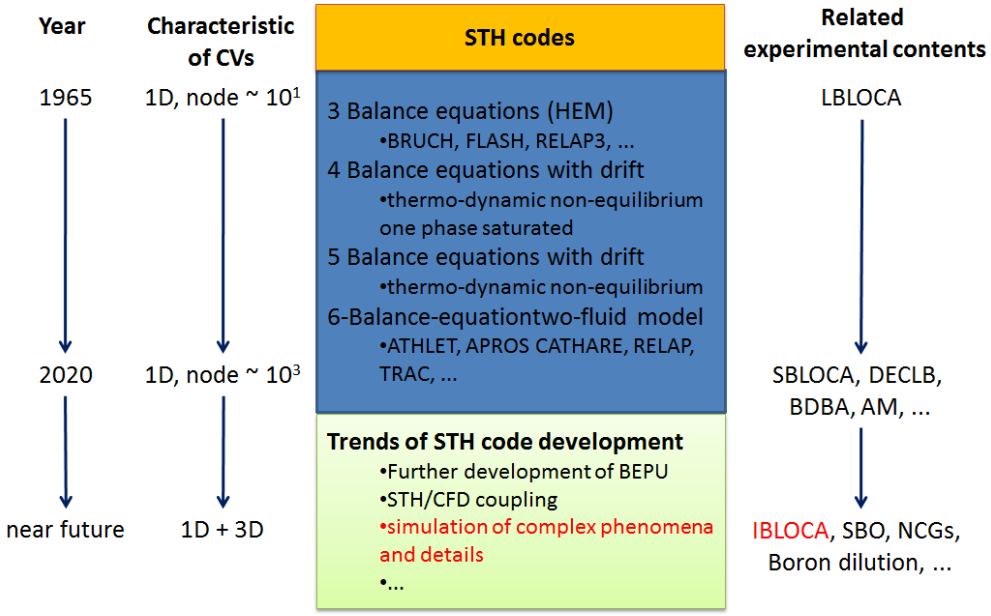

Figure 1.4: STH Codes - Code Development Activities and Direction

The United States safety authority that sponsored the work until late 1960s developed the first generation of these codes [28]. Since that time, different research groups over the world have started with the development of their own codes. Before Three Mile Island Unit 2 (TMI-2) accident, the STH codes considered only LBLOCA scenarios, and were based on the homogeneous equilibrium model (HEM), assuming equal velocities and temperatures of vapor and liquid phases. After that, the focus

was moved to another typical scenario – SBLOCA; the effort in code development was the implementation of new models to allow for the separation of vapor and liquid by gravity, gradually resulting in models with at least six balance equations. Plant models were extended by considering control and balance systems of primary and secondary sides. Therefore, several complex STH codes have been developed for simulating the transient behavior of water cooled reactors during such off-normal conditions. Accordingly, with the development of computation capability, the magnitude of control volumes in typical simulation cases was increased from 10^1 to 10^3 [29]. During the same period, the contents of test facilities were shifted to SBLOCA, Double Ended Cold Leg Break (DECLB), Beyond Design Basic Accident (BDBA) and Accident Management (AM) etc.[30][31]

Nowadays, especially after the Fukushima nuclear accident, the trends for STH codes are (1) from conservative approach to best estimate approach [32]; (2) STH/CFD coupling [33] and (3) more powerful simulation capabilities to deal with complex phenomena in nuclear accidents.

The requirements for STH codes are higher and higher. Recently, it concentrates on station blackout (SBO) [34], IBLOCA, non-condensable gases (NCGs) behavior [35], boron dilution[36] etc. For these complex phenomena, the STH codes should be validated against the test data. This study is concentrated on the recent test of PKL facility - an IBLOCA benchmark - and assesses the validation of ATHLET for this scenario (included in the trend item with red font in Figure 1.4) since previous STH simulations showed obvious uncertainty of IBLOCA. After that, according to the assessment results, the model which leads to the discrepancy between simulation and test data will be confirmed and then a modification of the model will be achieved in this study.

1.3 Structure of this thesis

The present work focuses on the ATHLET simulation of PKL I2.2 IBLOCA benchmark, evaluation of ATHLET simulation results comparing with PKL measurements, assessment of ATHLET thermal hydraulic models on IBLOCA phenomenon prediction, confirmation of the most IBLOCA sensitive model - which leads the discrepancies compared with benchmark test, new model development and validation. In this way, ATHLET may be more powerful and reliable for nuclear thermal hydraulic simulation and consequently more useful for nuclear safety evaluation. The dissertation is divided in seven chapters and two appendixes.

Chapter 1 is introductive, containing the background information of nuclear safety and the motivation of the activity.

Chapter 2 is about fundamental issues for benchmark simulation and STH model sensitivity study, i.e. background of IBLOCA benchmark including PKL description, simulation tool – STH code ATHLET, and the methodology for ATHLET assessment (including the fast Fourier transform based method (FFTBM), the method for nodalization of ATHLET and the Morris screening method (MSM) for sensitivity study.

Chapter 3 will introduce the procedure to prepare the ATHLET input deck, the simulation results compared with test data, including steady state calculation and transient simulation. At the end of this chapter, an assessment about the validation of ATHLET on IBLOCA will be given.

Chapter 4 will introduce the sensitivity study results, which are used to find the most sensitive model for the discrepancy. According to the sensitivity results, critical flow model (CFM) is chosen for modification/improvement. A new developed sensitivity study methodology called FFTBM-MSM two-layer method will be used in this chapter.

Chapter 5 will focus on the new CFM development. The model is called non-equilibrium and non-homogeneous two phase critical flow model (hereinafter abbreviated as NNTPCM). For verification and validation (V&V), the new model is compared in this chapter with measured data from 5 experimental facilities (Al-Sahan, Dobran, Sozzi, Celata and Henry tests)

Chapter 6 focuses on the use of the new developed CFM model in ATHLET. The new model is plugged in ATHLET as a table in input deck. Both SET facility (called Marviken, in which the interference of other phenomena is not so strong) and ITF facility (i.e. PKL, which is the original object of interest of this work) are chosen for the new model application in this chapter.

Chapter 7 summarizes the results of this study. An outlook for further IBLOCA simulation issues and for further investigations and improvements of CFM are given in this chapter.

The appendix of the dissertation provides a detailed discussion on the choking criterion, as a complement for Chapter 5.

2 Background, Tool and Methodology

In this chapter, the following three issues will be concentrated on before the introduction of benchmark simulation: some background about IBLOCA scenario (section 2.1) and the benchmark, including the PKL facility (section 2.2), a short description of the system thermal-hydraulic (STH) code ATHLET (section 2.3), the Fast Fourier Transform Based Method (FFTBM) for the assessment of ATHLET results (section 2.4), the nodalization methodology (section 2.5) and the basic sensitivity study methodology - Morris screening method (MSM, section 2.6).

2.1 IBLOCA

For each design of a NPP, the regulatory authority establishes a set of design basis accidents (DBAs). The supplier of NPP is correspondingly obliged to prove that the plant parameters during DBAs do not violate the acceptance criteria [37]. A loss-of-coolant-accident (LOCA) is a typical class of accident investigated during the whole history of nuclear engineering. There is a strong need to understand the characteristics of the LOCA as well as the automatic countermeasures of the protection and safeguard systems, designed to provide the withstand of the NPP for any break size and break location in the primary circuit.

Before the 1979 TMI-2 accident, the safety research had been mostly focused on a large break loss-of-coolant accident (LBLOCA) [38] since the limiting peak cladding temperature (PCT) normally happens in the LBLOCA [39]. Studies on pipe integrity have shown that the probability of a complete rupture of a pipe depends on the pipe size and, in particular, that this probability is higher for smaller pipes [40]. Therefore, LBLOCA and small break loss-of coolant-accident (SBLOCA) were studied in detail during the last century. The analysis of hypothetical LBLOCAs and SBLOCAs in a PWR determine many of the safety-related operating limits for a plant. Most of the development has been directed toward LBLOCAs since for PWRs the LBLOCA generates the limiting peak cladding temperature (PCT).

As plant life durations are increased in this century and researchers continue to seek improved operating efficiencies, the intermediate break loss-of-coolant-accidents (IBLOCAs) may become a concern; therefore, further understanding of nuclear thermal hydraulic phenomena in accident scenario is mandatory.

An IBLOCA scenario has been recognized as a very important topic in terms of risk-informed regulation (RIR). There is a widespread opinion that the frequency of double-ended guillotine break (DEGB) of primary coolant circuit piping (such as hot and cold legs) of PWR is quite low. Therefore, consideration of rupture of intermediate-size pipe is becoming relatively more important than ever in RIR-relevant safety analyses. The USNRC (2005) proposed risk-informed changes to LOCA technical requirements - Appendix K to Code of Federal Regulations Part 50. In this proposal, an IBLOCA is

chosen as a DBA for the assessment of the effectiveness of emergency core cooling system (ECCS) [41]. After that, more research related with IBLOCA has been focused on, including specific designed thermal-hydraulic experiments and their simulations with STH code. On the other hand, France eliminated LBLOCA from the list of DBAs in 2016, which means that more licensing focus will be on the IBLOCA rather than on the LBLOCA[42].

The studies of IBLOCA scenarios, both in STH simulation and test, will be reviewed next.

2.1.1 Review of IBLOCA simulation

IBLOCA study started at the beginning of 1980s; during that period of time the idea of safety concerns was shifted from LBLOCA to SBLOCA. Vagner [43] has concentrated on the formation mechanics of the intermediate break, studying the influence of cladding and shape of defect on the critical crack size during a PWR IBLOCA. In order to predict the highest cladding temperatures of the maximum and minimum critical heat flux during IBLOCA scenario, different correlations related to maximum critical heat flux, minimum heat flux, the heat transfer coefficients (HTCs) etc. were verified by Vojtek [44]. Kmetyk[45] has assessed the STH code TRAC-PF1/MOD1 against an IBLOCA test primarily. But the results of the calculations diverged significantly for many parameters of interest, with the 3-D VESSEL model results in better agreement with data. Later on, a postulated double-ended guillotine break of a direct-vessel-injection line in an AP600 plant has been analyzed. This event is characterized as an IBLOCA performed with the TRAC-PFl/MOD2 code [46]. According to their numerical results, AP600 had no experience of core heat up during an IBLOCA scenario theoretically and a safe shutdown could be achieved. A number of modifications have been made to the WCOBRA/TRAC-MOD7A code to enable it to make realistic calculations of SBLOCAs and IBLOCAs in a Westinghouse PWR since the early version was only concentrated on LBLOCA simulation [47]. An IBLOCA scenario in Chashma nuclear power plant-1 (CHASNUPP-1) type NPPs has been analyzed using APROS [48]. The results obtained show that the proposed system works properly by performing its role in the transient, leading to cold shutdown conditions. At Warsaw University of Technology, Gurgacz et al. [49] use RELAP5 and CATHARE to simulate an intermediate-break LOCA benchmarking exercise for the European Pressurized Water Reactor EPR. Both of them gave low cladding temperature at the early-stage and had different characteristics in the transient, which reflected the difficulty and uncertainty for the phenomenon simulation of IBLOCA.

Several participants from all over the world have taken part in the IBLOCA test simulation in the last OECD/NEA ROSA-2 Project (2009-2012), which will be introduced next. In this project, different kinds of typical STH codes [50] [51] [52] were assessed by the test data of the Large Scale Test Facility (LSTF).

2.1.2 Review of IBLOCA test

Parallel to the development of the analytical tools, some experimental projects have been executed to improve the understanding of IBLOCA phenomena, to study system behavior during IBLOCA transient, and to provide the required data base for code development and code validation. Although integral test facilities (ITFs) have provided a large matrix of transient scenarios that are used to validate and further develop system codes. However, the number of experiments which considered IBLOCA scenarios is small, so that the validation of STH codes under these conditions is limited [53]. As a conclusion, based on the IBLOCA test literature review, the development history of IBLOCA tests could be divided into 4 phases, as following:

(1) Phase 1 (before 1990): preliminary study on IBLOCA test

IBLOCA related thermal hydraulic phenomena have been researched briefly during this period. Some experimental data on PWR IBLOCAs have been obtained by using such ITFs as LOFT [54] in the US, LOBI [55] in Italy and ROSA-III [56] in Japan in the 1980s. The obtained data, however, would be insufficient to clarify the IBLOCAs specific thermal-hydraulic behavior and the PCT phenomenon.

(2) Phase 2 (from 1990 to 2000): Stagnation period for IBLOCA test

For this period, very few literatures could be found. Two reasons may be responsible for that situation:

1) Firstly, before 2000 the common idea for nuclear safety analysis was based on conservative assessment. Comparing with LBLOCA (which is considered the scenario of largest harm) and SBLOCA (which is considered the scenario of largest risk), IBLOCA scenario does not have so strong relation with conservative conditions. With the development of best-estimation, the study on IBLOCA came back to the concerned contents of safety test.
2) Secondly, the typical phenomena of IBLOCA were though those both in LBLOCA and in SBLOCA. A STH code could simulate IBLOCA if it could reproduce the phenomena in LBLOCA and SBLOCA scenario. (But, actually, according to the test of ROSA-2 project, which will be introduced next, the phenomena in IBLOCA - especially the core heat-up - were closely related to the break size, safety injection operations etc. Such phenomena were difficult to be well reproduced by the STH codes.)

(3) Phase 3 (from 2000 to 2010): Return of focus on IBLOCA test

The OECD/NEA PSB-VVER project (2003–2008) has been set in Russia with the objective to obtain the required experimental data not covered by the VVER validation matrix [57]. There were five tests in total in the PSB-VVER project, including two IBLOCA tests: the first experiment is an IBLOCA scenario with 11% upper plenum break [58]; the fourth experiment of the test matrix is related to the primary-to-secondary intermediate break issue [59].

JAERI (of Japan) conducted the Rig of Safety Assessment (ROSA) Program to investigate the thermal hydraulic response of PWR (ROSA-II and ROSA-IV) and BWR (ROSA-III) to LOCAs in the last half century. Several experiments (Test-1, Test-2 and Test-7) were conducted for the OECD/NEA ROSA-2 Project (2009-2012) [60] using the large scale test facility (LSTF) [61], which simulated a cold leg IBLOCA with 17% or 13% break in a pressurized water reactor. Assumptions were made, such as single-failure of high-pressure and low-pressure injection systems of emergency core cooling system [62]. One of the main outcomes was that an un-expected temperature increase was reported in the 17% cold leg break. The maximum peak cladding temperature (PCT) for that transient was around 300 K higher than that reported in the other two tests[63]. The adaptability of STH codes was also checked during the OECD/NEA ROSA-2 Project. The results showed that most phenomena could be reproduced by the participants using STH codes except the core heat-up and the related PCT phenomena.

(4) Phase 4 (from 2011 until now): Counterpart supplementary IBLOCA tests for ROSA-2

The NEA Advanced Thermal-Hydraulic Test Loop for Accident Simulation (in the facility ATLAS of KAERI) Project is one of the NEA supported joint projects under the auspices and with the support of the NEA [64]. It started from April 2014, with a three-year project period. There were five types of tests performed in the NEA-ATLAS Project, including two tests related with IBLOCAs - A4.1 and A5.2 with respects to 13% and 17% IBLOCAs separately. The scaling methodology for these two tests was applied to set-up the test conditions which were performed as counterpart tests of the LSTF IBLOCA tests.

In order to provide a contribution to solving the PCT problem of LSTF, as described above, it was decided to include three LSTF counterpart experiments in the OECD/NEA PKL-4 project as three different runs of the benchmark test I2.2 in the PKL facility in Germany.

The common strength of LSTF and PKL facilities is that they consider the full height of the corresponding NPP. One contribution of the OECD/NEA PKL-4 project was to provide data for STH codes to assess their calculated core heat-up and PCT behavior during IBLOCA.

2.2 PKL facility and I2.2 IBLOCA benchmark

The ATHLET simulation in this study is based on the IBLOCA benchmark performed at the PKL facility. The prototype of PKL (German abbreviation for "Primärkreislauf" = Primary Loop) is a 1300 MWe PWR of Konvoi class (e.g. Group 2 of the NPP at Philippsburg). It is an ITF for nuclear thermal hydraulic studies, located in Erlangen, Germany. PKL facility was designed, built and commissioned by Siemens/KWU (now AREVA NP GmbH) in the seventies and has been in operation since 1977 [65]. Its objectives have changed considerably to match latest developments with focus on nuclear safety issues. The facility was focused on DBAs at the beginning and latterly also on beyond design basis accidents (BDBAs) of NPP. A notable characteristic of PKL is that it could be used to investigate not only symmetric loop behavior but also asymmetric loop behavior.

2.2.1 The structure and features of PKL Facility

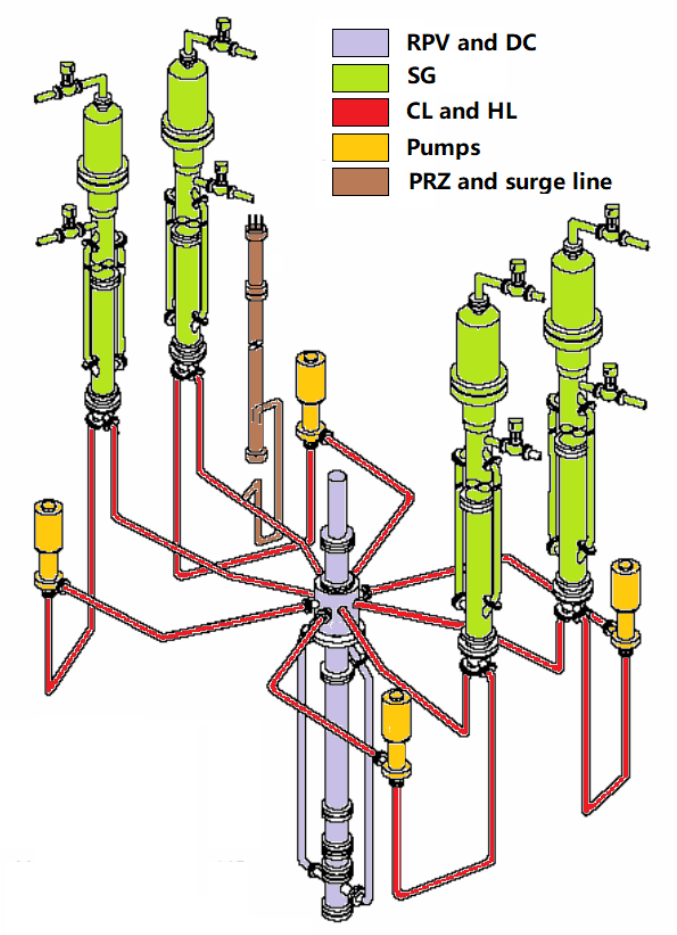

Figure 2.1: The Primary Structure of PKL facility

The PKL facility is a full-height facility, which means it has full-scale hydrostatic head of PWR and reproduces most of the PWR thermal hydraulic phenomena in primary and secondary loops. Its maximal power is 2.5MW (equivalent to about 10% of the nominal rate) [66]. As the essential construction principles of the most types of PWRs are similar, it is also possible to make statements concerning the behavior of other companies' NPPs.

The facility includes a Reactor Pressure Vessel (RPV), Steam Generators (SGs), the interfacing systems on the primary and secondary side and the break system. As shown in Figure 2.1, the reactor cooling system (RCS) mainly includes the reactor core model (including electrical heated rods, the upper head (UH), the upper plenum (UP) and the lower plenum (LP)), the downcomer (DC), the SG primary and secondary sides, the (four) reactor coolant pumps (RCP) and the pressurizers (PRZs, full-height and connected through the surge line to the hot leg HL #2) [67]. The (four) hot legs and cold legs (CLs) are also considered in the facility. The secondary loop includes main steam lines (MSLs) with all the characteristics of the original system except for turbine and condenser, feed water system, emergency feed water system and depressurization system.

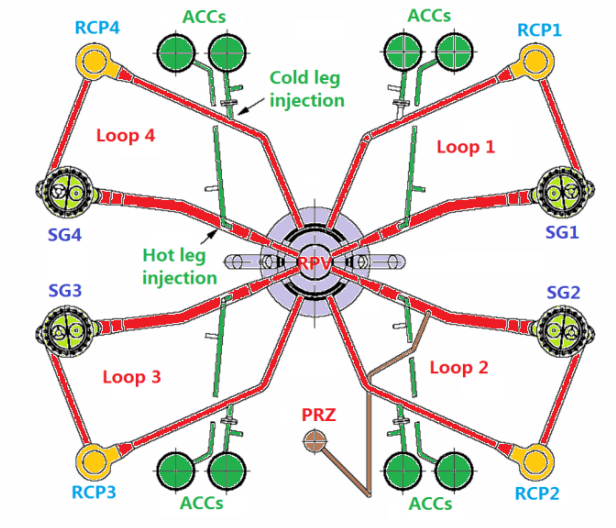

Figure 2.2: Top View of PKL facility

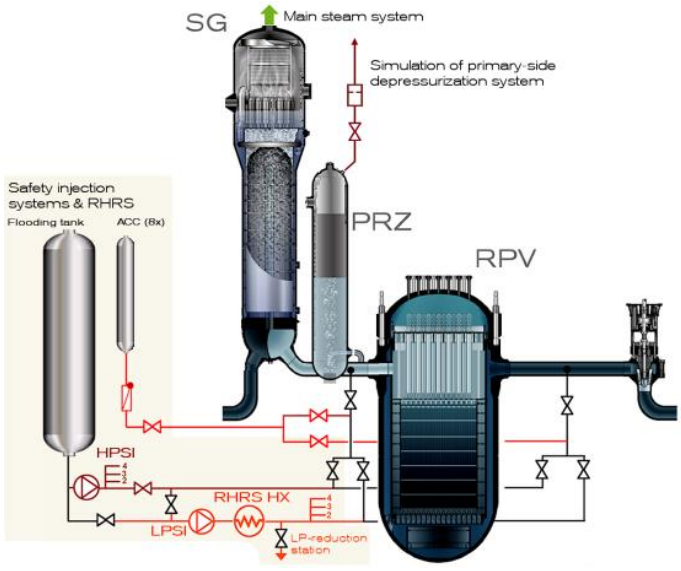

Figure 2.3: Configuration of the safety system of PKL facility

Figure 2.2 gives the top view of the PKL facility and Figure 2.3 gives the configuration of the safety system. The safety system is shown clearly in both figures. PKL facility is equipped with all relevant engineered safety and operational systems on the primary and secondary side - e.g. four independent high and low pressure safety injection systems connected to the hot and cold legs, RHRS (Removal system of residual heat), 8 accumulators (ACCs), coolant volume control system (CVCS) [68]. This allows the simulation of a wide spectrum of accident scenarios, the interaction between the primary and secondary side in combination with different safety and operational systems [69]. The basic design parameters of PKL facility are shown in Table 2.1 [70].

Table 2.1: Design Parameters of PKL facility

Design parameter	value	Design parameter	value
Reference Reactor Power	3400MW	**Reference Scaled Nominal Power**	28.36MW
Reactor Power/PKL Scaled Nominal Power	134	**Max Power**	2.5MW
Primary System Volume	≈2.4m^3	**Height of Pressurizer**	1.3m
Reactor primary loop volume /PKL scaled volume	145	**Reactor primary loop CSA/PKL scaled CSA**	145
Max Pressure of primary loop	4.5MPa	**Max Pressure of secondary loop**	5.6MPa
Number of electrical heated rods modeling reactor core	314	**Number of Control Rods**	26
Rod Cladding Max Temperature	750℃	**RCP operating flow rate**	40kg/s
Temperature of Primary fluid	300℃	**Temperature of Secondary fluid**	300℃
Number of SG U-tubes	28	**Measuring Locations**	>1500

2.2.2 The PKL I2.2 IBLOCA benchmark

Experiments related to IBLOCA scenario in a PWR were conducted for the OECD/NEA ROSA-2 Project using LSTF. Similar to PWR LOCA accident, in the LSTF tests the steam volume expansion involved concurrent liquid level depressions in the loop seal downflow leg and in the reactor core. The core uncover started simultaneously with liquid level drop in crossover leg down flow-side before loop seal clearing (LSC) and water remaining occurred on the upper core plate in the upper plenum. At this moment, minimum core collapsed liquid levels were taken. In the project, two IBLOCA sizes (13% and 17%) were considered for test study. While in the 13% break test the core heat up was not significant, the 17% break test showed an extensive increase of the rod cladding temperatures. The challenge for the LSTF IBLOCA scenarios simulations was that some STH codes or code users seemed not to be able to capture the core heat-up phenomena in both tests owing to the very dynamic behavior of the system.

Table 2.2: Significant changes between the 3 runs of PKL I2.2 IBLOCA benchmark

Test	Run 1	Run 2	Run 3
Break size	13%	17%	17%
HPSI	2 out of 4 in CL	2 out of 4 in CL	1 out of 4 in CL
ACC	2 ACCs in CL	2 ACCs in CL	2 ACCs in CL
LPSI	2 out of 4 in CL	2 out of 4 in CL	1 out of 4 in CL

For studying the scaling problems to extrapolate thermal-hydraulic phenomena observed in down-scaled facilities, an experiment was performed for the OECD/NEA PKL-4 Project with PKL, as a counterpart to a previous LSTF test and denoted as PKL I2.2 IBLOCA benchmark.

There are three runs in total for the I2.2 benchmark. Run 1 and run 2 were used for nodalization and model confirmation for STH code simulation and, in particular, the test run 3 [71] is selected for blind calculation in the benchmark.

Table 2.3: ICs and BCs of I2.2 test

Location	Parameter	Run 1	Run 2	Run 3
Break	Location	Cold leg 1	Cold leg 1	Cold leg 1
	Orientation	Upward	Upward	Upward
	Size	13%	17%	17%
	Break signal	0 s	0 s	0 s
Core	Core power	1965 KW	1972 KW	1965 KW
	SCRAM signal	0 s	0 s	0 s
Primary side	Mass inventory (w PZR)	2450	2440 kg	2440 kg
	Initial HL temperature	247.9	247.6	246.8 ℃
	Initial CL temperature	244.9	244.7	244.3 ℃
	Initial mass flow rate (each loop)	38.5	38.5	38.7 kg/s
	Subcooling CET	~8 ℃	~9 ℃	~10 ℃
PRZ	Pressure	44.6	45.02	45.8 bars
	Level	8.27	7.8	7.8 m
	Mass inventory	246	232	230 kg
	PZR heater shut-off	~5s	~5s	~4s
Secondary side	SG Initial pressure	35.0	34.9	35.3 bars
	SG fill level	11.97	12.2	12.1 m
	MFW temperature	243℃	243 ℃	244.3 ℃
	MFW closure	~11s	~10s	~8s
	MSS closure	~11s	~10s	~8s
RCP	rotation speed	2830	2830	2870 rpm
	RCP coastdown signal	~30s	~30s	~29s
	Butterfly valves	250s	250s	-
ACC	Injection location	CL loops 2 and 3	CL loops 2 and 3	CL loops 2 and 3
	Initiation of system	~13.8 bar		~16.3 bar
	Water temperature	25.6	24.7	26℃
	Water inventory	234	234 kg	235 kg
	Nitrogen inventory	7 kg	7 kg	7 kg
HPSI	Injection location	CL loop 2 and 3	CL loop 2 and 3	CL loop 3
	Initiation of system	~38.5 bar	~38.5 bar	~31.6 bar
	Water temperature	21 - 25℃	22 - 23℃	16 - 22℃
LPSI	Injection location	CL loop 2 and 3	CL loop 2 and 3	CL loop 3
	Initiation of system	~6.8 bar	~6.8 bar	~6.8 bar
	Water temperature	21 - 25℃	21 - 25℃	19 - 22℃

Table 2.2 shows the difference between the three runs, mainly in the break size and the control of safety injections. Comparing with test run 1, the break size of run 2 has been changed from 13% to 17% of nominal CL pipe size. Furthermore, from run 2 to run 3, the high pressure safety injection (HPSI) and low pressure safety injection (LPSI) have been halved, only existing in CL loop 1. The injection rates for the HPSI and LPSI have been both scaled down from ROSA/LSTF test 7 (13 % break case). Their capacity curves, as shown in Figure 2.4, were determined by a pre-test so that the safety injections started at a core power level which was comparable to the respective LSTF counterpart. The

HPSI (3.85 MPa) and LPSI (0.68 MPa) were controlled by functions of pressure signals at the upper plenum (UP) of the core vessel.

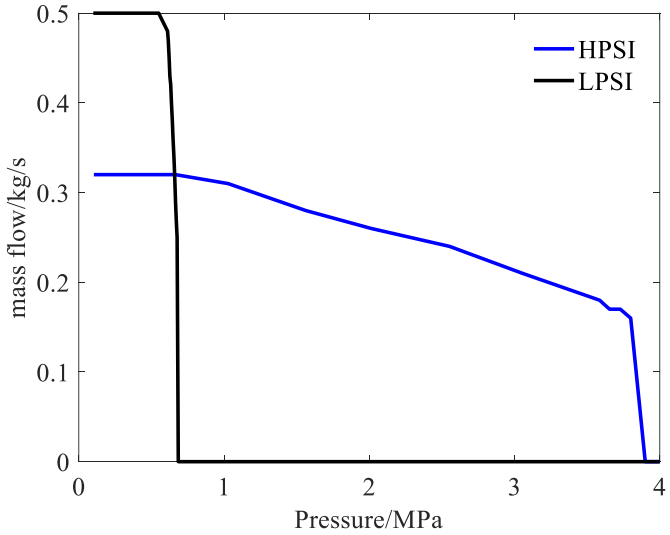

Figure 2.4: HPSI and LPSI in I2.2 run 1 test

In this study, run 1 will be analyzed in detail since the procedures and phenomena of the runs were similar.

In the project, 12 participants from different organizations, using a total of 8 different STH codes (RELAP5, ATHLET, CATHARE and MARS etc.), have performed benchmark calculations of the experiment [72].

The ICs/BCs for the PKL I2.2 IBLOCA benchmark have been derived from the appropriate ROSA/LSTF reference tests. For more detailed information of ICs/BCs in I2.2, Table 2.3 could be resorted to.

2.3 Simulation tool: ATHLET

As a typical STH code, ATHLET (abbreviation for Analysis of Thermal-hydraulics of Leaks and Transients) is used in this study for the simulation of IBLOCA benchmark and model modification/improvement. ATHLET is being developed by the “Gesellschaft für Anlagen- und Reaktorsicherheit (GRS) gGmbH". This study uses the version ATHLET Mod 3.1A[73], released in May 2018, as a part of the GRS code package AC^2[74], used for NPP safety analysis and accident assessment. The aim of ATHLET development is to cover the whole spectrum of design basis and beyond design basis accidents (without core degradation) for PWRs, BWRs, SMRs and future Gen IV reactors within one single code[75][76].

The structure of ATHLET could be illustrated by Figure 2.5, which is also similar to the most of other STH codes. At outermost layer of the program is the ordinary differential equations (ODEs) solver to be found, based on nodalization with given initial conditions (ICs) and boundary conditions (BCs). The system of ODEs is solved fully implicitly with the numerical integration method called Forward-Euler and Backward-Euler (FEBE) method. Solutions of a general non-linear system of ODEs of first order can thus be found. For the linearization of implicit systems, a Jacobian matrix is used. ODEs are mainly achieved from the discretization of conservation equations on meshes after nodalization. Under

the mathematical layer, the code contains two kinds of modules: physical model modules and Auxiliary function modules.

The physical model modules (as shown in Figure 2.5) have three dominant parts, to be stated next. Obviously, some parameters, e.g. heat transfer coefficients (HTCs), fluid temperatures etc., should be transferred among these modules during calculation in the practical usage of STH codes.

1) Two-phase fluid: here the most important are the 6-equations for mass, momentum and energy conservation in two-phase flow.
2) Solid: the heat structures (e.g. fuel rods, pipes etc.) are considered as solid in STH codes. The heat transfer in solid is considered as 1D and the traditional Fourier equation is used to describe it. A brief radiation model is also considered for a solid in ATHLET.
3) Nuclear physics: STH code needs the heat source term from nuclear reaction in accident scenario. Normally, point kinetics model or 1D kinetics model is used for the nuclear energy generation.

In order to solve the ODEs of ATHLET, as a STH code, several models related with the thermal hydraulic conservation equations should be included in calculation, e.g. closure law equations, state equations etc. Since some specific instruments (pumps, separators etc.) are used in nuclear engineering, in order to simulate them, their dedicated models are also included. For special or complex phenomena, some models are also considered for simplifications, e.g. critical flow model (CFM), counter-current flow limit (CCFL) model etc.

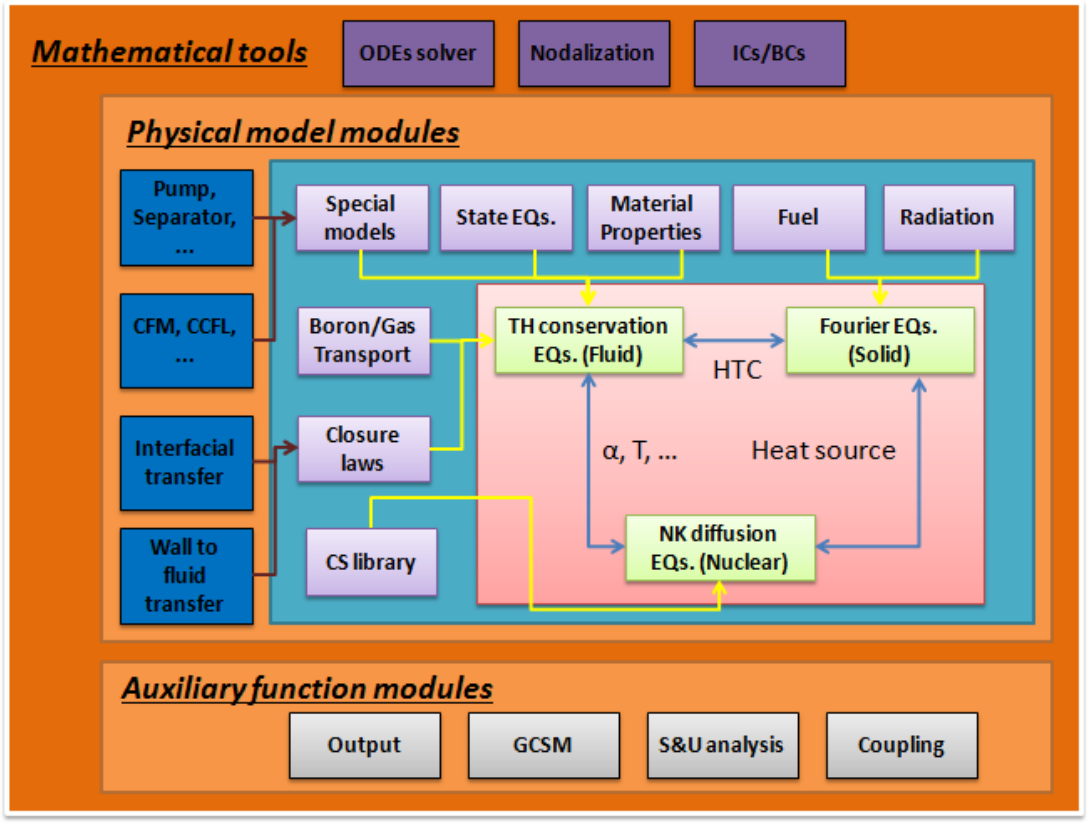

Figure 2.5: Brief structure of ATHLET

2.4 Assessment methodology: FFTBM

There are several approaches proposed and accepted in literature[77][78][79] to conduct an objective comparison between the STH code calculations and measured data. Among them, widely used, the fast

Fourier transform based method (FFTBM) developed by members of the Pisa University in 1990s [80]. It has been already applied for quantitative assessment of code calculations for various international benchmarks[81][82]. The details of this methodology may be found in this literature; the next sub-section will only recall it in its major aspects. It may be extended to many fields of research and generate some further functions/methods. In this study, several research contents are related with FFTBM as shown in Table 2.4.

Table 2.4: The usage of FFTBM in this study

Location in the study	Study objective	Function of FFTBM
Section 3.2	ATHLET steady state simulation	Assessment method of the rationality of ATHLET ICs/BCs and primary nodalization for PKL I2.2 IBLOCA benchmark simulation
Section 3.3	ATHLET transient simulation	Assessment method of nodalization for final nodalization chosen for PKL I2.2 IBLOCA benchmark simulation
Section 3.4	Assessment of ATHLET on IBLOCA simulation	Assessment method of PKL I2.2 IBLOCA benchmark results comparing with test data
Section 4.3	Sensitivity calculation	Assessment method of different sensitivity calculations
Section 4.4	Sensitive model evaluation	Couple with MSM to assess different sensitivity models and find the most sensitive model

For data analysis, FFTBM provides frequency-based accuracy measures for each single thermal hydraulic variable as well as for the whole calculation, using discrepancies between experimental data and calculated results in the transient duration. FFTBM easily provides quantitative and user independent accuracy indices using weighting factors based on experiment accuracy, safety relevance, and relative importance of each variable [83].

In FFTBM, fast Fourier transforms (FFTs) of the experimental and error signals functions are performed at first. According to the theory of FFT, functions must be identified by a number of values which is a power of 2 in order to fulfill the sampling theorem. Therefore, the number of points defining the function in the time domain may be written as $N = 2^{m+1}$.

The error function in the time domain $\Delta F(t)$ is defined as:

$$\Delta F(t) = F_{cal}(t) - F_{exp}(t) \tag{2.1}$$

where $F_{cal}(t)$ and $F_{exp}(t)$ are the calculated and the experimental signals, respectively. The code accuracy quantification for an individually calculated variable is derived out of amplitudes of discrete experimental $\left|\tilde{F}_{exp}(f_n)\right|$ and error signals $\left|\tilde{\Delta}F(f_n)\right|$ delivered by FFT at the frequencies f_n, with n=0, 1, ..., 2^m (m being the exponent, normally 8, 9, 10, 11).

$$AA_{exp} = \frac{1}{2^m + 1}\sum_{n=0}^{2^m}\left|\tilde{F}_{exp}(f_n)\right| \tag{2.2}$$

$$AA_{error} = \frac{1}{2^m + 1}\sum_{n=0}^{2^m}\left|\tilde{\Delta}F(f_n)\right| \tag{2.3}$$

The accuracy of a single variable is assessed by using the average amplitude (AA), defined as:

$$AA = \frac{AA_{error}}{AA_{exp}} = \frac{\sum_{n=0}^{2^m} \left|\tilde{\Delta}F(f_n)\right|}{\sum_{n=0}^{2^m} \left|\tilde{F}_{exp}(f_n)\right|} \tag{2.4}$$

AA in Eq. (2.4) means the ratio of the sum of the amplitudes of the error signal to the sum of the amplitudes of the experimental signal. It should be noticed that the AA is a dimensionless number, showing influences in terms of the average amplitude obtained in the frequency domain which represents the physical influence (e.g. temperature or pressure change). If the experimental and calculated signals are equal (i.e., the error signal is zero), AA becomes zero, which means perfect agreement. Inversely, if the calculated signal is zero, AA becomes 1.0, which means 100% error. The AA factor may be considered as a sort of average fractional error of the calculated variable of interest.

The overall picture of the accuracy for the given code calculation has to take into account many variables of interest and, therefore, one may define a total weighted average amplitude (total accuracy).

$$AA_{tot} = \sum_{i=1}^{N} (AA)_i \cdot \left(\omega_f\right)_i \tag{2.5}$$

with

$$\sum_{i=1}^{N} \left(\omega_f\right)_i = 1 \tag{2.6}$$

where N is the number of the considered variables, $(AA)_i$ and $\left(\omega_f\right)_i$ being average amplitude and weighting factor for the i-th analyzed variable, respectively. The weighting factor for the i-th variable is defined as:

$$\left(\omega_f\right)_i = \frac{\left(\omega_{exp}\right)_i \cdot \left(\omega_{saf}\right)_i \cdot (\omega_{norm})_i}{\sum_{i=1}^{N} \left(\omega_{exp}\right)_i \cdot \left(\omega_{saf}\right)_i \cdot (\omega_{norm})_i} \tag{2.7}$$

with ω_{exp} the contribution related to the experimental accuracy, ω_{saf} the contribution expressing the safety relevance, and ω_{norm} the contribution of primary pressure normalization. These parameters have to be assigned using engineering judgement. Weighting factors for STH code calculations for nuclear installations are given in Table 2.5 [84].

Table 2.5: Weighting factor contributions for analyzed quantities in nuclear installations

	ω_{exp}	ω_{saf}	ω_{norm}
Pressure drops	0.7	0.7	0.5
Mass inventories	0.8	0.9	0.9
Flow rates	0.5	0.8	0.5
Primary pressure	1.0	1.0	1.0
Secondary pressure	1.0	0.6	1.1
Fluid temperatures	0.8	0.8	2.4
Cladding temperatures	0.9	1.0	1.2
Collapsed levels	0.8	0.9	0.6
Core power	0.8	0.8	0.5

For the total accuracy, the following criteria were set for comparisons to experimental data (Prošek, 2002):

1) $AA_{tot} \leq 0.3$ characterize very good code predictions,
2) $0.3 < AA_{tot} \leq 0.5$ characterize good code predictions
3) $0.5 < AA_{tot} \leq 0.7$ characterize poor code predictions
4) $AA_{tot} > 0.7$ characterize very poor code predictions.

2.5 Nodalization methodology and procedure

As introduced in Figure 2.5, before the calculation of ODEs solver, a major step in the preparation of scenario simulation is the discretization or development of the nodalization of nuclear installations or test facilities. The nodalization must be determined and its uncertainty should be possibly eliminated prior to accident analysis through analytical studies. Recently, in order to emphasize the importance of code nodalization, D'Auria has interpreted the acronym BEPU as three parts [85], emphasizing the importance of the code nodalization:

1) the numerical (best estimate) code(s);
2) code nodalization;
3) the uncertainty method(s).

Furthermore, D'Auria has proposed a new powerful framework to demonstrate the capability of STH codes in nuclear engineering, which is called V&V&C (short for Verification, Validation and Consistency) [86]. Comparing with the current V&V (Verification and Validation), in this framework, more comprehensive topics, which connect with the development and the qualification of numerical codes, are considered in "consistency" activity. The consistency of geometry parameters between the STH codes and NPP or facilities, including code nodalization, is a typical topic of "consistency" activity [87].

All major existing STH codes follow the concept of a "free nodalization", that is, the code user has to build up a detailed nodalization which maps the whole system to be calculated into the frame of a one-dimensional thermal-hydraulic network. To do this, the codes offer a number of basic elements like single volumes, pipes, branches, junctions, heat structures, and so forth. In the frame of the input-deck set-up, engineering judgment is normally used to a wide extent. In practice, this approach provides not only a large flexibility with respect to different nuclear installations, but also a certain standardization for separate test facilities (STFs) and ITFs, which still might deviate considerably from the full-size reactor.

Historically, one of the major obstacles during nodalization development was related to the memory restrictions of STH codes[88]. Nowadays, due to the existing code limitations and economic constraints, the development of such a nodalization represents always a compromise between the desired degree of resolution and an acceptable computational effort. With the development of STH codes, it is more and more necessary to define a procedure to qualify the nodalization in order to obtain qualified (i.e. reliable) calculation results.

The problem is that the nodalization of STH codes usually provides large flexibility and, as a consequence, a large responsibility lies on the user to develop an adequate nodalization scheme. If the code nodalization is wrong, not only the reference results are wrong but also the results of the uncertainty calculations are unreliable. In the literature, some simple examples with different choices in nodalization have shown evidence of nodalization influence on results [89]. Furthermore, the development always becomes a compromise between the desired accuracy and computational effort due to the code and economic limitations.

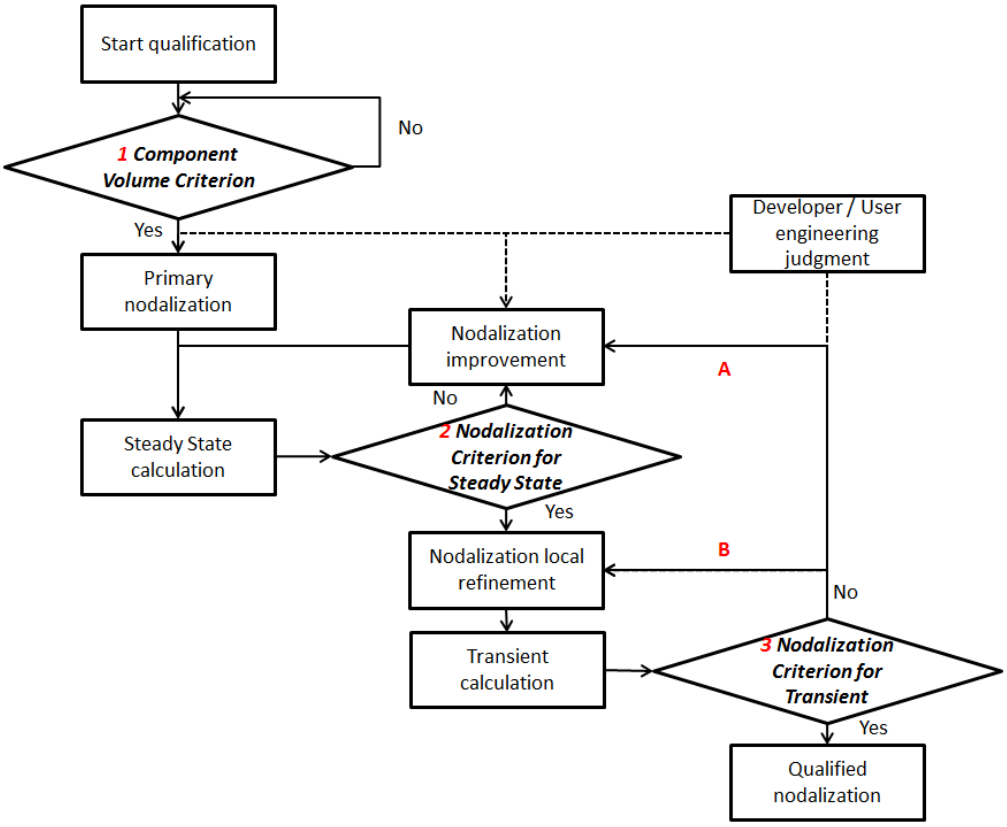

Figure 2.6: Flow chart for nodalization qualification

The continuous development and improvement of STH nodalization technology is not only a requirement but also a difficult task due to the large amount of information included in the nodalization of nuclear installation or ITFs. In that sense, methodologies designed to qualify NPP nodalization take a key role and can be used to both provide an insight in the quality of the produced analyses and, in addition, help the developer in the detection of possible deficiencies in the nodalization[90]. Based on the background, this study used a nodalization qualification methodology which is a modification of methodology from literatures [91] [92].

A major issue in the use of STH codes is constituted by the simulation capability to reproduce the nuclear installation or facility behavior under steady state and transient conditions. These aspects require three separate checks of the nodalization qualification, as shown also in Figure 2.6:

(1) Component volume criterion

The nuclear installations and test facilities can be divided into several components, such as RPV, HL, CL, SGs etc. These components should be reproduced in the STH codes to some extent. For code nodalization, the first criterion is for component volume judgment, which offers a necessary guarantee of geometrical rebuilding of the systems. The rebuilding items, which should be concerned, include not only the volume of each component but also the volume distribution at different elevation and the component materials. The qualified data from the official sources may be a great help for this task. Actually, this task is not nodalization but the basic for nodalization and code calculation. In this sense, it should be done before the first run of the steady state calculation.

In the component volume criterion, both qualitative and quantitative assessments are established to express the acceptability. According to the official documents of data, the volume variation as a function of elevation could be build. These data could be appropriately simplified (since the real geometries of some components may be very complex) and used for geometry description in the STH code. Comparison of the real and code-plugin volume-elevation curves could give a qualitative judgment of the code-plugin component volume and be a precondition for quantitative assessment.

In some literature, a relative error (e.g. 1% or 5%) between real volume and calculated volume in STH code is used as limit value for volume criterion. It is unreasonable since it does not consider the volume magnitude of different components. For example, if a component accounts for 20% of the system volume, a smaller (stronger) criterion of relative error should be introduced, comparing with a smaller component. On the contrary, a component, which accounts for 1% of total system volume, could use a larger (weaker) criterion value since its volume variation does not impact the total system volume much. Consequently, in this study Eq. (2.8) is introduced, which defines a volume fractional parameter for component volume criterion, considering there are K components in total in the objective system. In the equation, V_i and $V_{cal,i}$ $(i = 1, 2, \dots, K)$ are the real and calculated volume in STH code for the i-th component, respectively. The parameter $V_{tot} = \sum_{i=1}^{K} V_i$ stands for the total volume of the objective system.

$$R_i = \frac{V_i}{\sum_{i=1}^{K} V_i} \cdot \frac{\left|V_{cal,i} - V_i\right|}{V_i} = \frac{\left|V_{cal,i} - V_i\right|}{V_{tot}} \tag{2.8}$$

According to Eq. (2.8), the introduced volume fractional parameter considers not only the relative error of each component but also the volume fraction in the whole system. A suitable value should be chosen for R_i as volume criterion. In this study, 0.2% is chosen.

(2) Nodalization criterion for steady state calculation

The second criterion is related with steady state calculation, aiming to judge the capability of the nodalization to reproduce the steady state qualified conditions. The most direct and effective way for the criterion is to use the relative errors of calculated steady state values with respect to experimental ones for the selected parameters, as shown in Eq. (2.9). For j^{th} selected parameter, P_j is the calculated value, $P_{0j}$is the measured value and R_j is the relative error.

$$R_j = \frac{\left|P_j - P_{0j}\right|}{P_{0j}} \tag{2.9}$$

The selected steady state parameters may be pressures, temperatures, mass flow rates, etc.

In this study, the acceptable criterion value for the relative error for pressure and temperature is 1%, and 2% for water level. After the assessment of the steady state calculation, if the criterion is not satisfied, some modification (not only nodalization but also the topology of the geometry, physical models and related parameters etc.) should be done to decrease the relative errors of steady state parameters.

(3) Nodalization criterion for transient calculation

It is related to the capability of the code nodalization to reproduce the expected transient scenario. Some error types introduced during the nodalization set-up in steady state calculation can be detected

only after performing transient calculations. The criterion considers four aspects, both in qualitative and quantitative ways.

1) Since the transient results are related with several items, such as the physical model options, logic of some systems etc., all of them should be checked at the same time.
2) Qualitatively, the nodalization should confirm that the basic thermal hydraulic phenomena in the transient have been reproduced by the STH code.
3) Generally, based on the steady state nodalization, only limited nodalization components should be recognized and subdivided using "sliced approach"[93] to explore the influence of nodalization. The achievement of this step requires that the nodalization is detailed enough to offer results which are accurate enough in the critical positions (e.g. pressured vessel, steam generators) of the simulated system[94]. In this study, FFTBM is used to assess quantitatively the nodalization sensitivity for transient calculation.
4) The nodalization and CPU calculation time should be considered together since the STH code calculation is time-consuming, especially if sensitivity and uncertainty studies are concerned in the nuclear engineering design. A suitable nodalization also means high efficiency for the calculation.

The cases with different refined nodalizations could be run in parallel and then compared to each other. The procedure is iterative, requiring that a reasonable level of accuracy is satisfied. It should be emphasized that in some case from literature, transient results with different nodalizations were compared with experiment data, and the nodalization with minimum error (comparing with test data) was considered as the final nodalization. This process is not rigorous since the convergence of nodalization (i.e. the nodalization independent solution) is not verified and in the majority of cases there is no transient measured data that can be used for the calibration of the STH simulation. The suitable (nodalization) calibration case is not the experiment data itself but a more refined nodalization, and a convergence behavior towards it should be observed. An example will be shown and discussed in detail in section 3.3.

If the nodalization is not convergent, two possible options may be accessed, as shown by Figure 2.6. Option A is suitable for the situation when different refined nodalizations have different steady state results. In this situation, the primary nodalization should be modified and checked again. Option B is suitable for the situation when different refined nodalizations have the same steady state results but unacceptable discrepancy according to the criterion. In this situation, only the most refined nodalization should be modified.

2.6 Morris screening method (MSM)

Sensitivity (and also uncertainty) study is becoming increasingly widespread in many fields of engineering and sciences, encompassing practically all of the experimental data-processing activities and many computational modeling and process simulation activities. While building and using numerical simulation models, sensitivity analysis (SA) methods are very useful tools. They are used to study how the uncertainty in the output of a model can be apportioned to different sources of uncertainty in the model input [95]. It may be used to determine the most contributing input variables to an output behavior as well as the non-influential inputs, or ascertain some interaction effects within the model. The objectives of SA are numerous: model verification and understanding, model simplifying, factor prioritization, aiding in the validation of a computer code, justification in terms of system design safety etc. [96]. In my sensitivity analysis, the influences were determined by using the Morris screening method (MSM) acting on the FFTBM results.

The Morris method deals efficiently with models containing hundreds of input factors without relying on strict assumptions about the model (such as, for instance, additivity or monotonicity of the model input-output relationship). The Morris method is simple to understand and implement, and its results are easily interpretable. Furthermore, it is economic in the sense that it requires a number of model evaluations that is linear in the number of model factors. The method can also be regarded as quasi-global as the final measure is obtained by averaging a number of local measures (the elementary effects), computed at different points of the input space.

The experimental plan proposed by Morris is composed of individually randomized "one factor-at-a-time" experiments: the impact of changing one factor at a time is evaluated in turn. Each input factor may assume a discrete number of values, called levels, which are chosen within the factor range of variation. The sensitivity measures proposed in the original work of Morris[97] are based on what is called an elementary effect which is considered as the basis of the Morris screening method (aiming at identifying a few important inputs from a large collection of model inputs by using a small number of model evaluations). The elementary effect of Morris sensitivity technique is based on the EE_i [98][99].

$$EE_{ij}(\boldsymbol{x}) = \frac{\left[y(x_1, \dots, x_{i-1}, x_i + \Delta_j, x_{i+1}, \dots, x_k) - y(\boldsymbol{x})\right]}{\Delta_j} \tag{2.10}$$

where $\boldsymbol{x} = (x_1,\ x_2 \dots, x_k)$ is any selected input sample with totally k input parameters and y is the concerned output parameter. Δ_j (normally, a percentage change of the parameter value) is a certain change value of x_i (the rest of the parameters are kept fixed). The index EE_i defined in Eq. (2.10) expresses the ratio of the change of y by giving the i-th input x_i a certain change $x_i + \Delta_j$, which can measure the effect of x_i in a given scope on output y.

The MSM allows independent variables to be varied by a fixed percentage of the step size, and the final sensitivity discriminated factor is the average of multiple Morris coefficients. The corresponding formula is [100][101]:

$$S_i = \frac{\sum_{j=0}^{n-1} EE_{ij}(\boldsymbol{x})}{n} = \frac{\sum_{j=0}^{n-1} \frac{(y_{j+1} - y_j)/y_0}{(P_{j+1} - P_j)}}{n} \tag{2.11}$$

where S_i is the sensitivity factor of i-th selected parameter; y_j is the output value of the j-th run of the calculation; y_0 is the initial value of the calculated result after the parameter adjustment; P_j is the percent change of the parameter value after the j-th run model relative to the initial parameter value; n is the number of sensitivity calculations. According to the formula for Morris coefficients, one may remark that the Morris coefficient is the average slope between the calculated results and selected input sample. According to the S value of the parameter, Morris divides the sensitivity of parameters into four categories:

1) $|S| \geq 1$ for a highly sensitive parameter;
2) $0.2 \leq |S| < 1$ for a sensitive parameter;
3) $0.05 \leq |S| < 0.2$ for a moderately sensitive parameter;
4) $0 \leq |S| < 0.05$ for an insensitive parameter.

2.7 Summary

IBLOCA was highly concerned in this decade after the OECD/NEA ROSA-2 Project (2009-2012). PKL and its I2.2 benchmark test, which was a counterpart test related with the IBLOCA test of ROSA-2, were introduced in this chapter.

ATHLET was planned to use for the simulation of the benchmark. In order to verify the effectiveness of ATHLET simulation and its results, the assessment method (FFTBM) for STH code and the simulation nodalization were introduced in this chapter.

About the nodalization methodology, there are several differences of nodalization qualification methodology between literature and present work:

1) For component volume qualification, a more reasonable volume fractional parameter, which considers not only the relative error of each component but also the volume fraction in the whole system, was introduced.
2) FFTBM has been introduced for steady state nodalization qualification. A parameter called average amplitude (AA) is introduced by FFTBM and it is equivalent to absolute error between calculated and measured responses, relative to measured responses in steady state nodalization qualification.
3) Without using the a-priori knowledge of measured data, I developed a FFTBM-related method to judge the convergence and rationality of nodalization in transient simulation.

To find the most sensitive ATHLET thermal hydraulic model for IBLOCA scenario in PKL, a coupled methodology is developed. The basic sensitivity method – MSM has been introduced in this chapter.

3 ATHLET Simulation of PKL I2.2 IBLOCA benchmark

In this chapter, PKL I2.2 IBLOCA benchmark will be simulated by STH code ATHLET.

The issues related with benchmark simulation are divided into several parts:

1) Input deck preparation (section 3.1)
2) Steady state simulation (section 3.2)
3) Transient simulation (section 3.3)
4) The assessment of ATHLET on IBLOCA simulation (section 3.4)

At the end of this chapter, a summary will be made in section 3.5.

3.1 ATHLET Input deck preparation

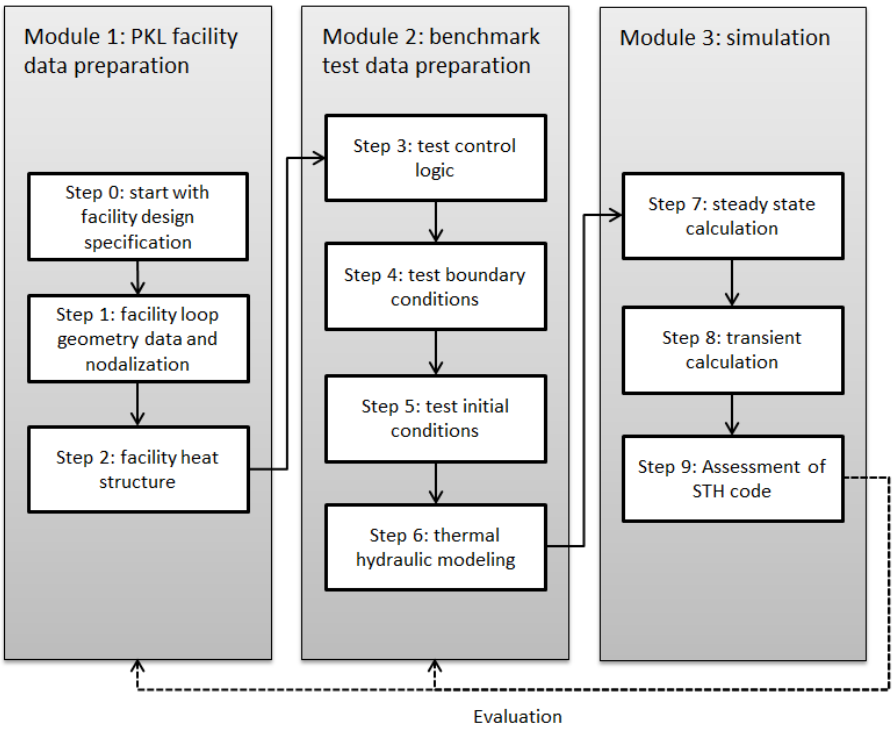

Figure 3.1: ATHLET modeling and simulation process of PKL I2.2 IBLOCA Benchmark test

Figure 3.1 gives the brief flow chart of ATHLET modeling and simulation process for PKL I2.2 IBLOCA benchmark. Module 1 (step 0-2) is the preliminary preparation for simulation - PKL facility

design data acquisition and processing. Module 2 (step 3-6) deals with the benchmark data (control logic, BCs, ICs, models), which are necessary inputs for calculation. The setting values of BCs and ICs for ATHLET calculation are nearly the same as their test values, as shown in the last section. Module 3 (step 7-9) comprises ATHLET simulation (steady state and transient calculations) and assessment of ATHLET on specified scenarios. The following part of this chapter will discuss all the steps, one by one.

The built-up input deck was based on the Framatome technical reports[102][103][104][105]. Since the ATHLET input deck preparations for three runs of I2.2 are similar - except for break size and ICs/BCs, the description of input deck in the following is only focused on run 1 test.

3.1.1 Geometry and primary nodalization

Before the calculation of benchmark, the geometry of PKL facility should be confirmed and a nodalization for its components should be done.

3.1.1.1 Geometry qualification

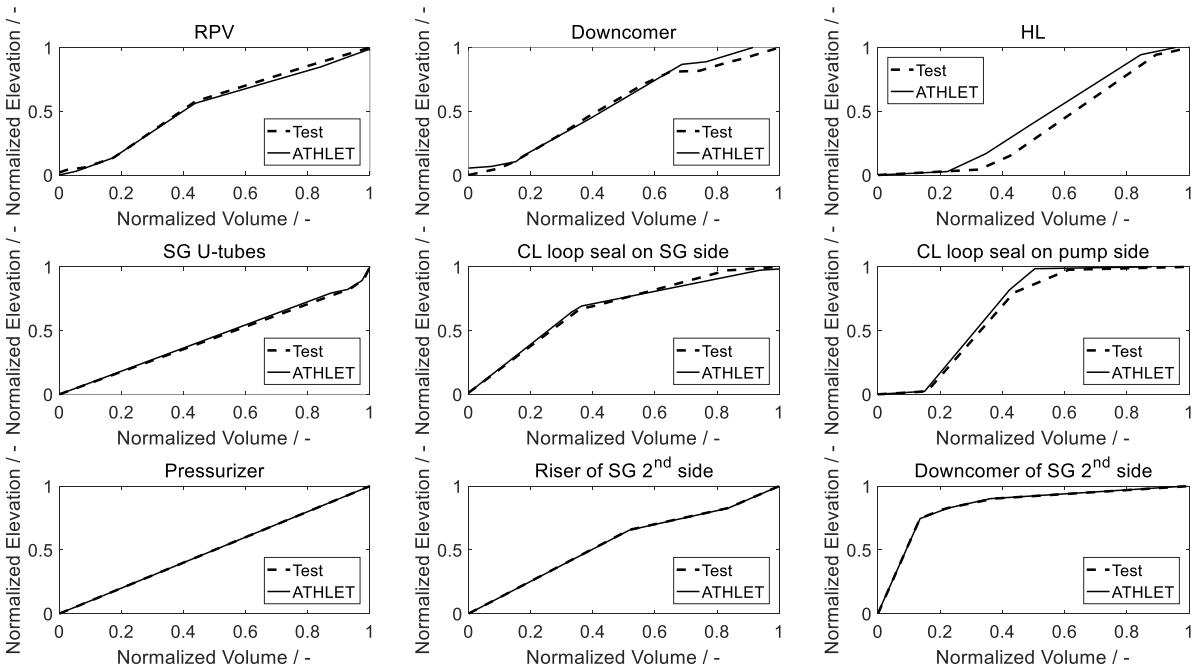

Figure 3.2: Volume vs. elevation (normalized values) in test and ATHLET input deck

As introduced in section 2.4, the assessment of the component volumes is a pre-requisite for calculation as well as for the interpretation of code results with regard to energy and mass balances. In Figure 3.2 the volume distributions as function of the elevation (normalized values) in each main component of the primary and secondary hydraulic sides are shown. According to the figures, qualitatively speaking, the calculated volume distributions are reasonable compared to the real ones.

Table 3.1 gives the component information and their assessment results of volume. The volume relative errors for some components (e.g. HL, loop seal, SG inlet and outlet plenums) are larger than 1%, but their volume fractional parameters are smaller than the criterion value of 0.2%, satisfying the criterion of component volume, since their fractions of total volume are not so large (smaller than 2%).

Table 3.1: Quantitative assessment of component volumes

Component	Fraction of total volume / %	Volume relative error / %	Volume fractional parameter / %
Core region	6.27	0.21	0.01
Cold leg (one loop)	0.46	-0.35	0.00
DC Annular	3.06	-0.40	-0.12
DC Pipes	8.83	-1.38	-0.12
Hot leg (one loop)	0.95	5.17	0.05
Lower plenum	4.10	-0.39	-0.02
Loop seal (one loop)	1.22	9.56	0.12
PRZ	15.53	-0.01	0.00
MCP (one loop)	0.24	1.62	0.00
Reflector gap	4.25	-0.14	-0.01
SG inlet plenum	1.93	-9.22	-0.18
SG outlet plenum	1.53	-8.22	-0.13
SG U-tubes (one loop)	4.74	0.00	0.00
Surge line	0.43	0.27	0.00
Upper head	3.73	0.25	0.01
Upper plenum	9.57	-1.52	-0.15

3.1.1.2 Primary nodalization

All of the fluid components in the pressure vessel, primary side and secondary side of loops, the break and safety injection systems have to be nodalized for simulation.

According to the design of PKL facility, the flow in the pressure vessel was simulated with pipes and branches for core channels, two downcomers, lower plenum, upper plenum and upper head. Three channels of core zones (inner part, middle part, outer part - related to the power distribution), the cross flows between them and the core bypass were modeled with the ATHLET pipe model. Each core zone was axially divided into several parts from inlet to outlet of the core. The cross flows were modeled by cross connect objects, as shown in Figure 3.3.

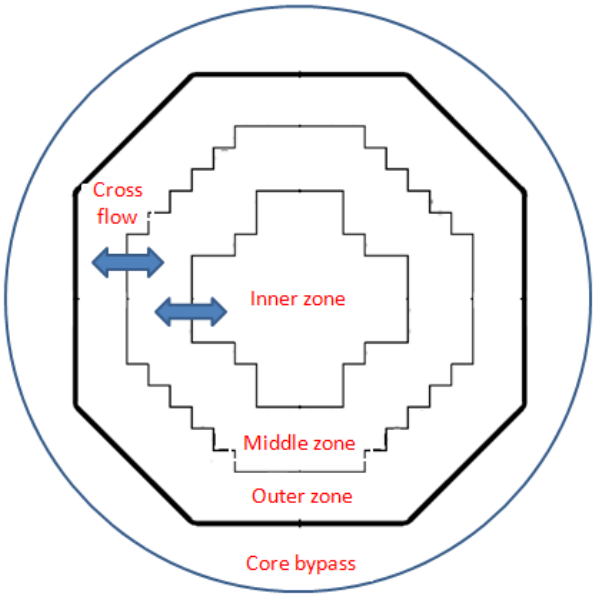

Figure 3.3: Top view of ATHLET core control volumes (CVs)

The coolant is separated into two ways at the inlet of the pressure vessel, most of the coolant flowing into the annular of the downcomer, and the rest (around 0.5%) flowing into the upper head. The flow split design of PKL facility was modeled in ATHLET with the branch type object.

The four loops of the primary coolant system were fully modeled. The U-tubes in each SG were divided into three groups, with different pipe lengths. The PRZ with surge line was on loop 2. The coolant systems of the 4 SGs' second sides, including the separators and the main stream line (MSL), were modeled in the simulation. HPSIs and LPSIs were considered by using the injection model and the ACCs as pipe models.

The system configuration of PKL facility is modeled just by connecting basic thermal fluid dynamic elements, called control volume objects (CVOs) and heat conduction objects (HCOs). To summarize, the PKL I2.2 IBLOCA simulation in ATHLET considered a total of 195 control volume objects and 33 heat conduction objects. The main objects are shown in Table 3.2.

Table 3.2 PKL main component control volumes for ATHLET simulation

CVO (control volume object), CV (control volume), HCO (heat conduction object) and HCV (heat conduction volume)

Component	Number of CVOs	Number of CVs	Number of HCOs	Number of HCVs
Core region	6	⩾12	6	⩾12
Cold leg (one loop)	1	5	0	0
DC Annular	22	22	0	0
DC Pipes	4	20	0	0
Hot leg (one loop)	1	7	0	0
Lower plenum	2	2	0	0
Loop seal (one loop)	2	11	0	0
PRZ	1	15	2	18
MCP (one loop)	1	2	0	0
Reflector gap	2	18	0	0
SG inlet plenum (one loop)	2	7	0	0
SG outlet plenum (one loop)	2	6	0	0
SG U-tubes (one loop)	3	⩾21	6	⩾24
Surge line	1	17	0	0
Upper head	1	1	1	1
Upper plenum	4	6	0	0

3.1.2 Heat Conduction

For the simulation of the temperature profile and the energy transport in solid materials, ATHLET provides a one-dimensional heat conduction model implemented in the module called HECU. In the simulation of the I2.2 benchmark, the following simplifications have been made:

1) The heat exchange between PKL facility and environment is considered as heat losses functions based on the experiment;
2) A melting process cannot be simulated.

There is no need to discuss all of the heat structures in PKL I2.2 IBLOCA benchmark simulation. Only two typical and most important heat structures (for core rod and SG U-tube respectively) and their relationship with CVs are given, as shown in Figure 3.4.

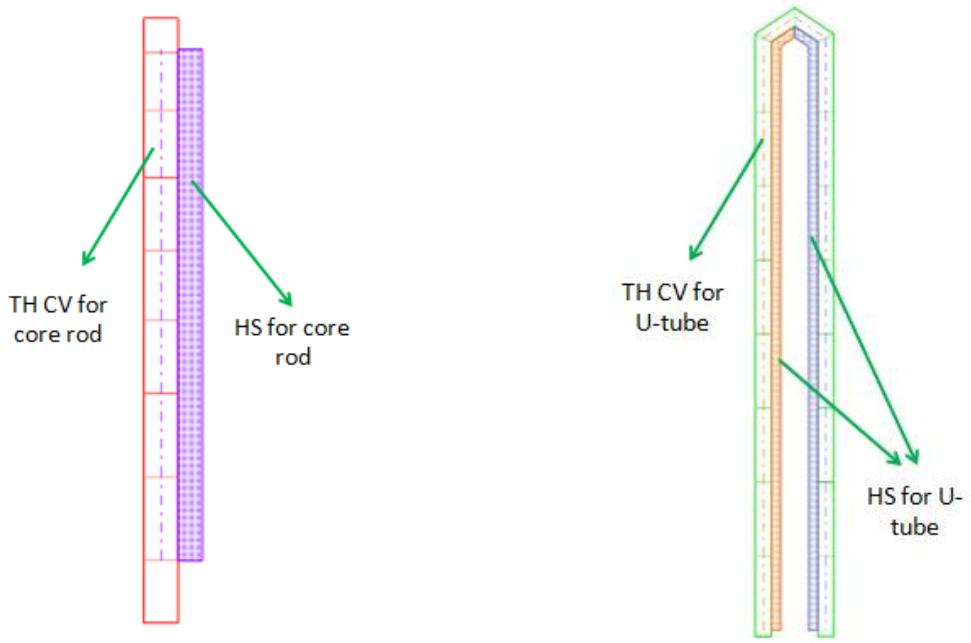

(a) Core rod (b) SG U-tube

Figure 3.4: ATHLET Model for core rod and SG U-tube

The different zones in the core contain different rods numbers and have different powers at the beginning, as shown in Table 3.3. During the transient, the power curve for each zone was given (see Figure 3.5).

Table 3.3: Description of different zones in core

Zone	Rod numbers	Total Power
Inner zone	63	398kW
Middle zone	118	728kW
Outer zone	133	839kW
Total	**314**	**1965kW**

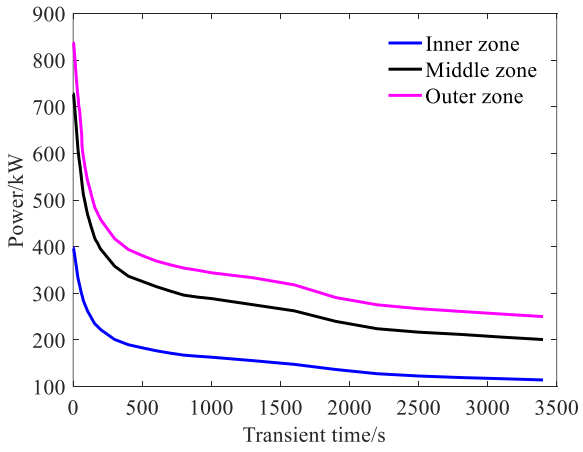

Figure 3.5: Powers for different zones in core

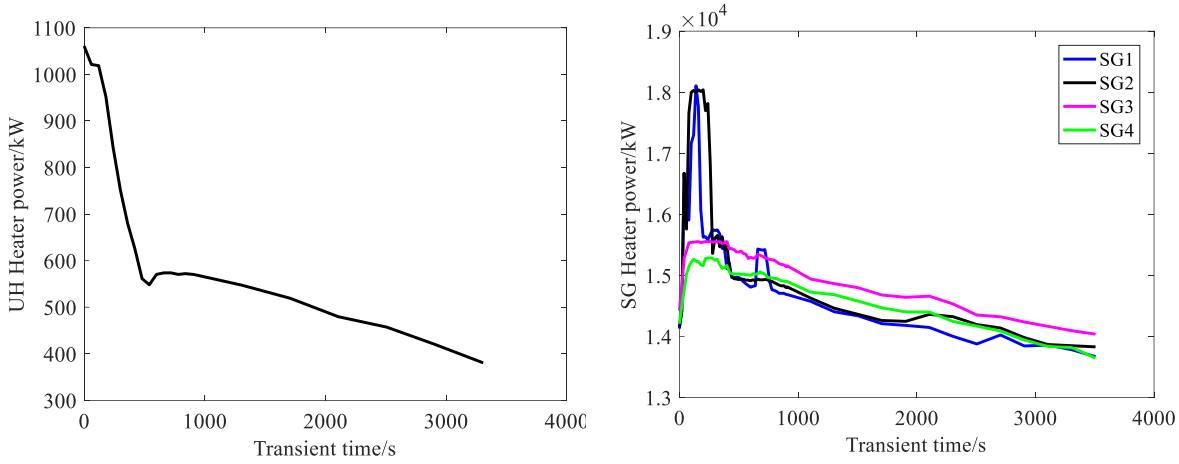

(a) Heater power in upper head (UH) (b) Heater Power in bypass of SG secondary side

Figure 3.6: Heaters for UH and SGs

Except for heat rods in core, there are also other three types of heaters in PKL which should be considered by ATHLET simulation.

1) In order to simulate the actual control instruments at the top of RPV, which could generate heat during operation and the accident scenario, a heater is set at the upper head (UH) of pressure vessel in the PKL facility. Its power is a function of time during the transient as shown in Figure 3.6 (a);
2) The heat loss in the secondary side of each SG side was also considered in the PKL facility. In each SG, it is compensated by a bypass heater at the bottom of SG in the secondary side. They were different from each other during the transient (see Figure 3.6 (b)).
3) There are two heaters in PRZ for bypass and supporting heating. But the support heating was not used in the I2.2 test. The bypass heater was closed at $t = 6$ s after the SOT.

3.1.3 Control signals and logic

Table 3.4: Control signals and logic

Control Signal	Type of trigger	Unit	Value	Remark
Water level in PRZ	Water level	m	8.27	SS
Water level in SG secondary side	Water level	m	11.8	SS
Start of steady state calculation	Time	s	-1500	-
SOT(break open and begin of core power decrease)	Time	s	0	-
Shut-off of PRZ heater	Time	s	6	-
Shut-off of feed water system	Time	s	11	-
Begin closure of MSL for SG 1	Time	s	10	-
Begin closure of MSL for SG 2	Time	s	20	-
Begin closure of MSL for SG 3	Time	s	30	-
Begin closure of MSL for SG 4	Time	s	40	-
Shut-down of all RCPs	Time	s	30	-
Closure of butterfly valves	Time	s	250	-
Start of HPSI	Pressure	bar	38.5	Pressure at UP
Start of ACC	Pressure	bar	13.8	ACC nitrogen Pressure
Start of LPSI	Pressure	bar	6.8	Pressure at UP

In ATHLET, the GCSM module is used to simulate the interconnected control signals in an accident scenario. A signal may be a process signal or a control signal which is a function of maximum four other different input signals. In the simulation of I2.2 IBLOCA benchmark, the following parameters were set using the GCSM module, as shown in Table 3.4. There were three types of signals in the benchmark to control the occurrence of typical events: transient time trigger, pressure trigger and water level trigger, respectively.

Signals for the water level in primary and secondary sides were set during the steady state calculation (during the transient, they were closed). The opening of the break marked the start of test (SOT) in the simulation. Simultaneously, the core power began to decrease. The heater of PRZ was closed at around $t = 6$ s. The SGs were closed on the main steam and feed-water sides approx. 10 s after SOT. In the simulation, the coast-down of the RCPs was started 30 s after SOT, the same as the set of test control. HPSI and LPSI were controlled by a pressure signal related with the upper plenum (UP). ACCs injection started when the pressure inside became larger than in the primary loop side.

3.1.4 Initial and Boundary Conditions (ICs/BCs)

Since in PKL facility the primary side pressure was limited to 5 MPa, a full pressure scaling of the complete transient was necessary to be able to reproduce the course of events as observed in the corresponding LSTF experiments. The steady state pressure for PKL I2.2 IBLOCA benchmark is around 4.6 MPa for all three runs. The reactor cooling system (RCS) was completely filled at start of test (SOT) and a symmetrical forced circulation existing in all 4 loops (pumps in operation).

The indicated values for ICs/BCs parameters could be found in Table 2.3.

3.1.5 Thermal hydraulic modeling

The six-equation two-fluid model (fully separated balance equations for liquid and vapor) was used in the primary system. Alternatively, the five-equation model (separate conservation equations for liquid and vapor mass and energy but a mixture momentum equation) together with mixture level calculation were applied in the pressurizer and in the secondary sides of the steam generators. Nitrogen from the ACC tanks has been simulated in the primary system.

Additionally, special models for pumps, valves, separators, critical flow etc. were also included in the benchmark simulation. In this section, the pump model and the critical flow model (CFM) were selected for introduction, since special attention was payed to them in IBLOCA experiment and simulation.

3.1.5.1 Critical flow model (CFM)

The mass flow is limited by the critical flow at the break location. Three different models are available in ATHLET:

1) The Homogeneous Equilibrium Model (HEM)
2) The Moody model
3) The CDR1D model [106]

The theory details of CFMs in ATHLET will be discussed in chapter 5. Here, only the usage of CFMs in PKL I2.2 IBLOCA benchmark simulation is focused on. Since only the CDR1D model considers the geometry information of the break pipe, it was selected for the PKL I2.2 IBLOCA benchmark simulation. It should be noted that no discharge coefficient (which is a modification multiplier for

CFMs) was set in the present work. The break pipeline was modeled up to the break valve and the break valve is fully opened at 5 s after SOT.

It should be noticed that in some cases the inherent capabilities of some two-fluid model are not fully exploited, and a separate special process model or correlation should be utilized. Critical flow is such an example. Although the integration of the two-fluid conservation equations may predict a choked condition, choking calculations in a component with a smooth area change could be done by using a sufficiently fine axial mesh during the occurrence of the critical conditions, being very time consuming[107]. Consequently, the early version of CDR1D model (early version, e.g. ATHLET 3.0[108]), as an auxiliary code for ATHLET, was used as tables in the ATHLET input deck, being executed and prepared separately before running ATHLET.

For PKL I2.2 IBLOCA benchmark test, the break pipeline is first oriented upwards, starting from the horizontal part of a clod leg (CL) downstream of the RCP in a loop without pressurizer, as shown Figure 3.7. Since the break valve is at around 7.6 m far away from the CL and the junction between the CL and break pipeline is a convergent – divergent throat, it is necessary to use the CDR1D model at both the throat and the break valve, as indicated in Figure 3.7. Critical flow may happen either at location 1 or at location 2.

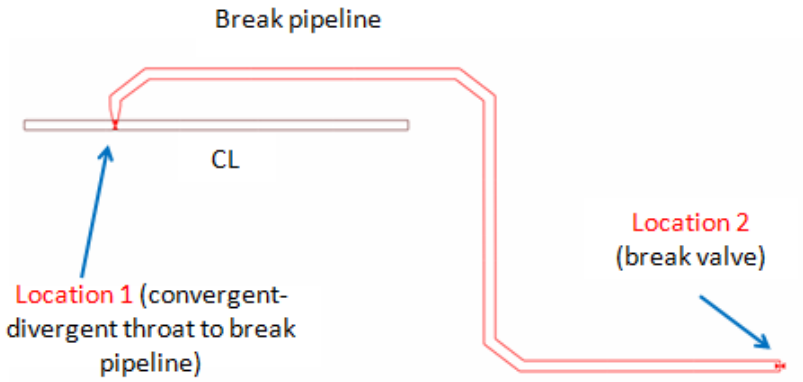

Figure 3.7: Locations for CDR1D model

3.1.5.2 Pump model

The pump model in ATHLET calculates the pump differential pressure (as a part of the momentum equation) and the pump power added to the fluid. In the benchmark, the signal for pump shutdown is at 30 s after SOT. Since the transient behavior of pump should be considered in the benchmark simulation and the pump speed in the transient is given (in Figure 3.8), both static pump model and dynamic pump model are suitable for the calculation. Some typical key parameters of pump model in the benchmark simulation are given in Table 3.5.

Table 3.5 Key parameters of pump model

Parameter	Unit	Value
Reference value of pump pressure differential	MPa	0.785
Rated pump speed	rpm	2830
Rated volumetric flow rate	m^3/s	0.0406
Rated pump head	m	98

It should be noticed that after the RCP closed down during the transient, it kept impacting the pressure loss of the loop because of the friction between pump and fluid. In order to simulate the friction loss, a

butterfly-valve was set at the loop seal, just below the pump, in each loop. The butterfly-valve area became smaller after the pump closed down.

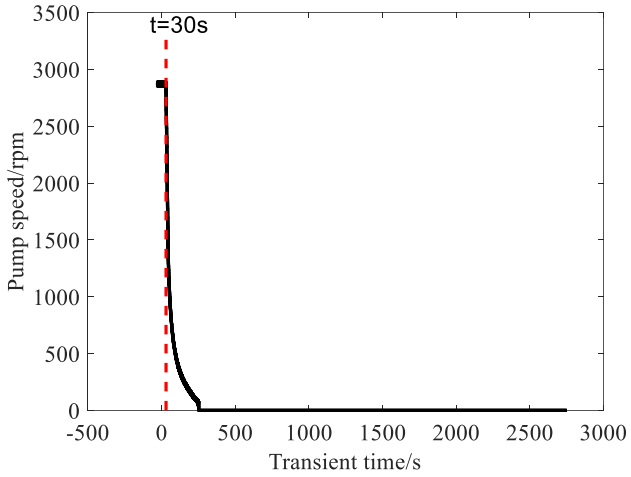

Figure 3.8: Pump speed during transient

3.2 Steady state simulation and results

It is similar to the stable operation conditions (pressure, temperatures, et al.) before the transient in the experiment; the steady state simulation was performed to confirm the ICs/BCs of test scenario before the transient calculation. In this section, two issues related to steady state simulation are introduced: (1) results of steady state calculation for benchmark to validate the steady state; (2) qualification of steady state calculation.

3.2.1 Results of steady state calculation

The steady state calculation was performed 1500 s before the transient (0 s is the SOT, consequently the steady state started at – 1500 s). Some important parameters were selected here for discussion.

The pressure of the primary loop is controlled by a constant pressure CV connected with the PRZ and a water level control signal of PRZ which keeps the PRZ water level at a specified value. In order to simplify the input, all of CVs on the primary side were set at the same pressure at the beginning of the steady state calculation. With the ongoing steady state calculation, all CVs go to their “real” values. Figure 3.9 shows the pressure at the top of PRZ (a representative pressure for primary side). It reaches a constant value quickly, only after few seconds.

All temperatures on the primary side were set at the same value at the beginning. With the generation of heat by core rods and other heaters, the heat losses to the surrounding, the heat transfer from the primary side to the secondary side in the loops, the energy balances in primary side and secondary side were achieved during the steady state calculation. Figure 3.10 shows the steady state temperatures results of core inlet and outlet. The difference between them was about 5.5℃.

The velocities of all CVs in primary loop were set 0 at the beginning. With the operation of pump in each loop, the mass flows in loops increase to the indicated values. Figure 3.11 shows the mass flow of CL (loop 1).

Based on the steady state results above, one may conclude that the steady state is achieved and maintained before transient.

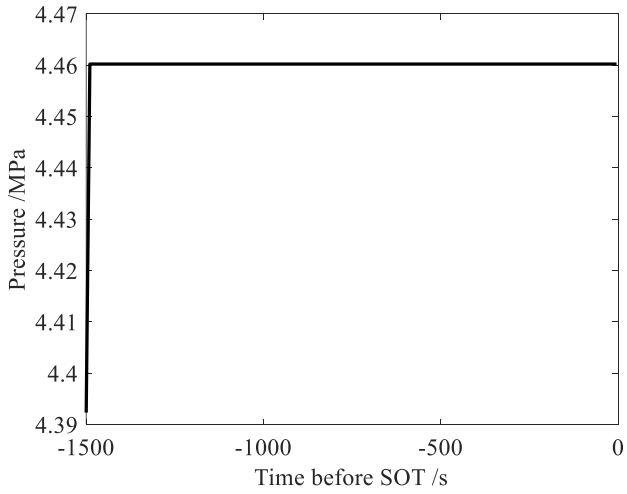

Figure 3.9: Pressure of PRZ (steady state calculation)

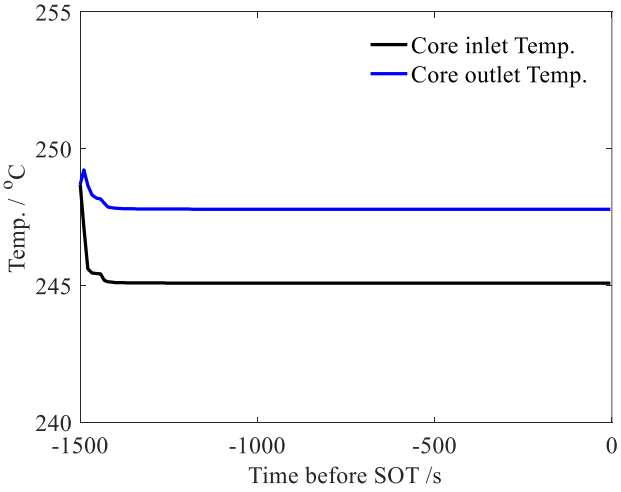

Figure 3.10: Temperatures of core inlet and outlet (steady state calculation)

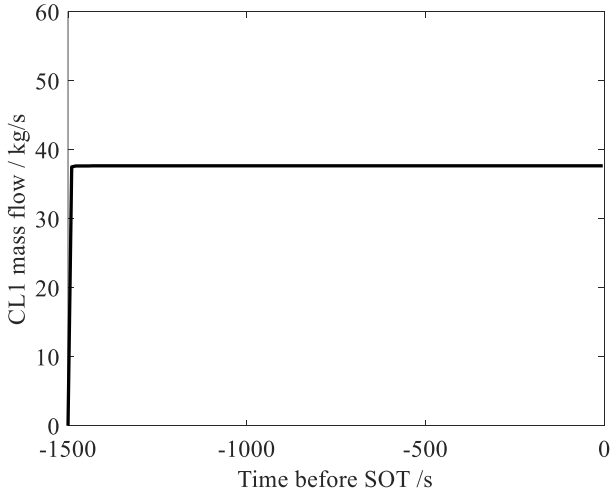

Figure 3.11: CL mass flow (steady state calculation)

3.2.2 Qualification of steady state calculation

The initial steady state conditions of the PKL I2.2 IBLOCA benchmark and the results from the simulation have to be compared to confirm the proper reproducibility of the ICs and BCs of the test, before starting the transient calculation. The FFTBM was employed to qualify ATHLET for the simulation of the IBLOCA scenario, steady state but also transient calculations (in section 3.3).

Table 3.6 presents some relevant quantities for evaluating the ICs and BCs, which indicates good reproducibility by simulation.

Table 3.6: Key parameters for ICs / BCs

ICs / BCs	Unit	Run 1 test	ATHLET	Error / %
Decay power	kW	1965	1965	0.00
Primary pressure at UP	MPa	4.55	4.56	-0.22
PRZ pressure	MPa	4.467	4.460	0.158
MSL pressure	MPa	3.48~3.5	3.5	-0.57~0.00
Coolant inventory in primary loop	kg	2450	2437	0.53
Pressurizer Inventory	kg	523.6	521.2	-0.46
ACC level	m	1.847	1.880	1.79
Upper head temperature	K	517.778	518.220	0.085
DC bottom temperature	K	518.856	518.240	0.119
RPV inlet temperatures	K	518.072	518.240	0.032
DC middle temperature	K	518.435	518.240	0.038
Rod K2 ME 6 temperature	K	521.902	521.860	0.008
Rod K10 ME 6 temperature	K	522.750	521.860	0.170
Rod L13 ME 7 temperature	K	525.173	521.860	0.631
Pressurizer level	m	8.300	8.269	0.370
Core level	m	6.193	6.077	1.879
Loop seal (SG side) level	m	6.256	6.290	0.541
Loop seal (MCP side) level	m	2.778	2.730	1.736
CL mass flow	kg/s	37.973	37.672	0.792

It should be noted here that a parameter was considered significant when it is of major relevance in determining the plant behavior and can be reliably measured. It was found that all the significant parameters are reproduced with acceptable error and satisfy the steady state criterion for nodalization assessment.

Furthermore, during the steady state assessment, the pressure drop in the primary loop should also be discussed since it is an important item for the reproducibility of test scenario. In ATHLET, the flow friction coefficients that are originally calculated through a wall friction model were tuned to achieve the corresponding pressure drops. The friction form loss of valves was set as an empirical value (provided by Framatome **[109]** **)** according to the pressure drop of the facility. It should be noted here that the pressure drop in the test had to be extrapolated according to the mass flow from range [0.5, 25] to 39.

Table 3.7 provides a comparison of the test and ATHLET calculated pressure drops along the primary system. The pressure drop differences between ATHLET and PKL measurements are quite small, except those of the lower and upper plenum, larger than 10%. They were considered as acceptable, compared also with the results of other benchmark participants **[110]**.

Table 3.7: Experimental and calculated pressure drops (in kPa)

Primary side section	Run 1 test	ATHLET	Error / %
Cold leg	15.8	14.3	-9.5
Downcomer vessel	41.2	41.0	0.5
Lower plenum	47.6	56.4	18.5
Core	90.3	89.8	0.5
Upper Plenum	27.3	35.7	30.7
Steam Generator	202.7	217.3	7.2
Loop seal	138.1	138.3	0.15
Butterfly valve	32.6	33.9	3.9
Total	**595.6**	**626.7**	**5.2**

3.3 Transient Simulation

This section is concentrated on transient simulation. According to the literature and my own experience, different nodalizations could come to the same steady state results but may cause large differences for the transient calculation. This means that, before the formal transient calculation, a sensitivity study should be done for some different detailed nodalizations, since the steady state calculation can only confirm the acceptance of primary nodalization. After the nodalization qualification, the results of transient simulation will be given in this section.

3.3.1 Transient nodalization qualification

The transient nodalization qualification phase is also called final qualification and demonstrates that typical transient phenomena are correctly reproduced by the calculation.

Based on the description of transient qualification in section 2.5, the nodalization of some significant components should be refined to show their sensitivity. According to the literature (Saghafi, 2016), the nodalization of the core region and steam generator (SG) U-tubes impacts the transient significantly. Therefore, 6 sensitivity cases, with different numbers of control volumes (CVs) and heat conduction volumes (HCVs) in the core region and SG U-tubes, as shown in Table 3.8, were chosen for the convergence analysis of the nodalization (also considering the calculation efficiency); the most reasonable one to be decided as the final nodalization. The number of CVs in the core region could be 2, 5 or 7. Similarly, the nodalization in SG U-tubes could be 5, 10 or 20 CVs. The numbers of HCVs were set the same or twice the number of CVs in each region.

Table 3.8: Number of control volumes and heat structures for refined cases

Case No.	Number of CVs in each core object	Number of HCVs in each core object	Number of Ave. CVs in each SG U-tube	Number of Ave. HCVs in each SG U-tube
1.	2	2	5	5
2.	2	4	5	10
3.	5	5	10	10
4.	5	10	10	20
5.	7	7	5	10
6.	7	14	20	20

As introduced in section 2.5, a suitable case with refined nodalization should be chosen as the calibration case for FFTBM, which is used for convergence analysis quantitatively. In this study, case 6 was chosen as calibration case. The considered time interval for the transient calculation was [0 s, 1000 s].

The results of the quantitative convergence assessment of ATHLET calculation on the transient I2.2 IBLOCA benchmark run 1 - using different refined nodalizations - are shown in Figure 3.12. According to the transient results, all of the cases have the same steady state results. This means the option B is chosen in Figure 2.6 since different refined nodalizations have the same steady state results. According to the *AA* values from Figure 3.12, the refined nodalization cases 3 to 6 could get smaller *AA* values than case 1 and 2. Furthermore, their results were at the same level comparing with case 6. In other words, nodalizations of case 3-6 were closer to convergence but case 1 and 2 did not.

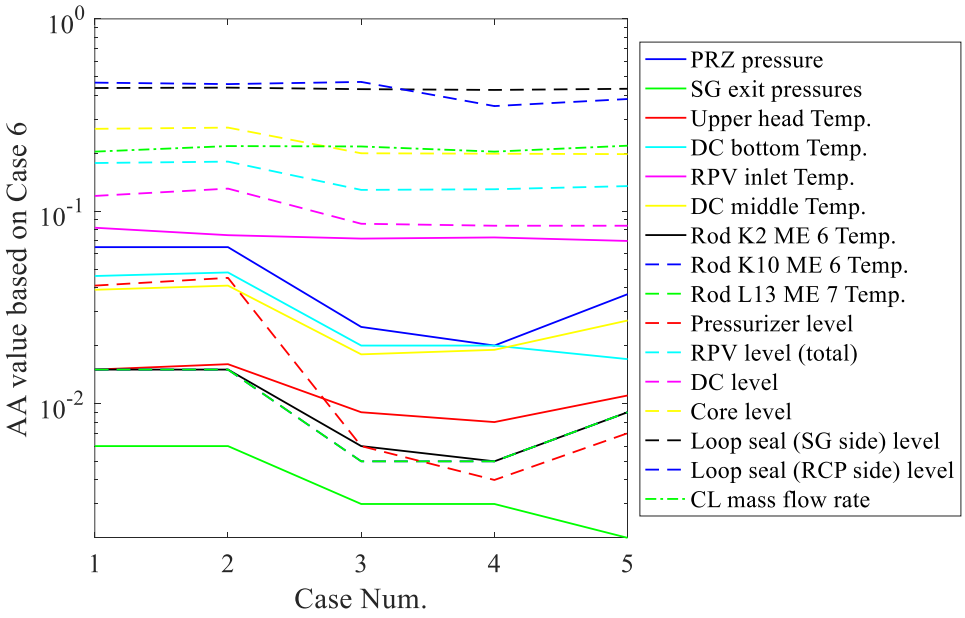

Figure 3.12: *AA* values of significant parameters for different cases

Table 3.9: CPU time of calculation for refined nodalization cases

Case No.	**1**	**2**	**3**	**4**	**5**	**6**
CPU time of calculation	35h14min	40h15min	52h1min	73h1min	67h7min	85h25min

On the other hand, a suitable nodalization also means high efficiency for calculation. In order to choose a suitable nodalization, the CPU time for each case were compared in Table 3.9. According to the table, the CPU time changes significantly even if only a small part of the nodalization changes. Case 3 with 5 CVs in each core object and 10 CVs in each SG U-tube is the most suitable case of nodalization.

Based on the nodalization qualification discussion for component volume, steady state and transient calculations, the modeling of geometry and nodalization for PKL I2.2 IBLOCA benchmark scenario has been developed, as shown in Figure 3.13. There is only one SG loop shown in the figure and “X4” stands for the 4 different loops in the PKL facility.

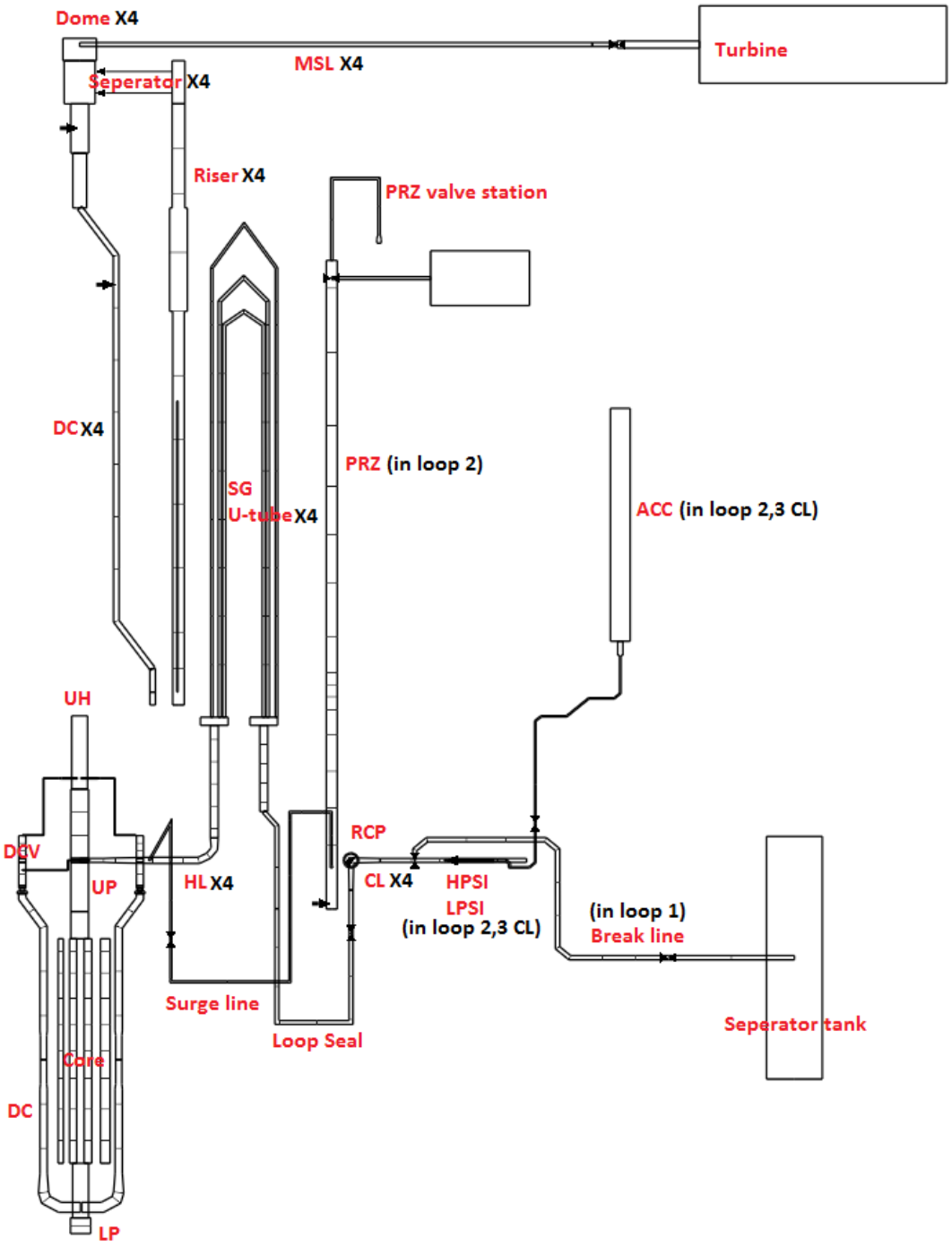

Figure 3.13: KIT final version of ATHLET nodalization

3.3.2 Selected Trends of PKL I2.2 IBLOCA benchmark scenario

The transient results of the ATHLET simulations will be presented and discussed in comparison with their measured (test) behaviors. The transient time [0 s, 2400 s] is considered since most of the injection and thermal hydraulic phenomena take place during this period. The significant events of the benchmark test are compared with the results of ATHLET simulation, as shown in Table 3.10 [111]. The discussion on these parameters will be made in next section, with the help of transient curves of the parameters. It should be noted that there was a core heat up process in the test from 103 s to 133 s. But ATHLET did not reproduce this phenomenon. Only the most significant parameters were selected here for discussion. For more information, the appendix A could be resorted to.

Table 3.10: Sequence of events

Event	Test	ATHLET
SOT	0	0
Close of PRZ heater	6	6
Start of HPSI	70	13
End of flow in loop 1	92	131
End of flow in loop 2	93	120
End of flow in loop 3	86	101
End of flow in loop 4	89	124
Start of core heat up	103	-
PCT	133	-
Loop seal clearing (LSC) in loop 1	193	120
Loop seal clearing (LSC) in loop 2	172	139
Loop seal clearing (LSC) in loop 3	179	153
Loop seal clearing (LSC) in loop 4	194	148
Minimum of core water level	120	348
Coast down of RCP	245	245
Start of ACC	410	318
Start of LPSI	2526	1828

Figure 3.14 displays the break mass flow. Figure 3.15 shows the primary side pressure and secondary side pressure. The break mass flow is one of the most relevant phenomena occurring in the present scenario. The discharge of coolant has strong impact on the pressure and, accordingly, on the general evolution of the system. The break mass flow is affected by several phenomena, especially by the critical flow (also called choked flow).

According to Figure 3.14, the calculated break mass flow approaches the test, with some slight underestimation at the beginning of the transient. The mass flow bulge around 450 s is related to the ACC injection and bypass flow of DC. When ACCs start to inject into the cold leg because of the pressure set point, the injection fluid is planned to go through the DC and then to the core. But in the ATHLET simulation, some of the injection flow at DC vessel (DCV) goes to the break. This phenomenon did not take place in test.

As shown by Figure 3.15, the evolution of the primary pressure can be reproduced quite well until ACC start-up. After that, the calculated and test pressures have the same trend, with the calculated one being slightly smaller because of the bypass of the ACC injection water into the DC vessel.

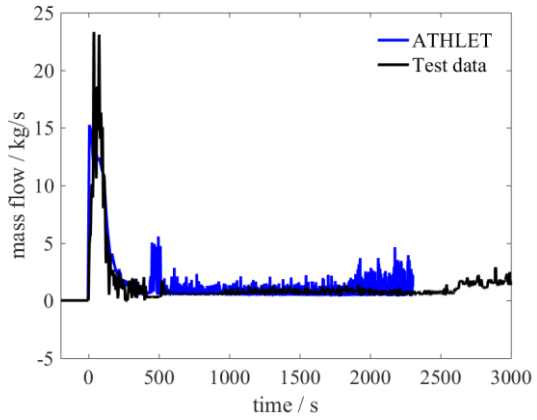

Figure 3.14: Break mass flows

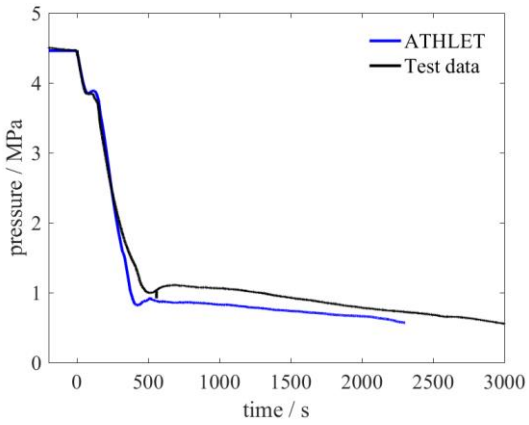

Figure 3.15: Primary side pressures

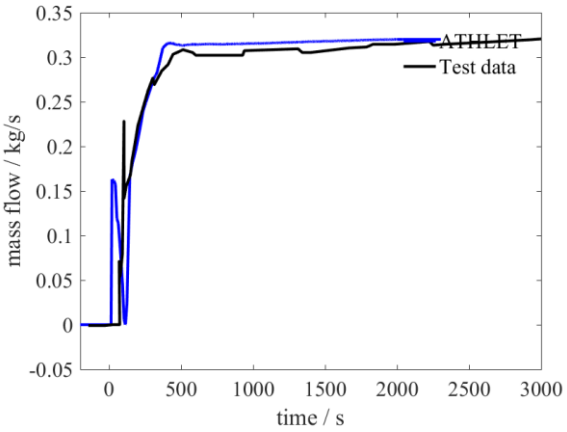

Figure 3.16: HPSI mass flows

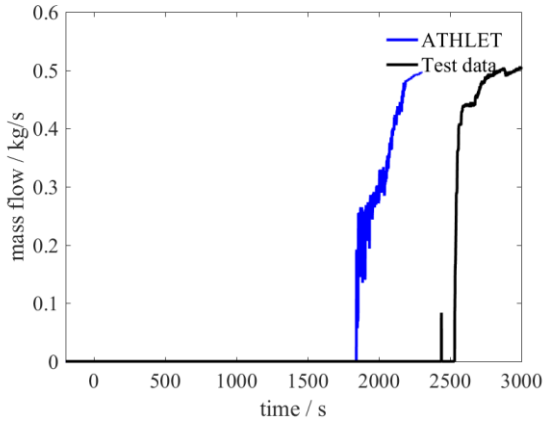

Figure 3.17: LPSI mass flows

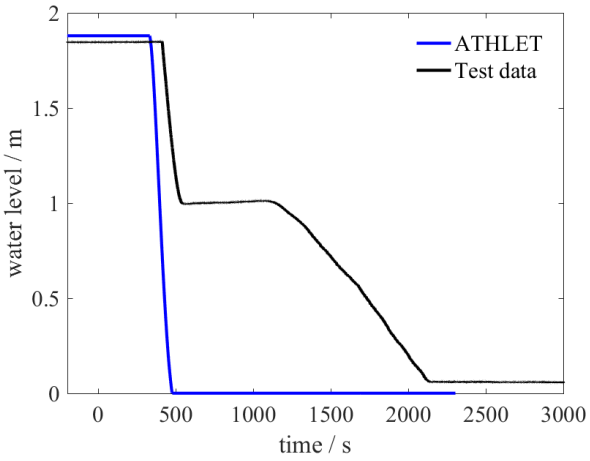

Figure 3.18: ACC water levels

Figure 3.16 shows the HPSI total injection which was started by a UP pressure signal. The experimental flow dependence was provided as a function of the primary pressure; therefore, if the pressure was correctly simulated, the HPSI should also be in accordance with the experiment. It shows that the HPSI injection evolution may be reproduced quite well but a little earlier than the test, since the HPSI was started at around 70 s in test. LPSI started much later than HPSI since the set point value for its pressure signal is lower. The comparison of LPSI (in Figure 3.17) has a similar situation as HPSI, happening earlier than in test.

When accumulator water is injected into the system, cold water may reach the core inducing a high amount of vaporization. The expansion of the steam phase may lead to an increase of the primary side pressure if the break is not large enough to mitigate this expansion. This phenomenon is captured in both test and simulation, as shown by Figure 3.15. If the primary side pressure increases, the ACC injection may be interrupted, ensuring a reduction of the vaporization and a subsequent pressure reduction will follow. Consequently, the ACC water level is very sensitive to the primary side pressure, as shown by Figure 3.18. Even a small pressure difference would decide the triggering of the ACCs injection.

In Figure 3.19 the collapsed water levels in the RPV show a good agreement, with a difference in the range of 0.3 m after 500 s. There are two things worth to be detailed. One is that the initial water levels are not equivalent because of the quite approximate geometry and contradictory data in the test reports. The other is that the timings were switched for the lowest RPV water level and the second lowest RPV

water level. The reasons for the inconsistence are the lower break mass flow at the beginning and the bypass of the ACC injection.

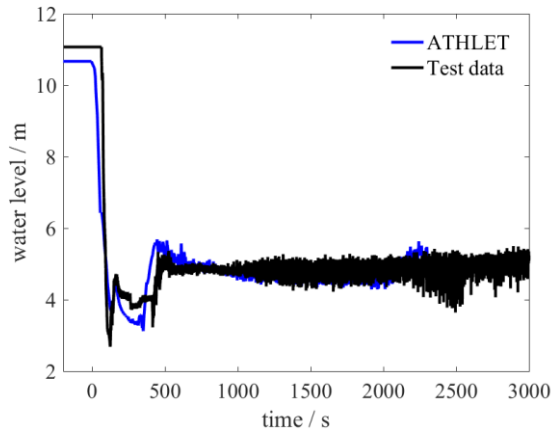

Figure 3.19: RPV collapsed water levels

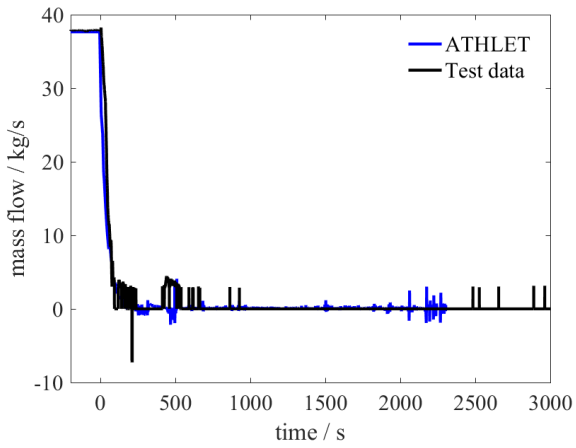

Figure 3.20: CL 1 mass flow rates

Figure 3.20 shows the mass flows in loop 1. Due to the considerable size of the break, the circulation in the loops ceases at about 83 seconds. At this moment in time, the RCPs coast down is still not finished; therefore, during these first 83 seconds, the circulation is a combination of forced circulation and natural circulation. This phenomenon is predicted remarkably well by ATHLET.

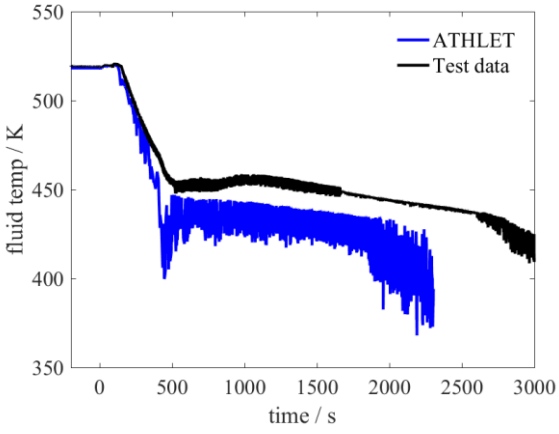

Figure 3.21: Core inlet temperatures

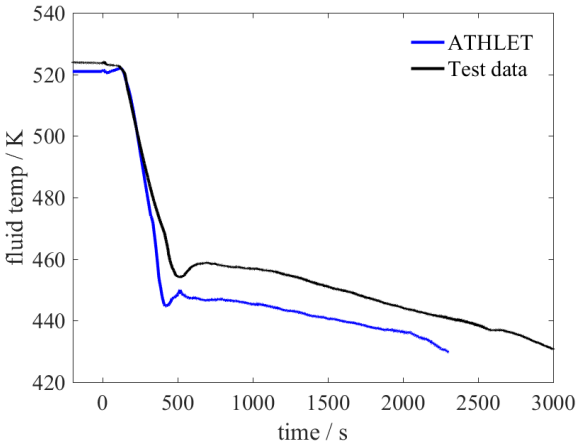

Figure 3.22: core exit temperatures (CET)

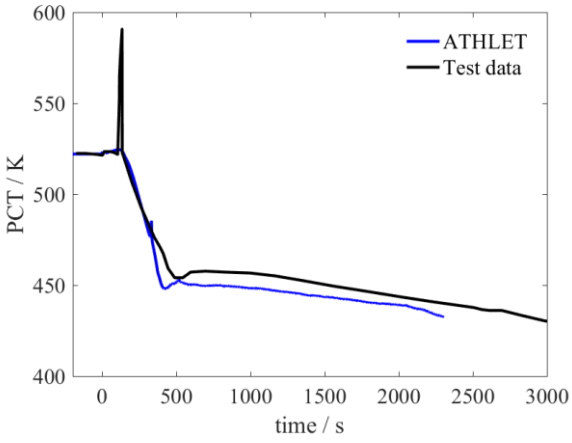

Figure 3.23: PCTs

Figure 3.21 and Figure 3.22 show the transient core inlet temperatures and core exit temperatures (CET) while Figure 3.23 shows the transient peak cladding temperatures (PCT). The calculated profiles are acceptable but the core heat up scenario is not reproduced by the ATHLET simulation. It is not a coincidence that the heat-up and the lowest RPV collapsed water level happen nearly at the same time. Both of them are impacted by the under-predicted break discharge flow rate.

The comparisons above were mainly concentrated on the transient trends of the crucial parameters. Although one may come out with a primary conclusion that ATHLET may predict such an IBLOCA scenario with reasonable results, the quantitative assessment introduced next would be more convincing in this respect.

3.4 Assessment of ATHLET simulation

The results of the quantitative assessment of ATHLET calculation on the transient I2.2 IBLOCA benchmark run 1 (at the test facility PKL) are shown in Table 3.11. According to the AA values, most of the variables are predicted very well by ATHLET, others (e.g. RPV level, HPSI mass flow, ACC level and CL 1 mass flow) are reproduced well and break mass flow poorly.

Table 3.11: Results obtained from FFTBM applied on PKL I2.2 IBLOCA benchmark run 1 calculation.

Parameters	AA values
PRZ pressure	0.083
SG-1 MSL pressure	0.126
Core inlet temperature	0.26
Core exit temperature	0.025
Maximum PCT	0.072
Pressurizer level	0.196
RPV level	0.398
Break mass flow	0.73
Integrated break mass	0.159
HPSI mass flow	0.378
ACC level	0.344
CL 1 mass flow	0.412
$\boldsymbol{AA_{tot}}$	0.1082

It has to be noticed here that if we recall the results from Figure 3.14 and Figure 3.20, the calculated mass flows almost coincide with the experimental ones, apparently better than given by the assessment estimators from Table 3.13. The reason is that, after 500 s, all the mass flow values are very small but with strong oscillations. The oscillations are really accounted for in the FFTBM; therefore, the corresponding AA estimators take large values.

Larger AA for mass flows and water levels may have as source the poorly predicted break mass flow, aspect to be addressed in a further study. The total AA is 0.1082, well below the acceptability limit of 0.4 [112][113]. One may conclude that IBLOCA scenario was reproduced well by ATHLET, up to some aspects (especially the break mass flow) still to be checked further.

3.5 Summary

The main steps for ATHLET input deck preparation and the simulation results (including steady state and transient) were described in details in this chapter. In order to make the results convinced, the related state-of-art methodology was used stepwise.

Firstly, the geometries of the PKL facility and that one implemented in ATHLET were quantitatively compared. The difference between them was acceptable based on the volume criterion. Subsequently, a primary nodalization for ATHLET simulation was made. In the steady state calculation, the primary nodalization was confirmed since the PKL ICs/BCs and the significant measured parameters of the stable condition before SOT were reproduced during this period.

In this chapter, a transient nodalization qualification method which was introduced in 2.5 was used and described step by step. After this procedure, it has been proved that my final nodalization in ATHLET was convergent, developed with necessary geometrical fidelity and reproducibility of the involved phenomena.

Based on the analysis of the transient results and the FFTBM results, one may come to the conclusion that most of the variables in PKL I2.2 IBLOCA benchmark were predicted very well by ATHLET, which confirmed its effectiveness on IBLOCA simulation.

But the PCT was not reproduced in the simulation. According to the AA values in FFTBM method, this is most likely related with the break mass flow simulation. In order to find the most influential model for the simulation, a sensitivity study for the thermal hydraulic models was performed, which will be introduced in the next chapter.

4 Sensitivity Analysis for Thermal Hydraulic Models

The previous chapter shows that the ATHLET code with existing models can simulate the IBLOCA scenario well compared with test data, except for the core heat-up phenomenon and PCT values, since these phenomena are found very sensitive to break size and safety injection operation in IBLOCA scenario. This study aims at finding the most sensitive model, which is responsible for the discrepancy between the ATHLET simulation and test data, and then modifying and improving the model in ATHLET. In order to identify the most sensitive model, sensitivity study is resorted to in this chapter. This is a precondition for the model modification.

In this chapter, a new method, called FFTBM-MSM two-layer sensitivity analysis, will be introduced in section 4.1. Then it will be applied in the sensitivity study of ATHLET simulation on the PKL I2.2 IBLOCA benchmark. Following the flow chart of the new method, the procedure of selection for sensitive input parameters and responses for sensitivity analysis will be given in section 4.2. In section 4.3, the results of sensitivity of the selected input parameters are described. Based on the results of FFTBM, a qualitative conclusion about the sensitive parameters could be given. In order to evaluate the sensitivities of these parameters quantitatively, MSM, coupled with FFTBM, is used in section 4.4.

4.1 FFTBM-MSM Two-Layer Sensitivity Analysis Method

A new method, which combines the FFTBM and Morris screening method (MSM), will be developed in this chapter to analyze the sensitivity of the thermal hydraulic parameters. Since FFTBM and MSM have already been described in section 2.4 and section 2.6, only the coupling mechanics of FFTBM-MSM are introduced here.

The structure of FFTBM-MSM two-layer sensitivity analysis method is shown in Figure 4.1. Since the transient time series (both measured test data and simulation results) are different to quantify and compare, in the first layer FFTBM is used to switch the time domain data into frequency domain data AA, in which the discrepancy between experiment and simulation could be quantified in an easier manner. According to the MSM methodology, after several percentage adjustments of the model parameters, the Morris coefficient S can be calculated for sensitivity analysis and model evaluation. The advantage of the two-layer method is that it combines the classical STH code evaluation method FFTBM with sensitivity analysis method and makes the sensitivity study more comprehensive.

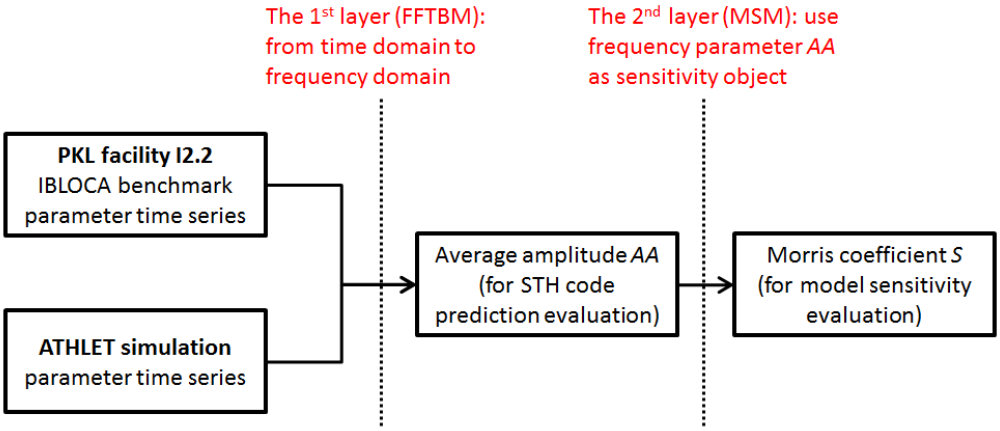

Figure 4.1: Structure of FFTBM-MSM two-layer sensitivity analysis method

This section will focus on the sensitivity analysis following the flow chart in Figure 4.2. A brief explanation to this flow chart is provided here.

Step 1 (selection of input parameters): based on the thermal-hydraulic phenomenon in LBLOCA, experience and results of previous sensitivity analysis, choose the several sensitivity parameters to be varied.

Step 2 (selection of the responses): the selected responses have strong relationship with nuclear safety. The selection depends on the safety criteria and important aspects which are derived from them.

Step 3 (sensitivity calculation with parameter variation): according to Morris screening method, several percentage variations for each parameter should be chosen and then use ATHLET to get the transient results. It should be noted that the parameter variations should be done one by one.

Step 4 (use FFTBM to calculate the average amplitude (*AA*)): use Eq. (2.4) to calculate the average amplitude for each response. Eq. (2.5) is used if the comprehensive sensitivity of some input parameters is of interest.

Step 5 (evaluate STH code predictions): using the results of step 4, not only the accuracy of ATHLET simulation (using the criteria at the end of section 2.4) but also the adaptabilities of the input parameters and responses as well as the amplitude of percentage variations for the sensitivity analysis could be evaluated. If the results do not show enough sensitivity, the parameters from step 1 to step 3 may be changed.

Step 6 (use MSM to calculate the Morris coefficient (*S*)): after the first 5 steps, the transient results which were in time domain were changed to the frequency domain, being much easier to use not only for prediction capability evaluation but also for sensitivity analysis. Let *AA* be the concerned output parameter of Eq. (2.11), and then use this formula to calculate the Morris coefficient.

Step 7 (model evaluation): based on the results of sensitivity analysis in step 6, the model sensitivity could be evaluated. If some parameters were ignored in the former evaluation, the procedure in the flow chart could be repeated again.

The new developed FFTBM-MSM two-layer method will be explained in detail using the PKL I2.2 IBLOCA benchmark sensitivity analysis as an example.

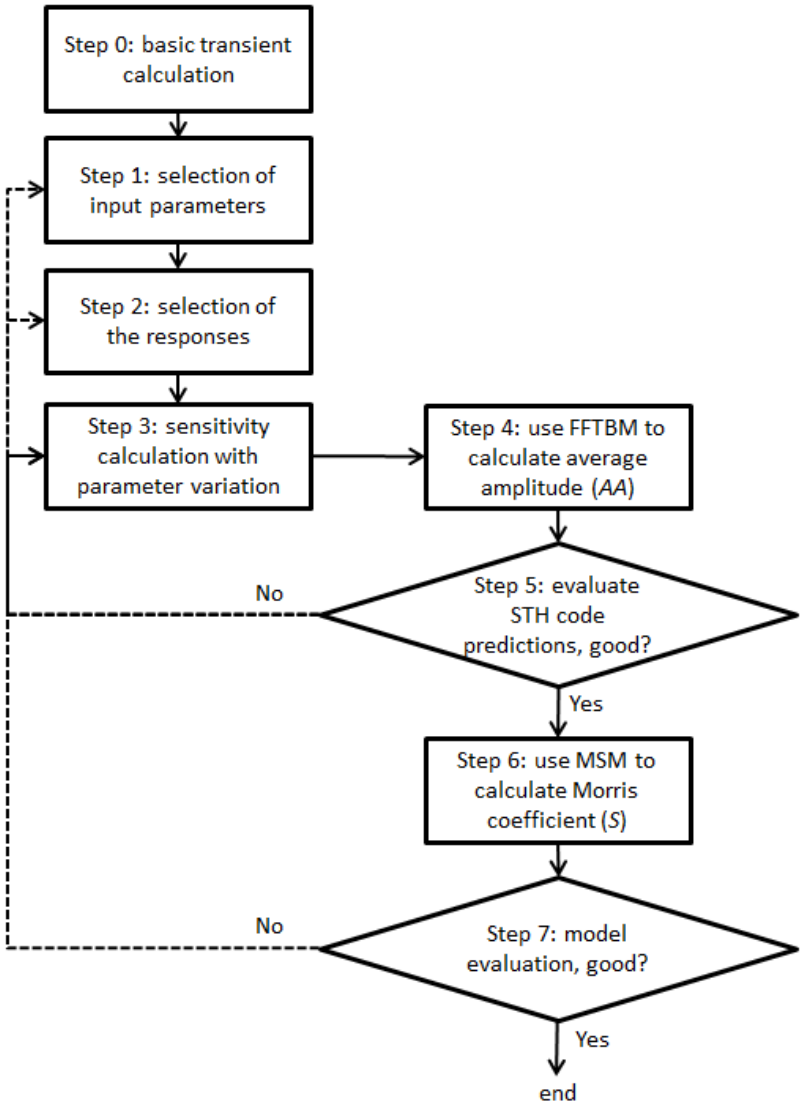

Figure 4.2: Flow chart of FFTBM-MSM two-layer method for sensitivity analysis

4.2 Selection of sensitive input parameters and system responses

The sensitivity study included sensitive input parameters and responses. For each case of calculation, one input parameter with a specified percentage change is considered in the ATHLET related module. The change will lead to the variation of simulation results. MSM is used on system responses to deliver quantitative sensitivity estimations.

(1) Selection of sensitive input parameters

This analysis is focused on the physical models involved in the prediction of the core heat-up behavior, which is a significant aspect of IBLOCA scenarios[114]. Initially, all the parameters in the uncertainty model of ATHLET called "MODELUNC", which is developed for uncertainty and sensitivity analyses for physical models and also used for corresponding code SUSA[115], were considered as potential input parameters. In this module, 29 input parameters are classified into 5 groups, as shown in Table 4.1. Furthermore, an input parameter OTURB, which allows (formally) the variation of the critical flow model parameter TURB (turbulence factor which is taken into account for the calculation of evaporation in critical flow model), is also considered in the Table 4.1.

Table 4.1: Sensitivity / Uncertainty parameters in ATHLET; in red: finally selected parameters

Group	Parameter	Interpretation	Preliminary selection	Final selection
Heating surfaces (HTC: heat transfer coefficient)	OHWFC	HTC for forced convection to liquid water	Yes	Yes
	OHWNC	HTC for natural convection to liquid	No	No
	OHWNB	HTC for nucleate boiling	Yes	Yes
	OHWFB	HTC for film boiling	Yes	No
	OHWPB	HTC for pool boiling	No	No
	OHVFC	HTC for forced convection to vapor	Yes	No
	OTMFB	HTC for minimum film boiling and maximum rewetting temperature	No	No
	OTRNB	HTC for critical heat flux	Yes	No
	OMCON	Condensation rate	No	No
Wall shear	OFI2H	Two-phase multiplier for horizontal junctions	Yes	No
	OFI2V	Two-phase multiplier for vertical junctions	Yes	Yes
	OFRIC	Wall shear distribution liquid – vapor	No	No
	OENBU	1M and 2M model	Yes	No
	OADDI	Evaporation rate at low pressure	No	No
Drift	ODANU	Rel. velocity in annulus	Yes	No
	ODBUN	Rel. velocity in bundle	Yes	No
	ODHPI	Rel. velocity in horizontal pipe	Yes	Yes
	ODHCC	Rel. velocity in horizontal cross−connection	No	No
	ODVPI	Rel. velocity in vertical pipe	Yes	Yes
Interfacial drag	OIHST	Horizontal flow: interfacial drag at stratified flow	Yes	Yes
	OIHSB	Horizontal flow: interfacial drag at intermittent flow	Yes	No
	OIHDI	Horizontal flow: interfacial drag at dispersed flow	Yes	Yes
	OIHT1	Horizontal flow: critical velocity for stratified – intermittent flow transition	Yes	Yes
	OIHT2	Horizontal flow: critical velocity for non−dispersed – dispersed flow transition	Yes	No
	OIANU	Vertical flow: interfacial drag in annulus	No	No
	OIBUN	Vertical flow: interfacial drag in bundle	Yes	Yes
	OIVPI	Vertical flow: interfacial drag in pipe	Yes	Yes
	OIVDI	Vertical flow: interfacial drag at dispersed droplet flow	Yes	No
	OIVTP	Vertical flow: critical velocity for non−dispersed – dispersed flow transition	Yes	Yes
Critical flow	OTURB	turbulence factor for the calculation of evaporation in critical flow model	Yes	Yes

According to a literature review[116] and the physical meaning judgment, a preliminary selection has been done and 22 input parameters were chosen for the ATHLET sensitivity calculation. For further selection, the criterion for parameters to be part of the final selection is that they should fulfill one of the following two conditions: either the variation of maximum cladding temperature is at least 50K or the variation of the quench time is at least 10% (of reference quench time, 128 s). As a result of this criterion, 12 parameters were chosen finally, as shown in Table 4.1.

(2) Selection of responses

The selection of responses is an important step for sensitivity study. In principle, any experimental data can be considered as a response to be compared with simulation results. But from the actual situation, these are normally the design parameters and threshold parameters for safety criterion or related parameters. When selecting the responses, it is important to take into account what is the final goal of the sensitivity analysis. For instance, for IBLOCA case, it is very important that both the heat-up phenomenon and the maximum PCT happen in all sensitivity trials. Referring to some literature [117], the response parameters considered for sensitivity analysis are the following:

Table 4.2: Response parameters for IBLOCA sensitivity analysis

No.	Parameter
1.	Primary side (PRZ) pressure
2.	Secondary side (SG exit) pressure
3.	Downcomer temperature
4.	Core exit temperature
5.	Typical rod temperature
6.	Maximum PCT
7.	RPV water level (total)
8.	Downcomer pipe WL
9.	Loop seal (SG side) WL
10.	Loop seal (RCP side) WL
11.	Break mass flow
12.	Cold leg mass flow rate

WL: water level

4.3 Sensitivity calculation and quantitative assessment of ATHLET simulations

After the selection of sensitive input parameters and responses, sensitivity calculation could be done using ATHLET, and then the ATHLET simulations could be assessed based on the sensitivity calculation results.

(1) ATHLET sensitivity calculations

After the selection of the influential parameters of specific physical models and responses of interest (to which these parameters are influential), the two-layer sensitivity analysis methodology in this study starts the ATHLET calculations with several percentage changes for each of the considered parameters. During the sensitivity analysis, a basic/reference calculation should be set. For reference calculation, nominal values have to be supplied. Unless otherwise noted, the data are multiplication factors, and the nominal values equal 1.0. A sensitivity analysis is performed for each parameter by varying the parameters in their a priori engineering judgment range and measuring its influence on the main responses of interest. After attempts with different variation values, in order to simplify the problem,

the parameters were adjusted with some fixed values in this study: 0% (reference/nominal calculation), ±5%, ±10%, ±15% and ±20%.

(2) Quantitative assessment of ATHLET simulations

The results of the quantitative assessment of ATHLET calculation on the transient I2.2 IBLOCA benchmark run 1 (at the test facility PKL) are shown in Table 4.3, which also gives the sensitivity results (take critical flow parameter OTURB as an example). The considered time interval was [0 s, 1000 s]. According to the AA values from Table 4.3, most of the responses were predicted very well by ATHLET, others (e.g. loop seal water level for both RCP side and SG side, CL mass flow) were reproduced well and break mass flow very poorly.

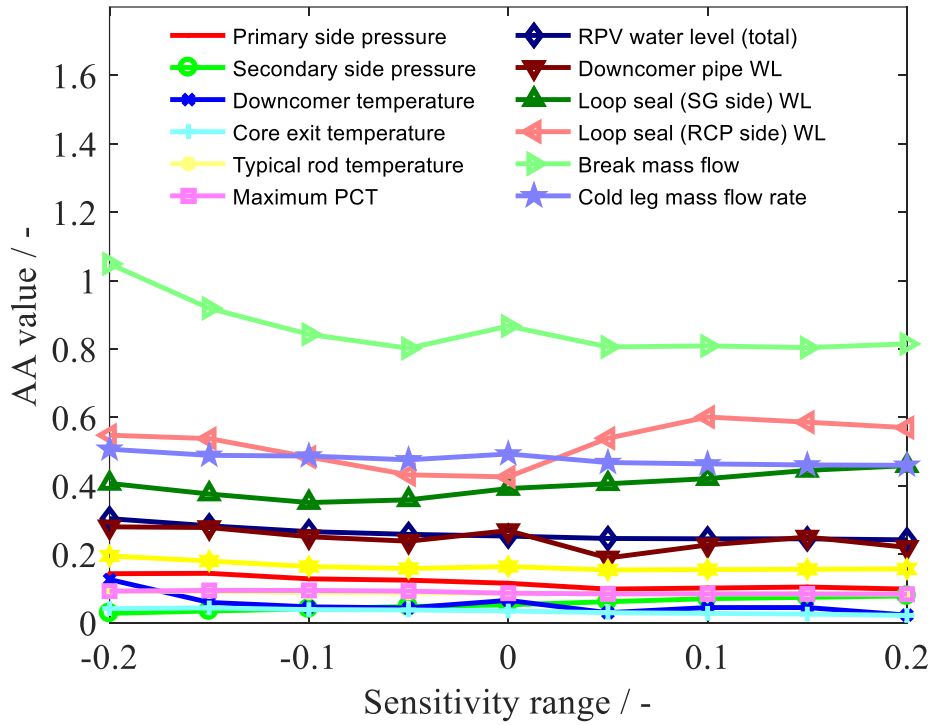

Figure 4.3: FFTBM quantitative assessment of ATHLET simulation

There are several points to be noticed here:

1) The PKL facility has four loops and the thermal hydraulic parameters for each loop are similar with small differences. The *AA* values for "Loop seal (SG side) WL" and "Loop seal (RCP side) WL" were chosen as the maximum values out of the four loops. The simulation of loop seals is different, owing to the strong volatility of two-phase mechanical equilibrium. As a consequence, it influences the AA values stronger than the RPV parameters.
2) The *AA* value for "Cold leg mass flow rate" was also chosen as the maximum value out of four loops. Furthermore, if we recall the results from Figure 3.14 and Figure 3.20, the calculated mass flows almost coincide with the experimental ones, apparently better than given by the assessment estimators from Table 4.3. The reason is that after 500 s all the mass flow values are very small but with strong oscillations. The oscillations are really accounted for in the FFTBM; therefore, the corresponding AA estimators take large values.
3) Larger *AA* for mass flows and water levels may have as source the poorly predicted break mass flow, aspect to be addressed further.
4) The total *AA* is calculated according to Eq. (2.5), which equals 0.163, well below the

acceptability limit of 0.4. One may conclude that IBLOCA scenario was reproduced well by ATHLET.

The sensitivity results based on FFTBM *AA* values could be intuitively displayed, as in Figure 4.3. It could be noticed that there is no big fluctuation between different percentage variations for each parameter. This means the assessment of ATHLET code by FFTBM is stable and is suitable for the sensitivity study, which will be shown in the next section.

4.4 Influence of the parameters on the responses

FFTBM is able to use complete time-trends as responses thanks to the transformation of the responses into the frequency domain. This provides little space for expert judgment, the only thing that needs to be decided is how much weight is given to each response. The weights are fixed within the methodology and should not be modified by the user. In this section, the results of the 2nd step of the two-layer sensitivity analysis method – MSM– will be shown.

All final chosen parameters in Table 4.1 have been selected as independent input sensitivity parameters, and the Morris coefficients for all responses are shown in Table 4.4. This table could be used for two applications: model evaluation and comprehensive sensitivity evaluation for input parameter, to be discussed further.

4.4.1 Model evaluation

Take the first parameter OHWFC, which means heat transfer coefficient (HTC) for forced convection to liquid water as an example. According to Table 4.4, two responses (downcomer pipe water level and loop seal (RCP side) water level) are sensitive to it; these responses reflect the thermal hydraulic phenomenon (especially collapsed water level) near the RPV inlet locally because of CCFL. This implies that the parameter OHWFC does not impact the global system response much, by impacting only some local regions. Around the RPV inlet, the heat transfer of forced convection to liquid water has a strong impact on the phenomenon. For the sake of qualitative analysis, it is also not difficult to come to this conclusion owing to strong volatility of two-phase mechanical equilibrium around loop seal (RCP side) and 3-dimensional effect at the downcomer vessel.

Take OTURB (input parameter for the critical flow model) as another example. As shown in Table 4.4, it has strong impacts on almost all responses (especially high influence regarding the secondary side pressure and some fluid and rod temperatures). As shown in Figure 4.4, the critical flow model does not impact the overall trends of PCT strongly, compared with other parameters. The reason for the lower sensitivity is that PCT is a local phenomenon, lasting a short time period. Furthermore, according to the figure, the critical flow model influences the PCT location and its value, aspect which is concerned in PKL I2.2 IBLOCA benchmark simulation.

Based on the FFTBM results in the last section and MSM in this section, we could come to a conclusion that critical flow model is not simulated well enough in PKL I2.2 IBLOCA benchmark test and it has high sensitive impacts on the simulation results, which means the critical flow would be the most likely a candidate model for modification in a further study.

On the other hand, researchers could use Table 4.4 to find the sensitive model with respect to chosen response. Taking PCT as response example, the OTURB (critical flow model) is the most sensitive parameter. Another response example “Cold leg mass flow rate”: it could be easily concluded that

OHWNB (HTC for nucleate boiling), OIVPI (Vertical flow: interfacial drag in pipe) and OTURB (critical flow model) are sensitive parameters according to the values in the Table 4.4.

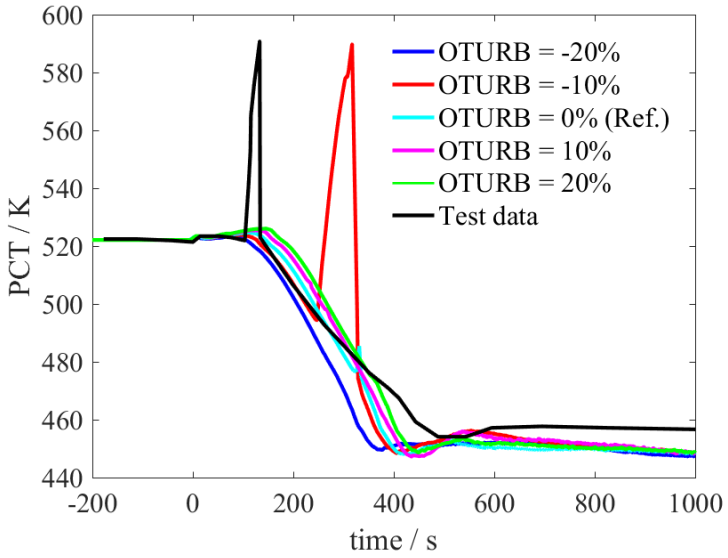

Figure 4.4: PCT response sensitivity to the Critical flow model

Table 4.3: *AA* results from FFTBM applied on PKL I2.2 IBLOCA benchmark run 1 test

Sensitivity Para. / **Response Para.**	OTURB **-20%**	OTURB **-15%**	OTURB **-10%**	OTURB **-5%**	**Ref. 0%**	OTURB **5%**	OTURB **10%**	OTURB **15%**	OTURB **20%**
Primary side pressure	0.143	0.144	0.128	0.124	0.115	0.098	0.101	0.104	0.098
Secondary side pressure	0.027	0.034	0.040	0.047	0.052	0.061	0.070	0.074	0.078
Downcomer temperature	0.126	0.059	0.046	0.043	0.065	0.029	0.044	0.044	0.022
Core exit temperature	0.041	0.043	0.038	0.037	0.034	0.029	0.027	0.025	0.021
Typical rod temperature	0.092	0.091	0.088	0.087	0.086	0.084	0.084	0.084	0.083
Maximum PCT	0.092	0.094	0.094	0.092	0.086	0.084	0.084	0.084	0.083
RPV water level (total)	0.304	0.283	0.266	0.258	0.253	0.246	0.245	0.245	0.242
Downcomer pipe WL	0.280	0.278	0.251	0.238	0.269	0.189	0.227	0.250	0.220
Loop seal (SG side) WL	0.407	0.376	0.351	0.359	0.392	0.406	0.421	0.445	0.459
Loop seal (RCP side) WL	0.548	0.538	0.484	0.432	0.426	0.539	0.601	0.586	0.570
Break mass flow	1.049	0.919	0.843	0.802	0.867	0.806	0.809	0.804	0.815
Cold leg mass flow rate	0.507	0.489	0.487	0.476	0.493	0.468	0.464	0.461	0.460
$\boldsymbol{AA_{tot}}$	0.195	0.180	0.164	0.158	0.164	0.154	0.155	0.156	0.157

$AA \leq 0.3$	very good prediction	$0.5 < AA \leq 0.7$	poor code prediction
$0.3 < AA \leq 0.5$	good prediction	$AA > 0.7$	very poor prediction

Table 4.4: *AA* sensitivity results from FFTBM-MSM applied on PKL I2.2 IBLOCA benchmark run 1 test

Sensitivity Para. / Response Para.	OHWFC	OHWNB	OFI2V	ODHPI	ODVPI	OIHST	OIHDI	OIHT1	OIBUN	OIVPI	OIVTP	OTURB
Primary side (PRZ) pressure	0.066	-0.141	-0.252	0.038	0.080	0.106	-0.175	0.335	-0.289	-0.439	0.374	-0.971
Secondary side pressure	0.013	-0.178	0.136	-0.009	0.021	-0.022	0.077	0.084	0.039	-0.149	0.042	3.359
Downcomer temperature	0.075	-0.174	0.796	0.042	0.229	-1.500	1.314	0.807	-1.692	0.773	1.730	-3.997
Core exit temperature	0.087	-0.155	-0.323	0.047	0.079	0.135	-0.181	0.422	-0.304	-0.492	0.395	-1.469
Typical rod temperature	0.018	-0.114	-0.041	-0.062	-0.056	0.047	-0.115	0.028	-0.066	-0.070	0.140	-1.641
Maximum PCT	0.015	0.018	-0.013	0.000	0.005	0.031	-0.018	-0.020	0.037	-0.032	-0.066	-0.254
RPV water level (total)	0.001	-0.012	-0.031	0.021	0.043	0.030	-0.079	0.048	-0.046	-0.042	0.075	-0.614
Downcomer pipe water level	0.276	-0.432	-0.401	0.144	0.223	-0.734	-0.640	0.420	-0.555	-0.583	0.561	-0.557
Loop seal (SG side) water level	-0.164	0.159	-0.228	-0.124	-0.013	-0.122	0.010	0.189	0.056	0.519	-0.016	0.504
Loop seal (RCP side) water level	-0.268	-0.537	-0.347	0.236	0.122	-0.219	-0.177	-0.217	-0.313	0.908	-0.005	0.549
Break mass flow	-0.121	-0.304	0.434	0.385	-0.106	0.135	-0.016	-0.006	-0.016	-0.155	-0.001	-0.673
Cold leg mass flow rate	-0.183	0.263	0.121	-0.106	0.055	0.177	0.023	0.007	0.066	-0.383	0.048	-0.377
AA_{tot}	-0.079	-0.160	0.216	0.191	-0.043	0.111	-0.052	0.029	-0.072	-0.190	0.079	-0.569

$0 \leq \lvert S \rvert < 0.05$	insensitive	$0.05 \leq \lvert S \rvert < 0.2$	moderate	$0.2 \leq \lvert S \rvert < 1$	sensitive	$\lvert S \rvert \geq 1$	high sensitive

4.4.2 Comprehensive sensitivity evaluation to input parameters

Except for the model evaluation, comprehensive sensitivity evaluation to input parameters is also important since it could provide some intuitive hints to researchers and make the judgment easier. There are two ways to proceed with the sensitivity analysis, based on Table 4.4.

(1) Direct usage of the Morris coefficient of AA_{tot}

Since parameter AA_{tot} is a comprehensive estimator from FFTBM, it may be used as input for MSM. In Table 4.4, the parameters OFI2V (Two-phase multiplier for vertical junctions) and OTURB (critical flow model) have significant comprehensive sensitivities based on the criterion in section 4.1.

(2) Criterion based on comprehensive sensitivity coefficient

Here we define the parameter "comprehensive sensitivity coefficient S_c" as the ratio between the number of sensitive or high sensitive parameters and the total number of responses. As a preliminary judgment, different comprehensive sensitivity could be classified into three categories: (1) $S_c < 0.3$, low comprehensive sensitive parameter; (2) $0.3 \leq S_c < 0.6$, moderate comprehensive sensitive parameter; (3) $S_c \geq 0.6$, high comprehensive sensitive parameter. According to this criterion, the parameters for PKL I2.2 IBLOCA benchmark ATHLET simulation could be classified as Table 4.5. Comparing the Morris coefficient of AA_{tot} for parameters OFI2V (=0.216) and OTURB (=-0.569) in Table 4.4, we could come to a conclusion that the 2nd method is more reasonable than the 1st method for comprehensive sensitivity evaluation for input parameters.

Table 4.5: categories for comprehensive sensitive parameters for PKL I2.2 IBLOCA benchmark simulation

Categories	Low	Moderate	High
Parameters	OHWFC, ODHPI, ODVPI, OIHST, OIHDI, OIVTP,	OHWNB, OFI2V, OIHT1, OIBUN, OIVPI,	OTURB

4.5 Summary

As presented in this work, the core heat-up and PCT could not be well reproduced in ATHLET PKL I2.2 IBLOCA benchmark simulation. A new generalized two-layer methodology of sensitivity analysis has been developed, based on two classical methods. The method in 1st layer is called Fast Fourier Transform Based Method (FFTBM), which is a tool to determine differences between code predictions and measurements in the frequency domain. The major calculated responses were compared with the test data using this method. By using the results of Morris screening method (MSM, the method of 2nd layer), we can analyze the sensitive relations between input parameters of thermal-hydraulic models and responses in detail.

Two methods of comprehensive sensitivity evaluation are proposed and compared, and the method using a defined comprehensive sensitivity coefficient S_c is recommended in the studies. The evaluation criterion is as following: (1) $S_c < 0.3$, low comprehensive sensitive parameter; (2) $0.3 \leq S_c < 0.6$, moderate comprehensive sensitive parameter; (3) $S_c \geq 0.6$, high comprehensive sensitive parameter.

According to the trend analysis, FFTBM quantitative assessment and MSM sensitivity analysis, the critical flow model (CFM), which is not simulated well enough in PKL I2.2 IBLOCA benchmark test and it has high sensitive impacts on the simulation, is with high probability responsible for that, and it would be the most likely candidate model for modification. In the next chapter, a 6-equation model is introduced for CFM, as a potential improvement instead of the present CDR1D model, which is only a 4-equation CFM.

5 Development of a new 6-equation Critical Flow Model (CFM)

The phenomenon of critical flow occurs for both single phase and two phase flow systems and has been extensively studied due to its important role in a variety of industrial implementations. Critical flow of single-phase compressible fluids is well understood and mathematically described. Even a modified Bernoulli theory is used within the subcooled region to evaluate the critical flow rate. However, there are still cases, for which the existing models cannot be applied. Owing to this background, an idea of new CFM development and its application for ATHLET CFMs improvement has been generated.

5.1 Background of Critical Flow Models

The discharge mass flow from the break during a DBA or BDBA scenario should be predicted by STH codes. The transient plant parameters such as reactor water level, the amount of coolant (i.e. inventory), pressure, cladding temperature and others have to be evaluated accurately for safety issues[118].

The accuracy of these parameters is strongly related to the discharge mass flow of the break, normally a two phase flow because of the primary side system depressurization and evaporation of the discharged coolant. The prediction of the mass flow rate plays a major role in determining the core cooling requirements associated with the safety analyses of nuclear power plants[119].

Due to the huge pressure difference between the primary system and the reactor containment, the mass flow rate is choked at the break, resulting in the mixture velocity of the coolant through the breach equaling the local sound velocity [120]. Furthermore, the flow is also referred as being critical flow when the mass flow rate becomes independent of the downstream pressure, as shown in Eq. (5.1):

$$\left(\frac{\partial G}{\partial P}\right)_t = 0 \tag{5.1}$$

Here G is the mass flux and P the pressure. The subscript t means at the "throat", as shown in Figure 5.1. The Eq. (5.1) underlines that the pressure dependence of the mass flux vanishes as long as the downstream pressure remains below a certain critical pressure. This location (t) is called the critical cross section.

For single phase flow, the link between the critical flow and the velocity of sound is easily established. However, for the two-phase flow conditions, which nuclear accident scenario usually faces, the velocity of sound becomes more difficult to evaluate, especially if the two phases have large

differences in velocity and temperature[121]. Not only the interfacial interaction (transfer of mass and energy, interfacial force) but also wall frictions are not easy to calculate accurately in the situation of critical discharge flow, due to the lack of experimental data or correlations.

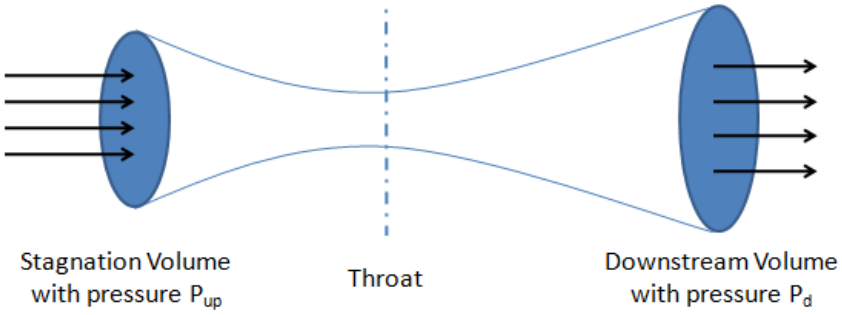

Figure 5.1: Converging-diverging throat

Accordingly, some simplified models were developed in the past. In the next section, the present CFMs in ATHLET and other classical models will be introduced.

5.2 Literature review of two phase CFMs

In this section, a literature review of critical flow models will be given, divided in three parts:

(1) The classification of CFMs
(2) The CFMs used in typical STH codes
(3) A brief introduction about ATHLET CDR1D model (since it will be used as the main contrast model for the validation of the new developed 6-equation model)

5.2.1 Classification of CFMs

The two-phase CFMs could be divided into several groups, based on different classification methods. For example, CFMs could be homogeneous equilibrium model (HEM) and non-homogeneous models. According to the application method, CFMs could be used as simple formula, fitted functions, interpolation tables or directly solving the system of ordinary differential equations (ODEs).

But the most well-known commonly used models for the description of critical one component two phase flows may be divided into hydrodynamic homogeneous and non-homogeneous (caused by the velocity and pressure differences). In the case of homogeneous flow, it is assumed that a pronounced mechanical coupling of the phases prevents a relative movement between the vapor and the liquid. This is true with strong dispersion of the discontinuous phase, e.g. in the case of short nozzle with blistering or spraying (high mass flux) [122]. But in the case of two-phase flows with higher void fractions (low mass flux), especially with largely separated phases, such as in the annular flow, the non-homogeneous fluid dynamics become more important.

The thermodynamic equilibrium and non-equilibrium (caused by the temperature difference between phases) were further considered for the classification of the critical flow models. In the models assuming thermal equilibrium, it is considered that the temperature difference between the phases is immediately and completely dissipated by heat transfer and phase transformations (i.e. evaporation or

condensation); therefore, the phases are always in the saturation state. Different temperatures of vapor and liquid are taken into account in thermal non-equilibrium models.

Therefore, according to these two features of classification, the critical flow models may be divided into four types, as shown by Table 5.1, depending on the thermal and fluid-dynamic behaviors assumed for the liquid and vapor phases. A literature review of existing models and correlations was too large to be included in this study; some references are provided in the Table 5.1 for more detailed information. A comprehensive review and discussion of the analytical models and key experimental results has also been compiled by D'Auria[123] and Elias[124].

Table 5.1: Classification of the Critical Models

Thermodynamic Hydrodynamic	Equilibrium	Non-equilibrium
Homogeneous	Wallis model[125], Pana model[126] et al.	Levy model[127], Elias model [128], CDR1D model et al.
Non-homogeneous	Slip model[129], Moody model [130] et al.	General drift flux model[131], Richter model[132], Dobran model[133]et al.

5.2.2 CFMs in STH code

The estimation of critical flow through the break is important to ascertain safe designs of piping system in NPPs and, consequently, is a basic function for all STH codes. In this section, there is no willing to repeat the details of CFMs in typical STH codes such as RELAP5, TRACE and MARS etc. but a brief summary of these models. Some detailed information about ATHLET CFMs will be described in section 5.2.3 since it is the objective STH code, planned to be improved within a certain model.

Burnell model [134] is an empirical correlation for the critical pressure. The liquid temperature and density at the exit were assumed to be equal to the stagnation (vessel) values. The Bernoulli equation, between the vessel and the critical location, was applied to calculate the mass flux.

A one-dimensional choked flow model developed by Ransom and Trapp is employed in RELAP5/MOD3. Trapp and Ransom developed an analytical choking criterion, using a characteristic analysis of a two-fluid model that included relative phase acceleration terms and derivative dependent mass transfer [135]. In other words, an overall mass conservation equation, two-phase momentum equations, and the mixture energy equation are used for Trapp and Ransom model. The equation set is written without non-differential terms, such as wall drag and heat transfer, since these terms do not enter into the characteristic analysis. An extended Henry-Fauske model (EHF) is introduced in the later version of RELAP5 [136]. TRACE and MARS has the same CFMs as RELAP5 except for the extended Henry-Fauske model.

RETRAN-3D is a flexible general purpose, thermal/hydraulic computer code that is used to evaluate the effects of various upset reactor conditions in the reactor cooling system. This code models the reactor coolant as a single phase or as two equilibrium phases with the exception that a non-equilibrium pressurizer component can be included. There are three options for CFMs in RETRAN-3D, which combine the EHF model, Moody model and HEM in different ranges of use [137].

TRAC (early version) [138] used a simplified, five-equation model that had a single momentum equation for both liquid and vapor phases. A drift flux model was used to determine the velocity of

each phase, since the solution of a single momentum equation cannot provide separate velocity results for the phases. For critical flow simulation, the drift flux model was also used [139].

Table 5.2: CFMs in Typical STH codes

	RELAP5	RETRAN-3D	TRAC	TRACE	MARS	ATHLET
Burnell model	X			X	X	
HEM		X				X
Moody model		X				X
Extended Henry-Fauske (EHF) model	X	X				
Ransom and Trapp model	X			X	X	
CDR1D model						X
Drift flux model			X			

As a summary, the CFMs in typical STH codes are shown in Table 5.3. It is not necessary to compare these models in detail but some points of review are concluded and given as following [140].

1) HEM under-predicts the critical flow rates for short pipes and near-liquid saturation, or subcooled upstream conditions.
2) The equilibrium-slip model of Moody, although successful for some long tubes, under predicted the critical flow rates for short pipes [141]. This is particularly true if the upstream condition is subcooled, or near saturation.
3) The effects of thermal non-equilibrium must be taken into account for short pipes.
4) At present, there is no general model or correlation for critical flow to be valid for a broad range of pipe lengths, pipe diameters, and upstream conditions, including subcooled liquids.
5) In the implementation of these critical flow models, both RELAP5 and TRACE allow the user to specify a discharge coefficient (referred in TRACE as a critical flow multiplier). This is a multiplier allowing the user to adjust the predicted flow rate to account for inconsistencies between model predictions and experimental observation. Without application of discharge coefficients, the Ransom and Trapp model may over predict the critical flux (compared with Henry-Fauske data and Marviken facility data).

5.2.3 ATHLET CDR1D models

Since the CDR1D model is recommended for the simulation of a PWR LOCA scenario, this part focusses on the introduction of CDR1D model. A recommendation for the HEM and Moody models could be found in related ATHLET documents. The methodology for transition between subcritical flow and critical flow will be given at the end of this section.

5.2.3.1 Brief introduction of CDR1D model

CDR1D model is a special critical flow model used only in the STH code ATHLET. To determine critical discharge rates, a one-dimensional finite difference model describing the one- and two-phase flow is used to simulate the fluid flow in the flow path closest to the choking location, where local pressure drop is strongest. Thermodynamic non-equilibrium phenomena are taken into account. The magnitude of the thermodynamic non-equilibrium during evaporation and condensation processes is controlled by a mass transfer rate between the liquid and vapor phases. Since the CDR1D model does

not consider a velocity difference between the two phases (mechanically homogeneous model), the speed slip ratio equals 1.0. In other words, only one parameter u is needed for the speed along the discharge path.

CDR1D model is based on the following main assumptions [106].

1) the flow is treated as quasi-stationary due to the relatively slow variation of the discharge rate when the flow is critical;
2) frictional and potential energy effects are assumed to be negligible for the energy equation;
3) the vapor phase is assumed as saturated for "liquid-dominant" region (single phase liquid and two-phase upstream conditions up to a void fraction of 0.95);
4) the "vapor-dominant" region means the vapor phase may deviate from thermal equilibrium, while the liquid (if there is one) is assumed to be saturated;
5) the liquid phase might be subcooled, saturated, or superheated.

A set of 4 ODEs in space can be formulated, based on a 4-equation model where the field equations are derived from the one-dimensional steady state conservation laws for the liquid mass, vapor mass, mixture momentum and mixture energy.

The equations used in ATHLET to determine the mass transfer rate between liquid and vapor phases within the bulk during evaporation or condensation processes are based on correlations for the heat transfer, controlled growth and shrinkage of vapor bubbles or liquid droplets. For low void fractions, it is assumed that the vapor phase is composed of single droplets. For high void factions, the existence of single droplets is assumed. For the transition region, an average mass transfer rate, based on both assumptions, is used.

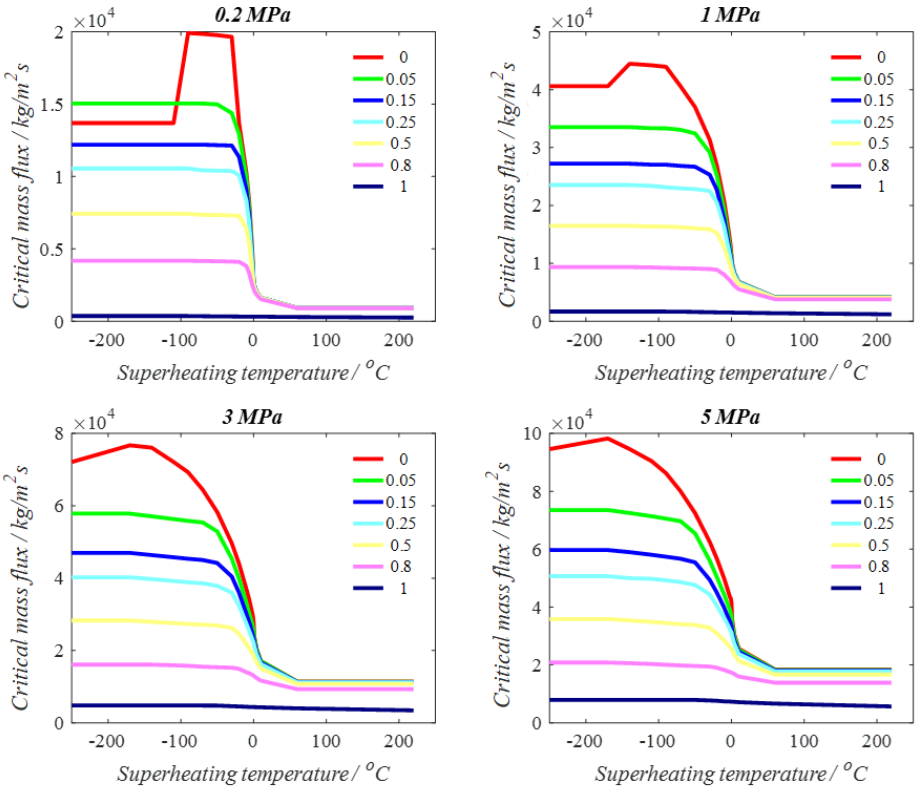

Figure 5.2 Critical mass flux of CDR1D model for PKL I2.2 IBLOCA simulation (Location 1)

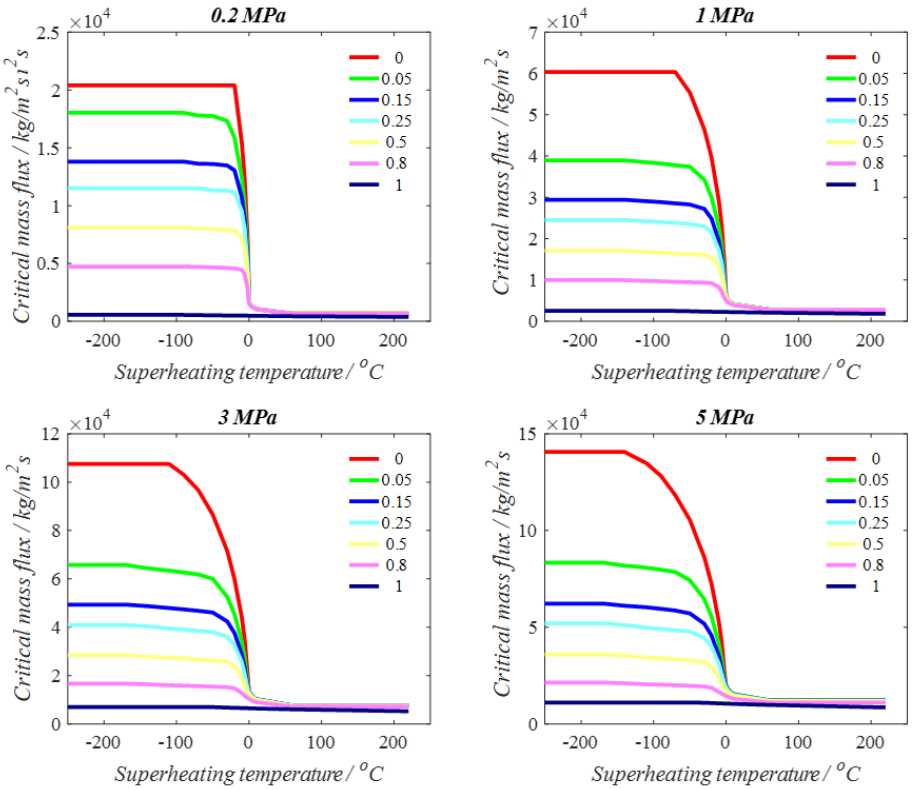

Figure 5.3 Critical mass flux of CDR1D model for PKL I2.2 IBLOCA simulation (Location 2)

As mentioned in section 3.1.5.1, there were two locations in the pipeline (see Figure 3.7), where CDR1D model should be considered for ATHLET simulation of PKL I2.2 IBLOCA benchmark scenario, since CDR1D model considered the geometry information of the discharge pipeline. At these two locations, the critical mass fluxes for different upstream pressures and superheating temperatures are shown in Figure 5.2 and Figure 5.3, respectively. The curves with different colors, i.e. the legends, represent the critical mass fluxes in different upstream void fractions of the critical flow locations.

5.2.3.2 Criterion for transition between subcritical flow and critical flow

Usually, the mass flow is limited to the critical flow at once although a transition time could be set in ATHLET input deck.

$$G_{mom} \geq G_{crit} \tag{5.2}$$

The mass flow time derivative according to the momentum equation is calculated also during the critical flow period. The transition from critical flow back to subcritical flow is assumed if its absolute value falls below the absolute value of the 'time derivative' of the critical mass flow.

$$\frac{dG_{mom}}{dt} \leq \frac{G_{crit,t_n} - G_{crit,t_{n-1}}}{dt} \tag{5.3}$$

where $dt = t_n - t_{n-1}$ is the time step size. Eq. (5.3) is equivalent to

$$G_{mom} \leq G_{crit,t_n} \tag{5.4}$$

5.3 Description of new developed 6-equation CDM

The flow regime to be expected in a two-phase flow depends on void fraction and mass flux. As an example, Figure 5.4 the flow regime map for vertical two-phase flow in pipes as used in RELAP5, cited by Todreas and Kazimi [142]. If the mass flux is greater than 3000 kg/m^{2}s, we get a fine dispersed bubbly flow for low void fractions and a fined dispersed droplet flow (or mist) for high void fractions, both with a strong mechanical interaction between both phases such that the slip ratio equals 1. In this range, the CDR1D model can well be applied.

If the mass flux is less than 2000 kg/m^{2}s, however, the bubbly flow, slug flow and annular flow to be expected will produce a slip ratio greater than 1, which is not foreseen in the CDR1D model. Here, we rather need a non-homogeneous two phase critical flow model (i.e. non-equilibrium and non-homogeneous two phase critical flow model, hereinafter abbreviated as NNTPCM). Since NNTPCM considers the interfacial interaction of two-phase fluid in detail, it may be a suitable extension for ATHLET to cover a larger range for IBLOCA scenario in PKL I2.2 IBLOCA benchmark test I2.2 and to get more realistic simulation results.

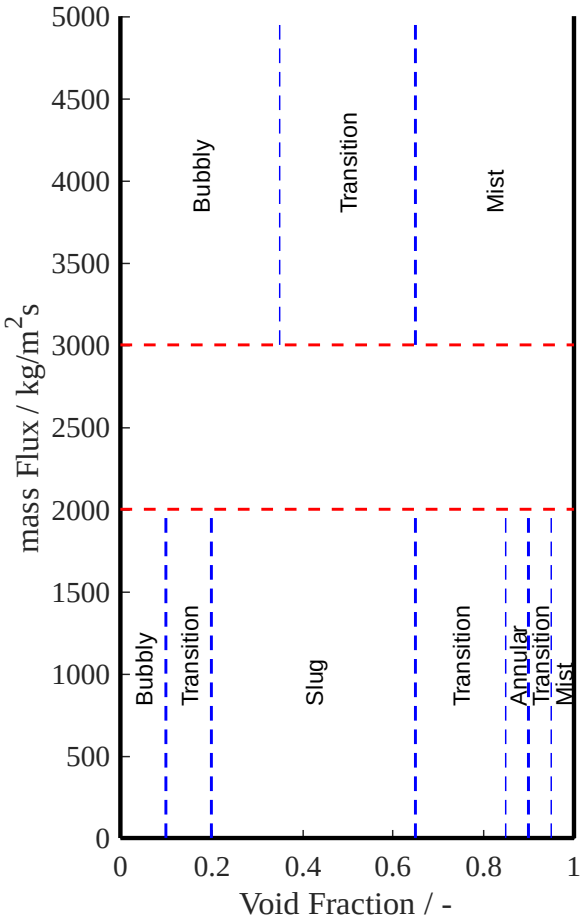

Figure 5.4 Vertical flow regime map of RELAP5 [143]

The NNTPCM has solid theoretical fundaments. It comprises six conservation equations (mass, momentum and energy for each phase) and takes into account a detailed description of the interfacial heat and momentum transfers. Although correlations are needed for some constitutive relationships, no major variable has to be determined empirically.

If the mass flux is greater than 2000 kg/m^{2}s, but less than 3000 kg/m^{2}s, the CDR1D model and the NNTPCM must be interpolated. Therefore, the NNTPCM model must also be checked with experimental data at a mass flux greater than 2000 kg/m^{2}s to get a smooth transition between both models.

The objective of this study was to introduce a general purpose two fluid model for choked flow in pipes starting from existing models in literature. The potential model comprises six conservation equations. It allows for hydrodynamic non-homogeneity as well as thermodynamic non-equilibrium, and includes the following flow regimes: single phase (both liquid and vapor), sub-cooled boiling, bubbly flow, slug/churn flow and annular flow. A droplet flow, however, is not included in NNTPCM. Therefore, according to Figure 5.4, it must be limited to a void fraction less than 0.95. Beyond this void fraction, we get a fine dispersed droplet flow, and the CDR1D model may be applied again.

As mentioned above, the NNTPCM will allow for the hydrodynamic non-homogeneity (caused by the velocity and pressure differences between phases) and thermodynamic non-equilibrium (caused by the temperature difference between phases) features. In order to simplify the modeling, some a-priori assumptions were needed:

(1) the critical flow through a tube can be modeled by one-dimensional conservation equations for the two phase flow;
(2) for time independent boundary conditions, the two phase critical flow is stationary;
(3) the gas phase is in thermal equilibrium at local saturation pressure;
(4) each phase is at the same pressure at any cross section of the tube (but the pressures in both phases are different due to surface tension);
(5) the wall friction of vapor (F_{WG}) has not to be considered because vapor does not contact the wall directly in the considered flow regimes;
(6) the two phase flow is assumed to be adiabatic to the wall during the process of choking.

The conservation equations and constitutive relationships will be introduced in this section, as inspired from Dobran, Schwelllus[144], Dagan[145] and Wein models [122]. All of these models from literature used the general 6 conservation equations; the main differences appear in the constitutive relationships and their combinations. In the present work, a selection of proper constitutive relationships was done and they were then optimally combined to minimize the errors of the corresponding critical flow predictions.

5.3.1 Conservation Equations

(1) Conservation of mass

Based on the conservation of total mass, the liquid and vapor mass changes are complementary:

$$\frac{d}{dz}[\rho_L(1-\alpha)u_L A] + GA\frac{dx}{dz} = 0 \tag{5.5}$$

$$\frac{d}{dz}[\rho_G \alpha u_G A] - GA\frac{dx}{dz} = 0 \tag{5.6}$$

After expanding the contents in brackets, mass conservation equations may be written as:

$$-\rho_L u_L\frac{d\alpha}{dz} + \rho_L(1-\alpha)\frac{du_L}{dz} + \rho_L(1-\alpha)u_L\frac{1}{A}\frac{dA}{dz} + u_L(1-\alpha)\left(\frac{\partial\rho_L}{\partial P}\right)_{sat}\frac{dP}{dz} + G\frac{dx}{dz} = 0 \tag{5.7}$$

$$\rho_G u_G\frac{d\alpha}{dz} + \rho_G\alpha\frac{du_G}{dz} + \rho_G\alpha u_G\frac{1}{A}\frac{dA}{dz} + u_G\alpha\left(\frac{\partial\rho_G}{\partial P}\right)_{sat}\frac{dP}{dz} - G\frac{dx}{dz} = 0 \tag{5.8}$$

In the process of derivation, it was assumed that the density change of each phase is related only to the saturated pressure.

(2) Conservation of momentum

Different forces, i.e. gravitation force, wall friction of liquid F_{WL}, interfacial force F_{LG} (including drag force F_D and virtual mass force F_{VM}) and forces for interfacial momentum transport F_{Li}, F_{Gi} are considered in two phase momentum conservation equations. The pipe angle θ represents the angle of inclination from the horizontal line.

$$\rho_L u_L(1-\alpha)\frac{du_L}{dz} + (1-\alpha)\frac{dP}{dz} = -F_{WL} + F_{LG} - F_{Li} - (1-\alpha)\rho_L g\, sin(\theta) \tag{5.9}$$

$$\rho_G u_G \alpha \frac{du_G}{dz} + \alpha\frac{dP}{dz} = -F_{LG} - F_{Gi} - \alpha\rho_G g\, sin(\theta) \tag{5.10}$$

The force terms on the right sides of the above momentum equations represent force magnitudes only, force directions being indicated by the signs in front of them. The concrete forms of these forces will be introduced in the next sub-section by using constitutive relationships.

(3) Conservation of energy

Since the two phase flow is assumed to be adiabatic, there is no external heat source for the choking flow. Under the given assumptions, the control volume energy balance on each phase may be written as:

$$-G\frac{dx}{dz}\left[h_L + \frac{u_L^2}{2}\right] + G_L\left[C_p\frac{dT_L}{dz} + u_L\frac{du_L}{dz}\right] + Gg\, sin(\theta) + q_i = 0 \tag{5.11}$$

$$G_G\left(\frac{\partial h_G}{\partial P}\right)_{sat}\frac{dP}{dz} + G_G u_G\frac{du_G}{dz} + G\frac{dx}{dz}\left(h_G + \frac{u_G^2}{2}\right) - q_i = 0 \tag{5.12}$$

The parameter q_i is the interfacial heat transfer rate per unit volume.

5.3.2 Constitutive Relationships

In order to solve the six equations, it is obvious that expressions for some of the unknown variables must be found. The equation of state can be used to correlate the thermodynamic properties of the liquid and the gas. This helps to reduce the number of variables but, as will be shown later, there are necessary requirements for the range and accuracy of the correlations. The other expressions are known as constitutive relationships. They are generally empirically based correlations for quantities which can be measured from some simple experiments. Relations for the following aspects must be found:

(1) bubble Growth;
(2) Wall Friction for Liquid;
(3) interfacial Transfer Terms;
    1) interfacial area
    2) interfacial force (including drag force and virtual mass force);
    3) interfacial momentum transport
    4) interfacial heat transfer

NNTPCM requires a great deal of information to complete (close) the model formulation, i.e. constitutive relationships to describe the interphase heat, mass and momentum transfers etc. These quantities have to be provided to close the conservation equations, for a well-defined solution. Actually, the constitutive relations have a very significant effect upon the final model's predictions, and therefore, careful selection or derivation of these terms is essential. Therefore, comparison of different constitutive relations with results from several different experiments is useful to determine, if possible, the best available form of the model.

5.3.2.1 Bubble Growth

NNTPCM of this work allows the choked flow starting from single phase, sub-cooled boiling or bubbly flow. Consequently, the bubble growth in bubbly flow has to be considered. The changes in quality and void fraction of bubbly flow are impacted by bubble diameter d_b and nucleate bubble density N. The correlation should be expressed as:

$$G\frac{dx}{dz} = \frac{dG_G}{dz} = \frac{d}{dz}(\alpha\rho_G u_G) \tag{5.13}$$

$$\alpha = \frac{N\pi d_b^3}{6} \tag{5.14}$$

After substitution and expansion, it takes the form:

$$\frac{dx}{dz} = x\left[\frac{3}{d_b}\frac{dd_b}{dz} + \frac{1}{\rho_G}\left(\frac{\partial\rho_G}{\partial P}\right)_{sat}\frac{dP}{dz} + \frac{1}{u_G}\frac{du_G}{dz}\right] \tag{5.15}$$

For bubbly flow, the bubble diameter has to be solved as the other unknown parameters of the conservation equations. This issue will be discussed later in the ODE solution methodology.

5.3.2.2 Wall Friction of Liquid

The wall friction of vapor (F_{WG}) is not considered in the model but the wall friction of liquid has to be considered. There are several correlations available for frictional pressure drop. Most take the form similar to that of the single phase Fanning or Moody friction factor equations, such as McAdams, or use modifiers for the entire single phase friction pressure drop, such as Martinelli-Nelson [146]. The most commonly used correlations appear to be curve fits for the friction factor using the Fanning or Moody expressions in single phase. There are several options which were considered further for the wall friction of liquid - Martinelli-Nelson correlation, Chisholm correlation [147] and Friedel correlation [148].

5.3.2.3 Interfacial Transfer Terms

It has been demonstrated experimentally that fluid mixture passes through several different flow regimes before choking, from bubbly flow to churn flow, to annular flow, to dispersed droplet flow. The interfacial terms of force and heat transfer are very strong functions of flow regime and, in one-dimensional models, usually take the form of an area times a driving force. Since simple relations that would be useful for the whole range of flow regime transitions do not exist, it is necessary to use individual correlations for each flow regime or approximations of them.

As mentioned previously, NNTPCM has solid theoretical fundaments by using six conservation equations which describe more accurately transients with rapidly changing flow conditions and non-equilibrium between phases. For example, the time lag of energy transfer at the interface may cause a temperature difference between the gas and liquid phases. Consequently, several constitutive relationships related with the interfacial transfer terms have to be considered to close the conservation equations. The details of the corresponding interfacial terms are further presented.

(1) Interfacial area

The interfacial area a_i (also called interfacial area concentration) is the total surface area between phases per unit of mixture volume. It is strongly dependent on the particular flow regime because of

different mechanisms[149][150]. In bubbly flow, the bubbles are assumed to be spherical; this is a good approximation for disperse bubbly flow. The interfacial area is simulated in bubbly flow as the surface area of the bubbles in the flow using the bubble diameter and the number of bubbles as in Eq. (5.16), derived directly from Eq. (5.14).

$$a_i = N\pi d_b^2 = 6\alpha/d_b \tag{5.16}$$

For annular flow, the interface geometry is better assumed to be a cylinder with a cylindrical gas core and a liquid film at the wall. A droplet entrainment is not considered. The interfacial area is calculated as the surface area of this cylinder:

$$a_i = \frac{4\sqrt{\alpha}}{D} \tag{5.17}$$

For slug/churn flow, there are no dedicated correlations available for the interfacial area. The existing method is the linear interpolation (see Eq. (5.18)) between points from the bubble to slug/churn flow transition and from the slug/churn to annular flow transition[151]. The parameters α_b and α_a are the interfacial areas for bubbly flow and annular flow, respectively.

$$a_i = \left(\frac{a_{ia} - a_{ib}}{\alpha_a - \alpha_b}\right)(\alpha - \alpha_b) + a_{ib} \tag{5.18}$$

(2) Interfacial force

The interfacial force represents the force applied from one phase to another across the interface due to the relative motion of the two phases. The liquid to gas interfacial force in this work was modeled as composed out of two terms only, the constant relative velocity interfacial drag force and the virtual mass force (due to the relative acceleration between phases):

$$F_{LG} = F_D + F_{VM} \tag{5.19}$$

Drag and virtual mass forces are the most important components of the interfacial momentum transfer; their concrete expressions are introduced below, respectively.

(a) Drag force

This force arises from the viscosity and pressure along the interface and is related to the local interfacial gradients. It has to be noted that the drag forces and bubble interaction mechanisms for bubbles flow are quite different with respect to slug/churn and annular flows.

In the bubbly flow:

$$F_D = \frac{3}{4d_b}(C_D)_{1-\alpha}\alpha(1-\alpha)^3\rho_L(u_G - u_L)|u_G - u_L| \tag{5.20}$$

The parameter $(CD)_{1-\alpha}$ is the bubble drag coefficient [144]:

$$(CD)_{1-\alpha} = C_D(1-\alpha)^{-4.7} \tag{5.21}$$

with the parameter C_D denoting a single bubble drag coefficient. In the present work, C_D in bubbly flow was considered as a function of the bubble Reynolds number Re_b [152]:

$$C_D = \begin{cases} \frac{24}{Re_b}\left(1 + 0.15Re_b^{0.687}\right), if\ Re_b \leq 1000 \\ 0.44, \qquad\qquad\qquad if\ Re_b > 1000 \end{cases} \tag{5.22}$$

where Re_b is expressed as:

$$Re_b = \frac{\rho_L(u_G - u_L)(1-\alpha)d_b}{\mu_L} \tag{5.23}$$

In the annular flow, the drag force may be expressed as:

$$F_D = \frac{C_{fi}}{2}\rho_G(u_G - u_L)|(u_G - u_L)|a_i \tag{5.24}$$

The parameter C_{fi} above is the interfacial drag coefficient replacing the drag coefficient C_D:

$$C_{fi} = 0.005\big(1 + 75(1-\alpha)\big) \tag{5.25}$$

The exact modeling of interfacial drag force for slug/churn flow is usually very difficult. Existing work on steady critical flow usually adopts simple interpolations between the other two flow patterns for calculating the corresponding interfacial drag coefficient. This approach was also adopted in this work. Considering the large variation in magnitude between the values of the drag coefficient at the two transition points, the interfacial drag coefficient is interpolated exponentially on void fraction:

$$C_{fi} = me^{n\alpha} \tag{5.26}$$

The parameters *m* and *n* are interpolation parameters to be determined by the values at the transition points.

(b) Virtual mass force

The virtual mass force is associated with the work needed from the (faster) moving phase to accelerate the fluid displaced by its body when translating to a new position. Usually, virtual mass force is considered as a second order effect when compared with drag force [153]. However, with the strong relative accelerations, the correct modeling of the virtual mass force is of fundamental importance in order to achieve accurate predictions of the flow variables, including pressure and velocity fields[154]. Simulation results show that for accelerated flows, the introduction of the virtual mass force significantly improves the results, indicating that this force is not negligible[155][156]. A well-known virtual mass force correlation was developed by Ishii and Chawla[157]:

$$F_{VM} = C_{VM}\rho_L\alpha_{VM} \tag{5.27}$$

$$\alpha_{VM} = [u_L + (1-\lambda)(u_L - u_G)]\frac{du_G}{dz} + [-u_G + (1-\lambda)(u_G - u_L)]\frac{du_L}{dz} \tag{5.28}$$

The parameter C_{VM} is called virtual mass force coefficient, which describes the fraction of displaced fluid that contributes to the effective mass of the fluid; in some sources, it was set constant at 0.5 for bubbly flow. Other authors used the following correlations:

$$C_{VM} = \frac{1}{2}\frac{(1+2\alpha)}{(1-\alpha)} \tag{5.29}$$

and

$$\lambda = 2(1-\alpha) \tag{5.30}$$

The sensitivity analysis done by Schwellnus demonstrated that the virtual mass effect needs to be included for the bubbly flow regime only. For slug/churn or annular flow, it equals zero.

Michael Wein [122] proposed the correlation:

$$F_{VM} = C_{VM}\rho_m \alpha(1-\alpha)\left(u_L \frac{d}{dz}u_G - u_G \frac{d}{dz}u_L\right) \tag{5.31}$$

with

$$\rho_m = \alpha\rho_G + (1-\alpha)\rho_L \tag{5.32}$$

In the present work, the virtual mass force coefficient $C_{VM,ba}$ was set to 0.5 for both bubbly flow and annular flow. For slug/churn flow, C_{VM} was considered as following: firstly, the void fractions of transition points (from bubbly to slug/churn flows and from slug/churn to annular flows, respectively) are set as α_b and α_a respectively; then α_1 and α_2 were defined as:

$$\alpha_1 = \frac{1}{1-\alpha_b}\left\{\alpha - \alpha_b\left[1 - \left(\frac{\alpha-\alpha_b}{\alpha_a-\alpha_b}\right)(1-\alpha_a)\right]\right\} \tag{5.33}$$

$$\alpha_2 = \alpha - \alpha_1 \tag{5.34}$$

secondly, an intermediate virtual mass force coefficients $C_{VM,i}$ considering the effect of larger bubble for slug/churn flow was set to 0.125; finally, the virtual mass force coefficient for slug/churn flow was defined:

$$C_{vm} = \frac{\alpha_1}{1-\alpha}\cdot C_{VM,i} + \frac{\alpha_2}{\alpha}\cdot C_{VM,ba} \tag{5.35}$$

(3) Interfacial momentum transport

When liquid is vaporized, the gas phase receives the momentum that the vaporized liquid had. There is an additional consideration, however, that the newly created vapor is moving at the liquid velocity in a faster gas phase. Therefore, it must be raised to the gas velocity by taking some momentum from either of the two phases. In essence, there must be two momentum sinks which will supply the necessary momentum, and the proportion being taken from each phase should be related by a coefficient[158]:

$$F_{Li} = (1-\eta)(u_G - u_L)G\frac{dx}{dz} \tag{5.36}$$

$$F_{Gi} = \eta(u_G - u_L)G\frac{dx}{dz} \tag{5.37}$$

i.e. parameter η above, called the phase distribution factor and set at 0.5.

(4) Interfacial heat transfer

The interfacial heat transfer in the separated critical flow models assumed that the conductive heat transfer was the dominant mode. Because of this, the general form of the heat transfer term is:

$$q_i = h_i a_i (T_L - T_G) + \Gamma(h_G - h_L) \tag{5.38}$$

where h_i is the convective heat transfer coefficient, being a function of the velocity differences between the two phases and the fluid properties. Again, correlations for bubble spheres and for the assumed cylindrical annular interface are used.

Consequently, the interfacial heat transfer rate per unit volume was modeled as the sum of sensitive and latent heat transfer components:

$$q_i = a_i h_i (T_L - T_G) + G \frac{dx}{dz}(h_G - h_L) \tag{5.39}$$

The interfacial heat transfer requires a surface area a_i which was already discussed above, and a heat transfer coefficient h_i. Empirical correlations are normally used for calculating the heat transfer coefficient during a choking process. For bubbly flow, h_i is given by Schwellnus [144]:

$$Nu = \frac{h_i d_b}{k_L} = 2 + C \cdot Re_b^{1/2} Pr_L^{1/3} \tag{5.40}$$

Consequently,

$$h_i = \left(2 + C \cdot Re_b^{1/2} Pr_L^{1/3}\right) d_b / k_L \tag{5.41}$$

In this work, the coefficient *C* takes the value 0.15. For annular flow, h_i is based on the Reynolds-Colburn analogy[159][160]:

$$h_i = \frac{C_{fi}}{2} \rho_L C_{PL} (u_G - u_L) Pr_L^{-2/3} \tag{5.42}$$

The heat transfer coefficient above is dependent upon the relative velocity. Since the gas accelerates dramatically through slug/churn flow, the relative velocity at the bubbly/churn transition point may be over an order of magnitude less than at the churn/annular transition point. Obtaining the heat transfer coefficient in churn flow by interpolation requires prior estimate of the relative velocity in annular flow. Inspired by the work of Schwellnus, a smooth interpolation was achieved by using a heat transfer parameter instead:

$$HTP = h_i / (u_G - u_L) \tag{5.43}$$

HTP does not require prior knowledge on the relative velocity for annular flow. The introduction of this parameter eliminated also the unrealistic sudden rise in the heat transfer coefficient encountered by previous models, as was shown by Schwellnus. The exponential interpolation was chosen:

$$HTP = m e^{n\alpha} \tag{5.44}$$

The parameters *m* and *n* are interpolation parameter to be determined by the values at the transition points.

5.3.3 Numerical Solution Scheme

5.3.3.1 Flow Regime Transform

NNTPCM involves several flow regimes, i.e. single phase, sub-cooled boiling, bubbly flow, slug/churn flow, and annular flow. Consequently, the flow regime transition has to be considered in the solution method. This is a fundamental feature of the solution method, to be introduced firstly.

For subcooled inlet condition, the calculation proceeds along the test section until the condition for vapor nucleation is satisfied. As the pressure decreases along the test section, mainly due to wall friction, it decreases below the saturation pressure corresponding to the fluid temperature. This saturation pressure is assumed to equal the vapor pressure inside the nucleation sites. Nucleation is assumed to occur when the excess vapor pressure in the bubble nuclei overcomes the surface tension forces:

$$P_{sat}(T_b) - P_L \geq 4\,\sigma/d_{b0} \tag{5.45}$$

where d_{b0} is the initial bubble nucleus diameter. As nucleation starts, values for the initial bubble diameter d_{i0} and initial bubble nuclei density N_0 are required. These bubbles are presumably present as dissolved gases acting as nucleation sites at the onset of flashing. The initial bubble diameter is equivalent to stating an initial void fraction. With this initial bubble diameter, the superheat at onset of flashing can be evaluated. Following Richter and Schwellnus, these initial values for bubble diameter and bubble nuclei density were used in this work:

$$d_{b0} = 2.5 \times 10^{-5} \tag{5.46}$$

$$N_0 = 1.0 \times 10^{11} \tag{5.47}$$

In opposition with Richer [132] and Dobran [133], assuming the bubble diameter and the bubble nuclei density as constants for bubbly flow, my work used a different methodology: the two parameters were solved using Eqs. (5.14) and (5.15), coupled with the 6 conservation equations.
Since different constitutive relationships were used for bubbly, slug/churn and annular flows, the flow regime transition points from bubbly to slug/churn and from slug/churn to annular had to be set. According to experimental information[161], the void fraction values for these two points were assumed as 0.3 and 0.8, respectively.

5.3.3.2 Solution Methodology

The system of equations to be solved contains at least 6 equations, i.e. the conservation equations of mass, momentum and energy for the liquid and vapor phases (Eqs. (5.7)-(5.12)). The 6 equations are sufficient in the case of slug/churn and annular flows. In the case of bubbly flow, an additional equation has to be considered in the set of equations, i.e. Eq. (5.15), coupling pressure P, quality x and velocity of vapor u_G with the bubble diameter d_b. Therefore, the system to be solved contains 6 or 7 first order ordinary differential equations (ODEs) with nonlinear parameters. No matter the system of ODEs should be solved in its 6-equations form (for slug/churn and annular flows) or 7-equations form (for bubbly flow), it may be written in matrix form:

$$[\boldsymbol{A}]\frac{d}{dz}[\boldsymbol{X}] = [\boldsymbol{b}] \tag{5.48}$$

where

$$[\boldsymbol{X}]^T = [P, x, \alpha, T_L, u_L, u_G] \tag{5.49}$$

is the vector of unknown parameters for the 6-equations form and

$$[\boldsymbol{X}]^T = [P, x, \alpha, T_L, u_L, u_G, d_b] \tag{5.50}$$

the vector of unknown parameters for the 7-equations form of the system of ODEs.

The coefficients of matrix $\boldsymbol{A}$ and vector $\boldsymbol{b}$ depend on the unknown parameters and the independent variable z, to be solved step by step. The solution of the above system of equations can be accomplished by utilizing the initial conditions, i.e. inlet parameters in terms of the tube geometry

(tube length, flow cross-sectional area and its derivative along the pipe). The system of ODEs for critical flow problems becomes stiff or illness (from the linear equations (LEs) of view) when the choking point is approaching [162]. Basically, the numerical integration in this work was accomplished by a variable step implicit Runge-Kutta procedure with a first stage that is a trapezoidal rule step and a second stage that is a backward differentiation formula of order two [163].

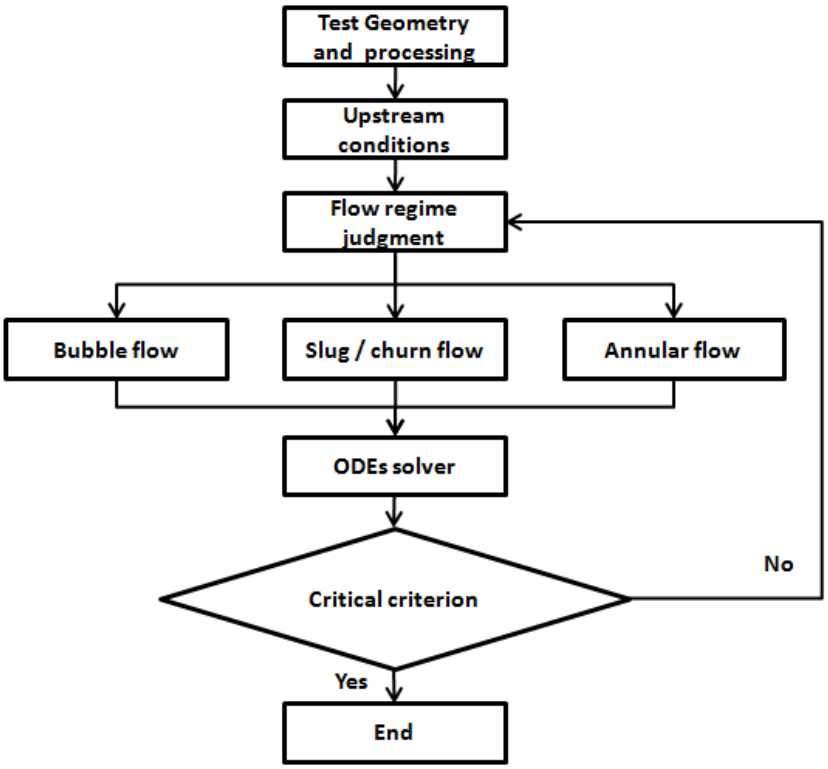

Figure 5.5 Calculation flow chart of NNTPCM

The NIST thermodynamic property data tables[164] were used during solving the system of ODEs. Figure 5.5 shows the flow chart for NNTPCM program.

The critical condition indicating the choking plane was used to terminate the calculation; a very large pressure drop was used as critical condition:

$$\frac{dP}{dz} < C_c \tag{5.51}$$

according to the references[165]. A detailed discussion about the choking criterion will be provided as appendix of the dissertation.

5.3.3.3 Shooting Method for the Inverse Problem

For a given mass flux at the inlet of the discharge pipe, it is not known before calculation where the choking appears. The choked point may be established after a distance shorter or longer than the length of the discharge pipe. Therefore, the initial mass flux should be chosen iteratively until the choked point appears at the end of the discharge pipe, i.e. the boundary condition formulated by Eq. (5.51) is satisfied there.

This is an inverse problem, requiring an inverse solving process to confirm some constitutive parameters of the system of ODEs [166] (Kabanikhin, 2008). The inverse solving process just recalled

above is denoted as shooting method. The shooting has been used by other authors in their studies [167] (Wolfert, 1977, Burtt, 1984) on critical flow and was adopted also for the present work.

The idea of shooting method is to reduce the given boundary value problem to several initial value problems. Roughly speaking, one 'shoots' out trajectories corresponding to different initial mass fluxes until a trajectory has a desired boundary value (according to Eq. (5.51)) at the end of the specified pipe length.

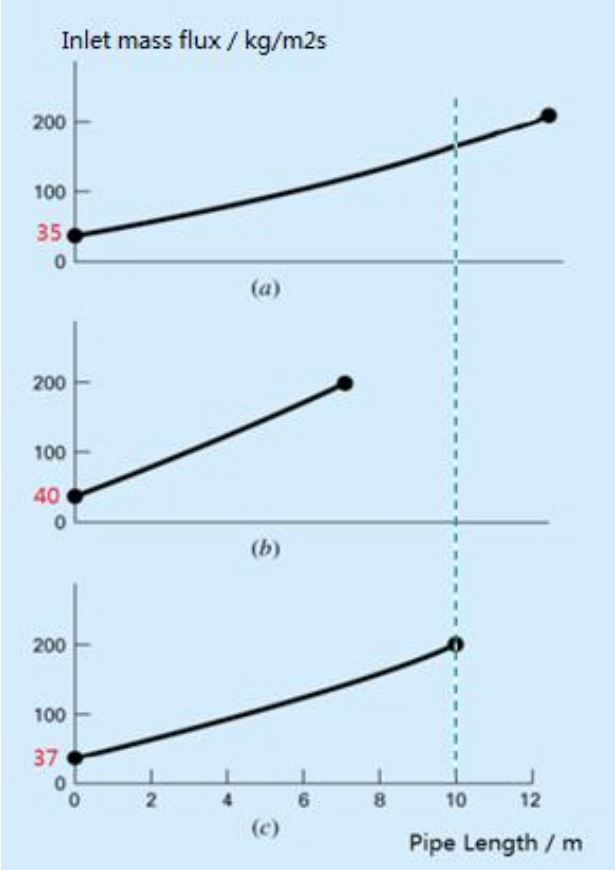

Figure 5.6 Schematic diagram for shooting method

Take Figure 5.6 as an example, assuming L_0 = 10 m is the real length.

(1) Step 1 (Figure 5.6 (a)): for the first shoot, the inlet mass flux is assumed as a small value (35 kg/m^{2}s). A longer critical length L_1 is achieved.
(2) Step 2 (Figure 5.6 (b)): for the second shoot, the inlet mass flux is assumed as a large value (40 kg/m^{2}s). A shorter critical length L_2 is achieved.
(3) Step 3 (Figure 5.6 (c)): according to the results above, a new mass flux value at the inlet is interpolated based on the pipe lengths L_0, L_1, L_2. Use the new value for critical length calculation L_3. If the new length L_3 is between the real length L_0 and L_1, L_3 will replace L_1. Otherwise, L_3 will replace L_2. This procedure is iterated until the real length L_0 is achieved.

The flow chart for shooting method could be clearly described by the Figure 5.7. The convergence criterion of relative error between the real length L_0 and the calculated length is set 10^{-3}.

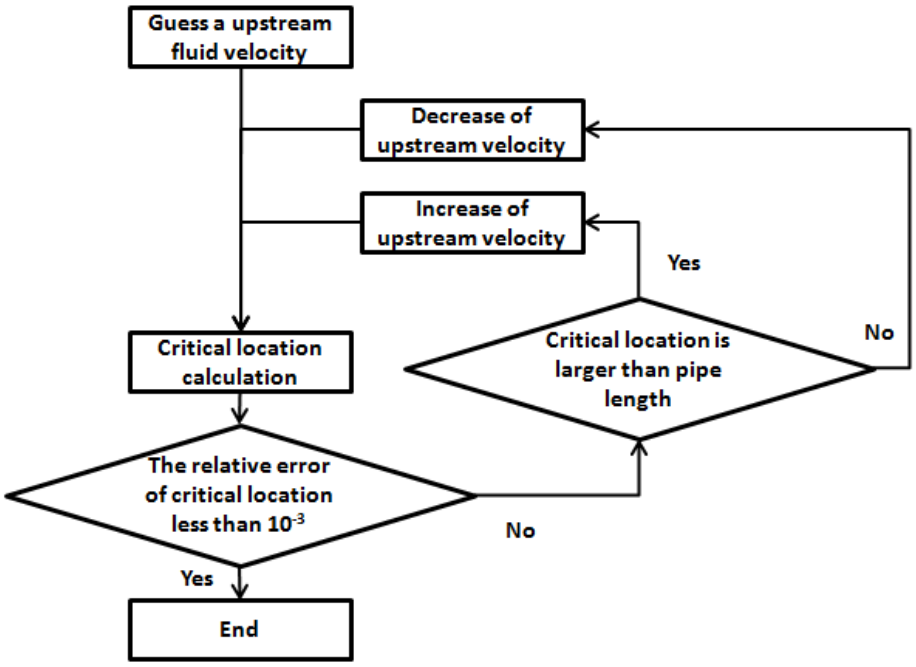

Figure 5.7 Logic flow chart for shooting method

5.4 Validation

5.4.1 Test selected

From the beginning of 1950s, a large number of critical flow experiments have been performed. An interesting listing of some 50 or so references may be found in the NEA report [168]. Most of them were also included in the report of Ilic [169]. After that, in the literature of Elias & Lellouche [124], 66 tests with different lengths, diameters, and pressures were reviewed. There is no need to review them in detail but some of the test information is shown in Table 5.3 as example.

Isbin et al. [170] published the results of their investigation of a two-phase critical flow of steam-water mixtures over a pressure range from 0.275 to 2.96 bar and a quality range from 0.01 to saturated vapor, both evaluated at the critical section. Zaloudek [171] published the results of an experimental study of a critical flow of steam-water mixtures flowing in a long pipe with constant area (diameter 13.2 or 15.8 mm, and lengths up to 1.2 m). The corresponding critical pressure ranged from 0.275 to 0.758 MPa. Henry et al. [172] published data on a steam-water critical flow in long tubes (L/D > 40.0). The mass flux ranged from 2500 to 31540 kg/m^{2}s. The pressure at the critical section was in the 0.275 to 1.034 bar range. Three test sections, all 0.914 m long, were used. Two of them had a circular cross-section with different inlet geometries (test C7 and C120). The third test section had a rectangular cross section (test R7). The data from these three tests were used for the validation of HEM, which revealed the under-prediction of HEM.

Fauske [173] studied experimentally the critical two-phase flow of steam-water mixture at high pressures. Four test sections with different internal diameters and lengths were built for tests. Celata [174] has investigated the critical flow of liquid through orifices with the aim of measuring the time extension of metastable states, due to strong depressurization. An upper limit of these metastable states of the order of 10^{-4}s has been detected. Cruver [175] examined the metastable states in a two-phase, steam-water critical flow. Simultaneous measurements of pressure and temperature were used to determine deviations from the thermodynamic equilibrium. Sozzi and Sutherland [176] published the results of critical flow rate and pressure ratio measurements for saturated and subcooled water. Tests

were conducted with seven different flow nozzles. The tests were conducted by blowing down a vessel, from an initial fluid pressure of 6.9MPa with the discharging fluid temperature between 232 and 287 °C. The results demonstrated the importance of the thermal non-equilibrium effect on flow fields with a length of less than 0.127 m. The data showed that the critical two-phase flow at high pressures and low qualities is strongly dependent upon upstream (stagnating) conditions. This dependence decreases with an increase in the flow field length. The strong effect of the tube length on the critical flow rate was attributed to the thermal non-equilibrium between the two phases.

Ardron and Ackerman [177] studied the critical flow of subcooled water in a pipe. Experiments were performed using pipes of 25 mm nominal diameter and 1.0 m long. Pressures at the inlet to the test section were up to 3.5 bar and temperatures were up to 140°C. A non-equilibrium two-fluid model has been used for comparison with the test data. The pressure and void fraction profiles were met well with the test data, but predicted bubble growth rates and the bubble number densities were not in agreement with the observations. The discrepancies were attributed to the role of convective heat transfer in bubble growth and the deficiencies in the existing models of heterogeneous nucleation.

Table 5.3: Brief review of Critical Flow tests

Researcher	Length / m	Diameter / mm	Pressure / MPa	Critical mass flux / kg/m^{2}s
Isbin		6.35-25.4	0.0275- 0.296	
Zaloudek	1.2	13.2-15.8	0.275-0.758	488-4882
Henry	0.914	3.32	0.275-1.034	2500-31540
Fauske	1.428-2.794	3.17-12.25	0.275-2.068	2440-21000
Celata	0.001	1.25	0.95-1.7	28485-39740
Cruver	0.609	13	0.1-0.28	432-6146
Sozzi and Sutherland	0.05-0.72	12.7-76.2	6.9	-
Ardron and Ackerman	1.0	25	<0.35	5000-14000
Al-Sahan	0.127-0.635	3.175	0.4-1.4	1840-5175
Abdollahian et al.	0.3-1.8	200-500	2.5-5.0	-

Al-Sahan [178] studied the critical flow of initially subcooled water in long tubes with a range of stagnation pressures from 0.4 to 1.4 MPa, stagnation temperatures from 127 to 190 °C. The critical mass flow rates, the critical pressure ratios and the axial pressure profiles were measured for each test section, under different stagnation conditions. The results compared with non-equilibrium two-fluid model showed that the pressure profile, the critical mass flux and the critical pressure ratio are strongly dependent on the stagnation pressure and temperature, at constant (L/D).

Abdollahian et al. [179] reported the results of the Marviken full scale critical flow tests. These are among the few experiments which provided two-phase critical flow data at a scale comparable to the nuclear reactor size. A total of 27 tests were carried out in this project. The parameters which were varied included the nozzle diameter, from 0.2 to 0.5 m, the nozzle length, from 0.3 to 1.8 m, and the initial sub-cooling, from 0 °C to 30 °C. The stagnation pressure ranged from 2.5 to 5.00 MPa.

The range of critical mass flux ranges from less than 2000 kg/m^{2}s, for which the NNTPCM is expected to be more precise, to more than 3000 kg/m^{2}s, for which the CDR1D model should be better. The data from the above-mentioned Celata test, Henry test, Sozzi and Sutherland test, Al-Sahan test, and Marviken full scale facility will be considered in this study.

As discussed above, the new 6-equation CFM requires many assumptions, approximations, and several closure laws. Therefore, its use in the framework of ATHLET for nuclear safety analysis needs an assessment process to ensure the capacity to simulate transient scenarios with a sufficient degree of reliability and accuracy. As a universal model development procedure, the two relevant aspects that have been identified for the assessment strategy are: Verification and Validation (V&V).

V&V are a crucial part in a code or model development and assessment processes. Verification is a process to assess the code correctness and numerical accuracy of the solution of a given mathematical model, defined by a system of differential or integral equations derived from the physical reality. In other words, verification is performed to demonstrate whether the equations are correctly solved by the code. In the case of the validation process, the aim is to quantify the accuracy of the model through comparisons of experimental data with simulation outcomes from the computational model.

Since the basic numerical solution scheme is based on MATLAB ordinary differential equation toolbox, there is no need to verify the toolbox. In this section, test data from five test facilities were used only for the validation of NNTPCM. Validation is a key step in the field of thermal hydraulic models and plays a crucial role in the implementation of system codes or models.

There are different kinds of discharge pipes, with different pressure ranges, geometries etc. In order to test the model effectively, it was necessary to use typical experiments for validation. Although a large collection of experimental data on critical discharge flow was reported in the literature, experiments with detailed geometry description and measurements of the axial distribution of flow parameters along the test section are rare. Based on the literature, Schwellnus and Al-Sahan tests **[180]** (long pipe discharge), Celata test (nozzle discharge), Dobran test (long pipe discharge), Sozzi–Wutherland tests (short pipe discharge) and Henry tests **[181]** were chosen. The results from Schwellnus model were also introduced, for comparison. They used different kinds and shapes of discharge pipes.

5.4.2 Critical process analysis

Before validation, two items about critical process will be discussed firstly in this section.

5.4.2.1 The convergence process of ODEs solution

NNTPCM will be validated on different test geometries, from nozzle to long pipe. Since the choking processes for different geometries (long pipes, short pipes or nozzles) are quite similar (scalable), the choking process study in this section will only focused on two extreme L/D cases: a test of Al-Sahan and a test of Celata with the initial upstream pressures of 1 MPa and 0.95 MPa, respectively. The test of Al-Sahan focused on the critical flow for long straight pipe and that of Celeta on orifice critical flow. Their lengths of the test discharge pipes are 0.635 m and 0.001 m, respectively. The diameter in Al-Sahan test was 0.003175 m, which makes a large length-to-diameter ratio (L/D = 200), and 0.00125 m in Celata test (L/D = 0.8). The inlets of the discharge pipes were considered with a converging geometry. The results displayed in this sub-section were obtained with a pressure gradient criterion at -2×10^{12} Pa/m.

Figure 5.8 shows the convergence trends of the calculations corresponding to the tests of Al-Sahan and Celata. The horizontal axis represents the serial step number of the calculation point and the vertical axis represents the corresponding step length. Both of them were automatically generated using the implicit Runge-Kutta scheme. The total step numbers are very large compared to the non-critical flow, 1343 and 600 steps for Al-Sahan and Celata tests, respectively. Since Al-Sahan test corresponds to a long pipe geometry, it requires more steps to converge. Both curves are serration-shapes because of the algorithm of the Runge-Kutta method. Each step of the Runge-Kutta method will try the old step size as long as it may converge, otherwise a smaller step size will be tried. The step sizes are overall

decreasing along the discharge pipe. As mentioned earlier, the ODEs for two-phase non-equilibrium critical model are stiff, which make both of the step sizes at the critical points less than 10^{-10} m.

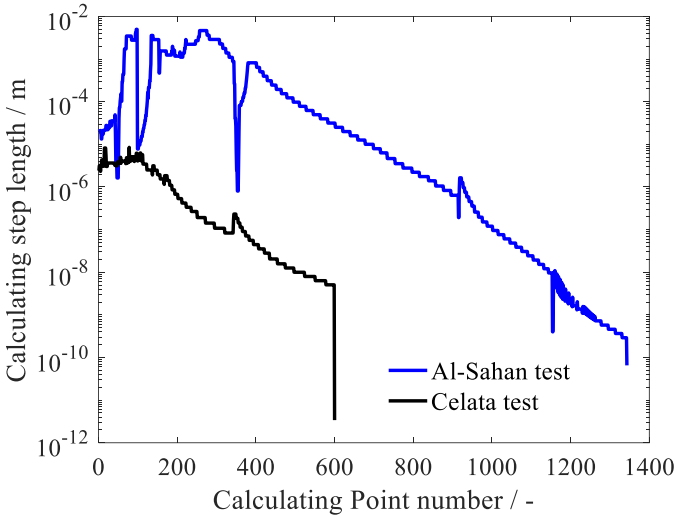

Figure 5.8: Calculation step size during choking process.

5.4.2.2 Choking Criteria Comparison

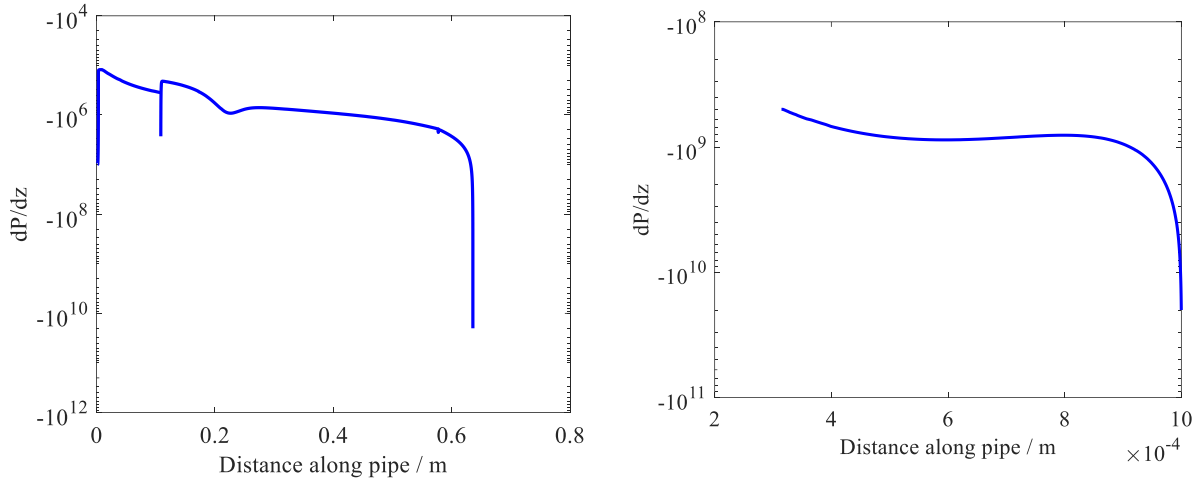

(a) Al-Sahan test

(b) Celata test

Figure 5.9: Pressure gradient changes during choking process.

According to the discussion about the choking criteria, they are equivalent when the pressure gradient is approaching infinity. From the numerical point of view, “infinity” means a very large number. In this section, the trends of pressure gradient and the determinant of coefficient matrix will be given firstly since they are the basics for criteria. After that, the comparison of the criteria will be discussed.

Figure 5.9 shows the pressure gradient changes along the pipeline during the discharge for both Al-Sahan and Celata tests. Compared with the near inlet upstream range, the pressure gradient variation becomes then much sharper. At the pipe end the flow becomes choked, satisfying the pressure gradient choking criterion (-2×10^{12} Pa/m). This gradient value is continuous for Celata test. But it is not continuous for Al-Sahan test due to the calculation instability caused by the different constitutive relationships owing to the flow regime transformation.

In order to show the variation of determinant $|\boldsymbol{A}|$, we use the relative value ($|\boldsymbol{A}|/|\boldsymbol{A_0}|$, where $|\boldsymbol{A_0}|$ is the determinant for initial condition). Figure 5.10 shows changes of relative value $|\boldsymbol{A}|/|\boldsymbol{A_0}|$ along the discharge pipeline during the choking process. The step sizes of ODEs around the choking point, when determinant criterion was used, were smaller than 10^{-15}m (which approaches the minimum value of ODEs allowed step size). It could be noticed that $|\boldsymbol{A}|/|\boldsymbol{A_0}|$ (also $|\boldsymbol{A}|$) is approaching 0.0 when the flow becomes choked. The discontinuous values in Al-Sahan test are caused by the flow regime transformation, making use of different constitutive relationships.

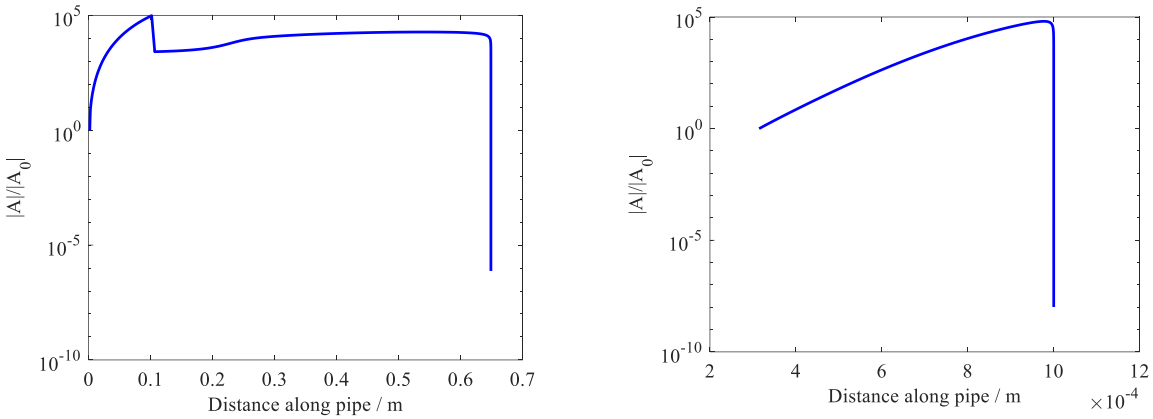

(a) Al-Sahan test (b) Celata test

Figure 5.10: Relative determinant value changes during choking process.

According to the discussion above, it could come to a conclusion that the results of NNTPCM reflect the trend of pressure gradient and determinant as the derivation of choking theory and now come to the discussion of pressure gradient selection as choking criterion.

In the literature, some authors used the determinant criterion. But most of the authors used the pressure gradient criterion for the judgment of choked flow and as termination criterion of the ODEs calculation. But they had different understanding on the critical pressure gradient, by using different threshold values. Ardron, Ewan and Dagan chose -5×10^9 Pa/m as the threshold value[182][183]. Richter and Javidmand chose -10^{10} Pa/m [184]. Schwellnus chose -2×10^{10} Pa/m. I did not find any motivation in literature for the choice of these particular values.

Therefore, I focused myselves on the impact of different thresholds values (of the pressure gradient criterion) on the results of critical flow rate obtained from the ODEs calculation. The impact was explored on all of the above-mentioned test facilities: Al-Sahan test with L/D=200 at 1.0 MPa, Dobran test with L/D=97 at 2.33 MPa, Sozzi - Wutherland test with L/D=3.5 at 6.34 MPa and Celata test L/D=0.8 at 0.95 MPa.

As shown in Figure 5.11, different threshold values were used in the pressure gradient criterion: from -4×10^4 to -2×10^{10} Pa/m for Al-Sahan test, from -8×10^5 to -2×10^{10} Pa/m for Dobran test, from -2×10^7 to -2×10^{10} Pa/m for Sozzi - Wutherland test and from -2×10^8 to -2×10^{10} Pa/m for Celata test; the threshold values on the x-axis have been considered as absolute values (in reality, they are negative). The relative deviations (relative errors) of the calculations (made using the pressure gradient criterion PGC or the determinant criterion DC) with respect to the test (experimental) ones are represented on the y-axis. It is obvious that, if the pressure gradient threshold (absolute) value is too small, the relative error is strongly negative as the calculated critical mass flows are much smaller than the

experimental ones. With the increase in the pressure gradient threshold (absolute) value, the calculated critical mass flow will increase. But if the threshold absolute value of the pressure gradient is larger than 2×10^7 for Al-Sahan and Dobran tests (long pipes), 1×10^9 for Sozzi - Wutherland test (short pipe) or 2×10^9 for Celata test (orifice), the relative error nearly keeps constant. It is because of the large pressure gradient around the choking point. Even if the pressure gradient changes, the mass flow remains insensitive to it. Furthermore, one may come to the conclusion that a larger pressure gradient threshold (absolute) value has to be introduced for the calculations of short pipes or orifices by comparison with the case of long pipes. In other words, if the two-phase flow remains closer to homogeneous equilibrium flow, a smaller (absolute) pressure gradient threshold is allowed, but for the two-phase flow where strong non-homogeneity and non-equilibrium arise, a larger (absolute) pressure gradient threshold have to be considered. According to the results, one may conclude that all the values above-mentioned, chosen as thresholds for the critical pressure gradient criterion, were particularly suitable.

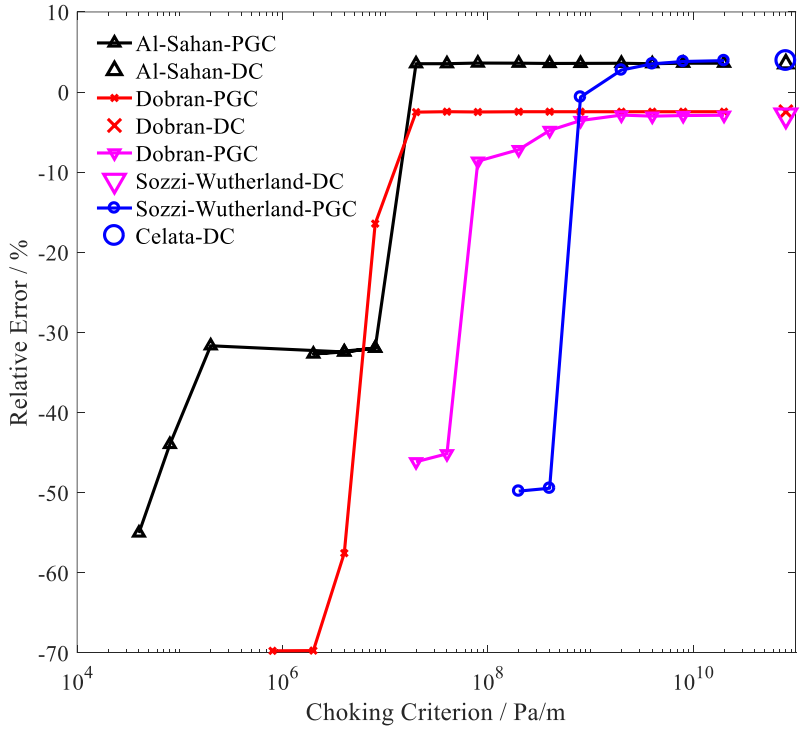

PGC: Pressure gradient criterion; DC: Determinant criterion.

Figure 5.11: Comparison of the two choking criteria.

At its upper-right corner, Figure 5.11 shows the relative errors by using the determinant criterion for the calculations corresponding to the two test cases. It is not unexpected that the results are consistent with the results using pressure gradient criterion. The difference between these two criteria is as small as 0.1%.

5.4.3 Results of Validation

For the validation, $C_c = -2.0 \times 10^{10}$ is chosen as the choking criterion.

5.4.3.1 Al-Sahan test

Al-Sahan tests were long straight pipe tests (in Figure 5.12). Al-Sahan obtained his data for critical discharge for long straight pipe (L/D = 200) with saturated inlet liquid in the pressure range 0.196 to 1.00 MPa, as shown in Table 5.4.

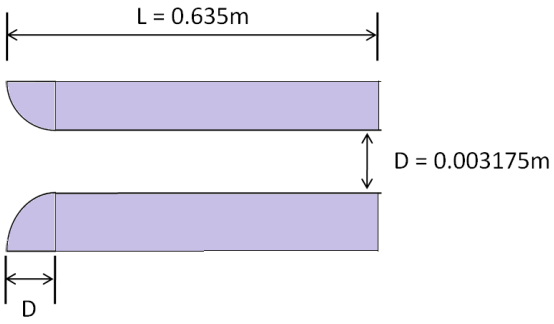

Figure 5.12: Geometry of Al-Sahan test section

Table 5.4: Information of the Al-Sahan tests

Data by	Length L / m	Diameter D / m	Shape	Pressure / MPa
Al-Sahan	0.635	0.003175	straight pipe	0.196
				0.300
				0.497
				0.703
				1.000

The critical mass flux data is the most crucial result to be delivered from the calculation. Although the other primary variables are of interest, only the critical mass flux would be considered for a subsequent computation, being used as source term for safety calculation and risk assessment in most applications[185]. The present model was compared with test data on critical flow as well as ATHLET CDR1D model and Schwellnus's calculated results, as summarized in Table 5.5. According to Table 5.5, the error of present model is between -7% and +4% in predicting the Al-Sahan test data, obviously better than ATHLET CDR1D model results in the range of -43% to 14% and Schwellnus's results in the range of -10% to 11%. The critical mass flux is under-predicted by the CDR1D model, in particular, at lower mass flux, presumably due to the missing slip ratio. It has to be noted that, for two low pressure cases of Al-Sahan tests, not only Schwellnus model but also the present model slightly under-predict the test data. This would be not acceptable from the point of view of the conservative safety analysis. Anyhow, the present model has a better prediction capability and can be implemented into STH codes with the mentioning of some slight tendency of underestimation of the critical flow in the small pressure range.

Table 5.5: Comparison of Al-Sahan test data with different CFMs

Pressure / MPa	Critical Flow of Test / kg/m²s	CDR1D model		Schwellnus Model		Present Model	
		Critical Flow / kg/m2s	Error / %	Critical Flow / kg/m²s	Error / %	Critical Flow / kg/m²s	Error / %
0.196	2426	1385	-42.9	2240	-7.666	2295	-5.385
0.300	2943	1887	-35.9	2675	-9.106	2742	-6.844
0.497	3364	2639	-21.5	3380	0.475	3403	1.149
0.703	4205	3466	-17.5	4400	4.637	4243	0.904
1.000	5175	4439	-14.2	5700	10.144	5352	3.427

The other primary variables of interest were also compared. As examples, Figure 5.13 and Figure 5.14 show Al-Sahan's measured axial pressure distribution compared with Schwellnus's model predictions and those of the present model for the stagnation pressures of 0.479MPa and 1.00MPa, respectively. The present model is in excellent agreement with Schwellnus's results and also with the measured profiles. The pressures at the inlet do not change too much because of the low velocities of the two

phases. At the end of the pipe, the pressures are larger than ambient ones and their derivatives approach infinity for both tests; they are choked before discharge to the surroundings.

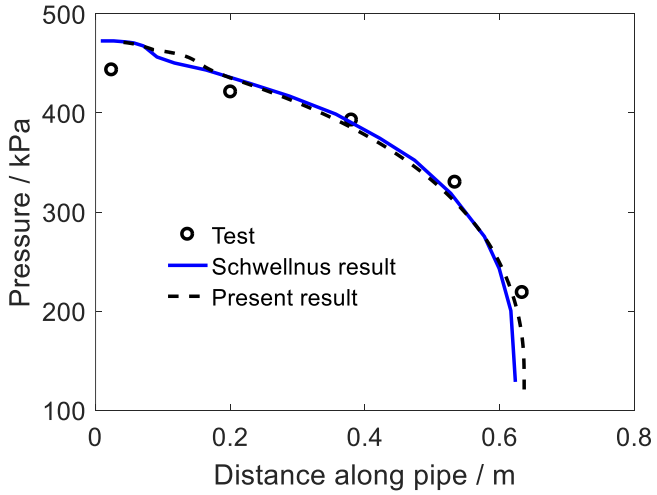

Figure 5.13: Comparison on axial pressure distributions for the Al-Sahan test at 0.479 MPa.

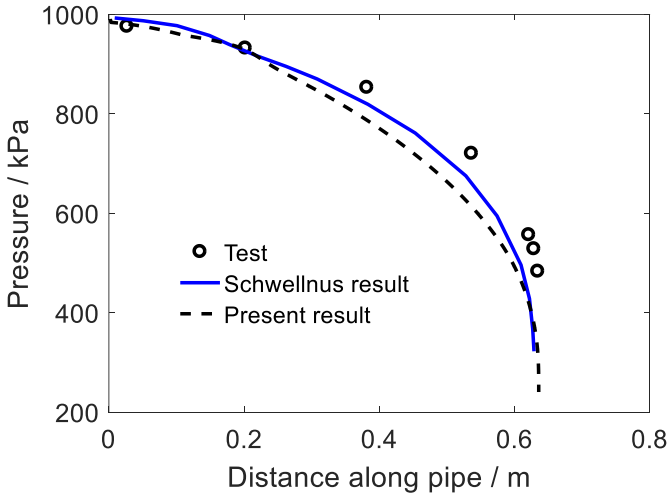

Figure 5.14: Comparison on axial pressure distributions for the Al-Sahan test at 1.00 MPa.

5.4.3.2 Celata test

The Celata test studied the critical flow through orifice. The length of the nozzle is 1 mm and the orifice diameter is 1.25 mm (length to exit diameter ratio of 0.8). The orifice geometry of Celata critical discharge experiment was a rounded entrance as shown in Figure 5.15. The pressure of the chosen test was 0.95 MPa. The predicted flow regime was bubbly flow. The present model was compared with test data on critical flow as well as ATHLET CDR1D model and Schwellnus's calculated results, as summarized in Table 5.6.

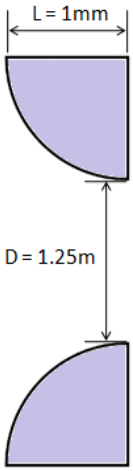

Figure 5.15: Geometry of Celata test section

Table 5.6: Comparison of Celata test data with different CFMs

Pressure / MPa	Critical Flow of Test / kg/m²s	CDR1D model		Schwellnus Model		Present Model	
		Critical Flow / kg/m2s	Error / %	Critical Flow / kg/m²s	Error / %	Critical Flow / kg/m²s	Error / %
0.95	28485	35855	25.9	31000	8.8	29600	3.9

The critical mass flux for Celata test was 28485 kg/m^{2}s. The result of ATHLET CDR1D model was 35855 kg/m^{2}s (relative error was 25.9%). Schwellnus got a result of 31000 kg/m^{2}s (relative error was 8.8%). But the calculated result for present model is 29600 kg/m^{2}s (relative error is 3.9%). Furthermore, it should be noted that Schwellnus has adapted (with some pipe-like prolongation) the geometry of the discharge orifice to get the result. The present NNTPCM model got a closer result (with a relative error of 3.9%) compared to the above-mentioned two models, even though the mass flux is far outside its limit of 3000 kg/m^{2}s.

5.4.3.3 Dobran test

Dobran tests were based on a long straight pipe test facility (Dobran, 1987). The information of the chosen tests are provided in Table 5.7. In this section, three tests with different upstream pressure values were chosen for the NNTPCM verification. The discharge pipe diameter is 0.0125 m, for which the pipe length could be 1.21 m or 3.6 m, with a rounded entrance, as shown in Figure 5.16. Dobran obtained his data for critical discharge for long straight pipe (L/D = 97 or 288, respectively) with saturated inlet liquid in the pressure range from 2.23 to 3.49 MPa.

Table 5.7: Information of the Dobran tests

Data by	Shape	Diameter D / m	Length L / m	Pressure / MPa
Dobran	Long pipe	0.0125	1.21	2.23
			3.60	2.58
				3.49

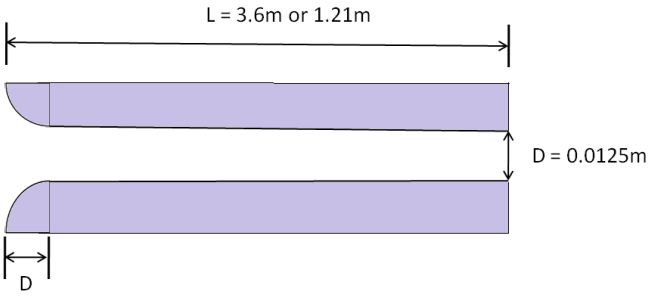

Figure 5.16: Geometry of Dobran test section

The present model was compared with the test data on critical mass flow provided by the Dobran tests, with prediction capabilities of ATHLET CDR1D model and Schwellnus model as summarized in Table 5.8. According to Table 5.8, ATHLET CDR1D model underestimated the critical flux (the relative errors in the range from -17.6% to -22.4%) and Schwellnus model overestimated the critical flux (the relative errors in the range from 0.05% to 19.9%). Two errors of the present NNTPCM model are between -3% and +4% excepting for one with an overestimation of +15.66%. Anyhow, this overestimation is smaller compared with other similar model in literature, with a corresponding overestimation at 19.9%.

Table 5.8: Comparison of Dobran test data with Schwellnus model and present model

Pressure / MPa	Critical Flow of Test / kg/m^{2}s	CDR1D model		Schwellnus Model		Present Model	
		Critical Flow / kg/m2s	Error / %	Critical Flow / kg/m^{2}s	Error / %	Critical Flow / kg/m^{2}s	Error / %
2.23	11155	8648	-22.4	11160	0.05	10882	-2.45
2.58	9080	6829	-24.8	9780	7.7	9408	3.61
3.49	10090	8310	-17.6	12100	19.9	11670	15.66

5.4.3.4 Sozzi-Wutherland test

The Sozzi-Wutherland test was based on pipes or orifices with different shapes. They have been used for several researches, comparing with the CFMs developed by them, e.g. Richter, Schwellnus. One of the geometries was used in this section for verification of NNTPCM. It was a short pipe (or called nozzle, length 44 mm) with rounded entrance (inlet diameter 43 mm, outlet diameter 12.7 mm), as shown in Figure 5.17.

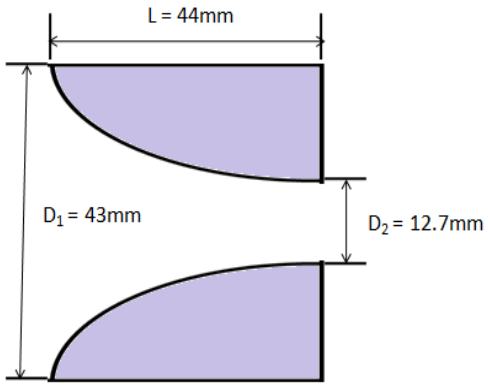

Figure 5.17: Geometry of Sozzi-Wutherland test section

The upstream pressure is 6.34 MPa. The critical flow in test is 61000 kg/m^{2}s. The calculated value for this test is 59240 kg/m^{2}s, i.e. the relative error is -2.89% (shown in Table 5.9), which is better than the result of ATHLET CDR1D model, even though the critical mass flux is far too high for the NNTPCM.

Table 5.9: Comparison of Sozzi-Wutherland test data with different CFMs

Pressure / MPa	Critical Flow of Test / kg/m^{2}s	CDR1D model		Schwellnus Model		Present Model	
		Critical Flow / kg/m2s	Error / %	Critical Flow / kg/m^{2}s	Error / %	Critical Flow / kg/m^{2}s	Error / %
6.34	61000	73021	19.7	-	-	59240	-2.89

5.4.3.5 Henry experiment

The Henry experiment facility for critical flow data comprised heater, blow-down vessel, test section and so forth. The facility was filled with demineralized water at 21℃. The water was circulated through the 85-kW electrical heater under sufficient pressure to retain a liquid state throughout the facility. This procedure continued until the water in the blow-down vessel attained the required temperature. The experimental run was taken by opening the valve to the test section while pressurizing the vessel with nitrogen from the top. The nitrogen was supplied at a sufficient rate to maintain a constant vessel pressure, greater than the corresponding saturation pressure, thereby ensuring a liquid state in the vessel. There were three test sections, with different geometrical configurations, in Henry experimental investigation. As an example, the test section C120 (in Figure 5.18) is chosen for validation.

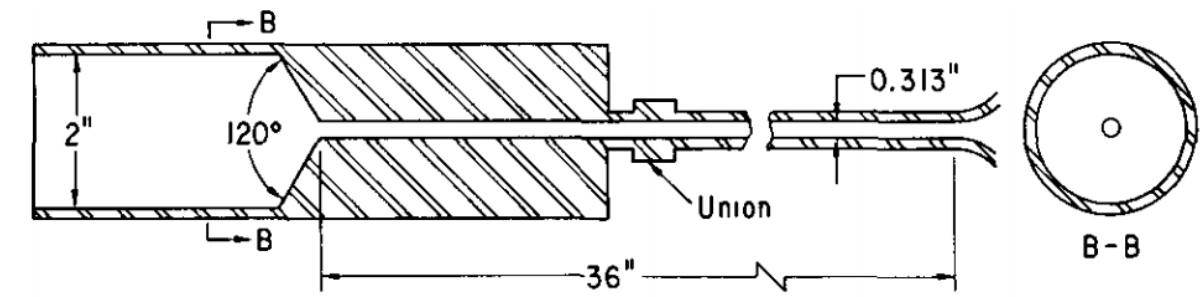

Figure 5.18: Test section C120 of Henry experiment

The test section C120, which contained 19 tests including 9 subcooled and 10 saturated inlet conditions, as shown in Table 5.10, were chosen for the validation in this study. The authors chose all of the test data without any result optimization. The thermo-hydraulic parameters are the upstream liquid pressure ranging from 0.538 to 1.060 MPa and the upstream liquid sub-cooling ranging from 0 to 21.16 ℃. The nozzle has a length of about 761.7 mm.

To validate the ATHLET potential critical flow model with NNTPCM, the obtained results were compared with experimental data extracted from the trials of Henry. Numerical results of the model were compared with three models in ATHLET, including HEM, Moody model and CDR1D model, which have been described in detail in the section 5.2.3.

From Henry's data, four magnitudes are especially significant for this work: liquid inlet parameters (the pressure and temperature), critical flow mass flux, and pressure profiles with void fraction traversing for the nozzles.

Table 5.10: C120 test section of Henry critical flow experiment

Test num	Pressure / MPa	Temp. / ℃	ΔT / ℃
1	0.669	150.10	-12.98
2	0.855	173.20	0.00
3	0.979	179.00	0.00
4	0.952	177.70	0.00
5	1.060	182.20	0.00
6	0.710	165.50	0.00
7	0.676	158.50	-5.04
8	0.565	153.00	-3.50
9	0.607	154.10	-5.18
10	0.559	152.90	-3.19
11	0.538	151.00	-3.63
12	0.593	157.40	0.00
13	1.030	181.10	0.00
14	0.607	159.30	0.00
15	0.579	147.70	-9.73
16	0.600	147.70	-11.15
17	0.690	163.70	0.00
18	0.586	148.40	-9.49
19	0.738	145.90	-21.16

Figure 5.19 (a) and Figure 5.19 (b) summarize and compare the numerical results of HEM, Moody model, CDR1D model and NNTPCM with respect to the critical mass flux test data, considering the subcooled upstream conditions and saturated upstream conditions, respectively.

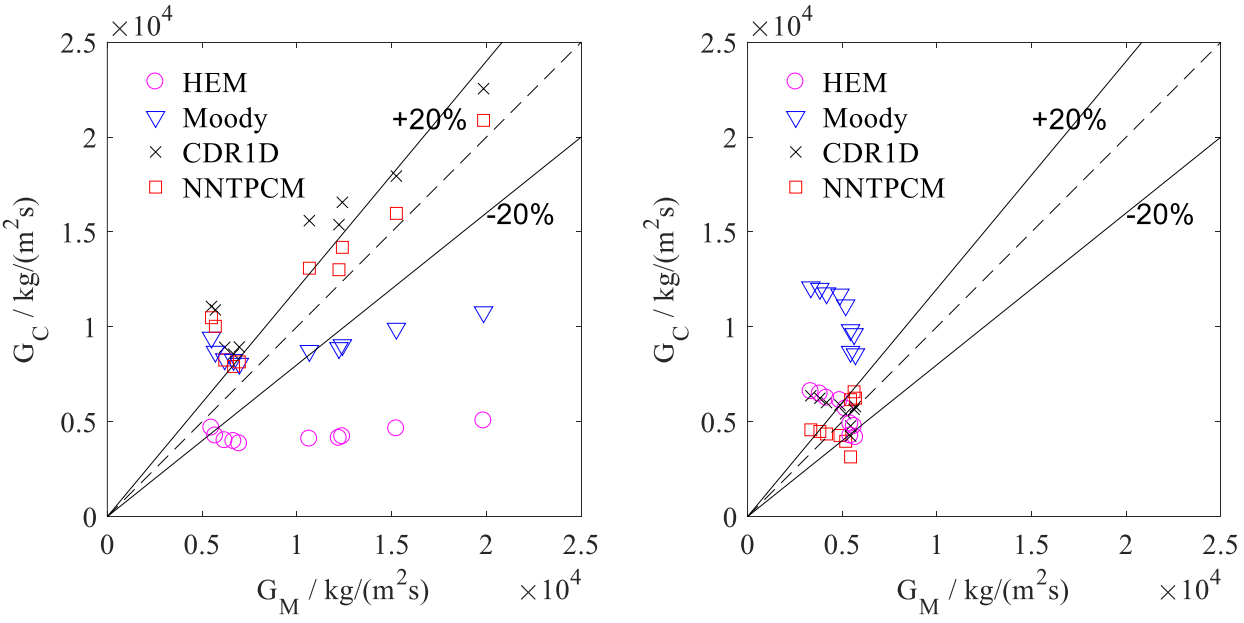

(a) Subcooled upstream conditons (b) Saturated upstream conditions

Figure 5.19: Predictions of critical mass flux with respect to Henry experimental data

For subcooled conditions, the relative larger test values mean deep subcooled conditions (larger than 10 ℃) and smaller values mean shallow subcooled conditions (less than 10 ℃). According to Figure 5.19, HEM underestimated the critical mass fluxes while CDR1D model and NNTPCM overestimated the results. Moody model overestimated the results for shallow subcooled conditions but overestimated for deep conditions. Regarding to saturated conditions, Moody model overestimated the results and other three models underestimated or overestimated the results. Table 5.11 shows the mean error (absolute value) for critical mass flux for different models. It shows that NNTPCM could predict the mass flow better than other chosen models of ATHLET.

Table 5.11: Absolute mean error for critical mass flux with respect to Henry experimental data

Model Abs. mean error	HEM	Moody	CDR1D	NNTPCM
Subcooled conditons	0.4979	0.3513	0.4306	0.2894
Saturated conditions	0.3621	1.3054	0.2879	0.1959
Total	0.4336	0.8032	0.3630	0.2451

In order to reveal the pressure profile along the discharge pipe, several pressure points along the discharge pipe were set for measurement. It is assumed that the upstream pressure is at z=0 and the pressure measure point is set at 0.381 m, 0.6096 m, 0.6922 m, 0.7239 m, 0.7492 m, 0.7612 m, 0.7617 m (the end of the discharge pipe, i.e. the choking point). The measure points were set more and more crowded when it was closer to the choking point since the pressure deviation was very high there. Figure 5.20 (a) and Figure 5.20 (b) show the prediction results of pressure profiles using NNTPCM with respect to test 1 and 2, which are typical subcooled upstream condition and saturated condition, respectively. Similar prediction results could be obtained in other test conditions. Comparing the pressure curves, it appears that there was a significant inflection point for the pressure deviation (sharp decrease) for subcooled conditions while the curves of saturated condition remained much smoother.

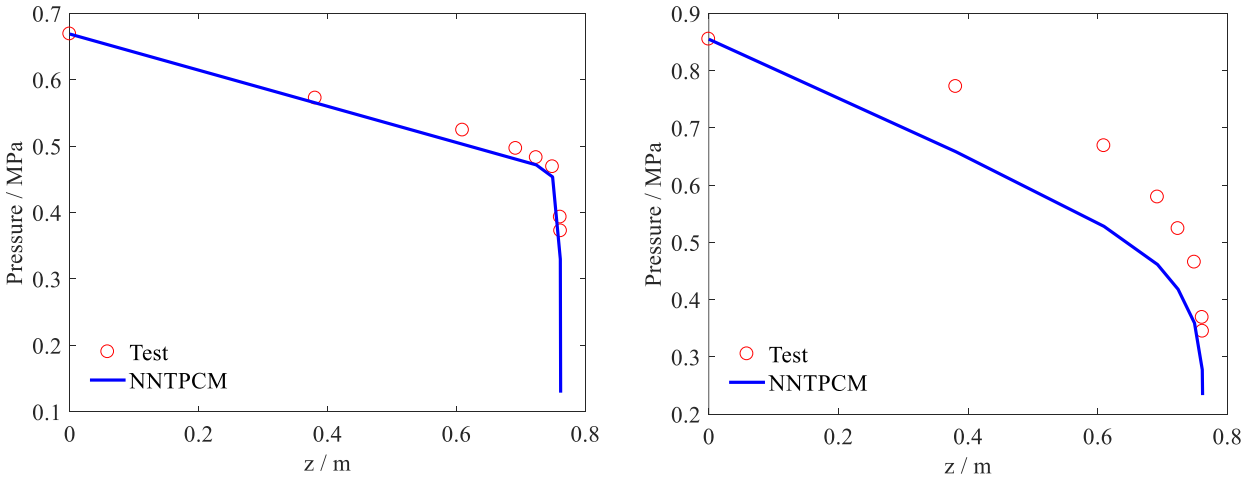

(a) Test 1 (subcooled upstream condition) (b) Test 2 (saturated upstream condition)

Figure 5.20: Typical calculated pressure along the pipe using NNTPCM for Henry test

According to the results of Figure 5.20 (a), NNTPCM could predict the pressure drop along the pipe quite well, except the choking point when the upstream fluids were in subcooled condition. At the choking point, NNTPCM delivered a lower choking pressure. This is expected from the theory of critical flow: the pressure gradient around choking point should approach the negative infinity. In

other words, the choking point is theoretically a singular point for sound speed propagation, which is very different to achieve or be measured in reality. On the contrary, for Figure 5.20 (b), the pressure profiles along the pipe for saturated conditions were a little bit underestimated by NNTPCM. It means that NNTPCM reproduces differently the two-phase interaction along the discharge pipe. This discrepancy may be caused by the bubble growth process along the pipe, especially the determination of flashing point, which will be studied in details further.

Figure 5.21 could be resorted to for more detailed comparison of pressure at each measured point of pressure along the discharge pipe. Most of the calculated values were within the range of ±20% band, except the values around the exits (choking points). This means the NNTPCM could repeat the pressure profiles well besides the critical mass flux. Furthermore, at the first half of the discharge pipes, both the measured pressures and the calculated pressures by NNTPCM are scatted. But at the other side of the discharge pipe (choking point), measured pressure values and the calculated pressure values have different characteristic. All of the measured pressure values were approaching to 0.35MPa, which means the choking pressures were nearly the same in the tests, which the calculated choking pressures were scatted and different from each other. This discrepancy is owing to the measurement accuracy of the pressure. According to the theory of critical flow, the choking pressure should be achieved when the fluid is closer and closer to the choking point. But around the choking point, the pressure deviation is so sharp that even an unlimited small amount *dz* could lead to significant changes of pressure. But the problem is that the measuring could not approach in reality the choking point asymptotically being impacted by the system accuracy at measuring points. This is the reason why the measure pressures approached to a relative higher constant pressure but the calculated pressures did not.

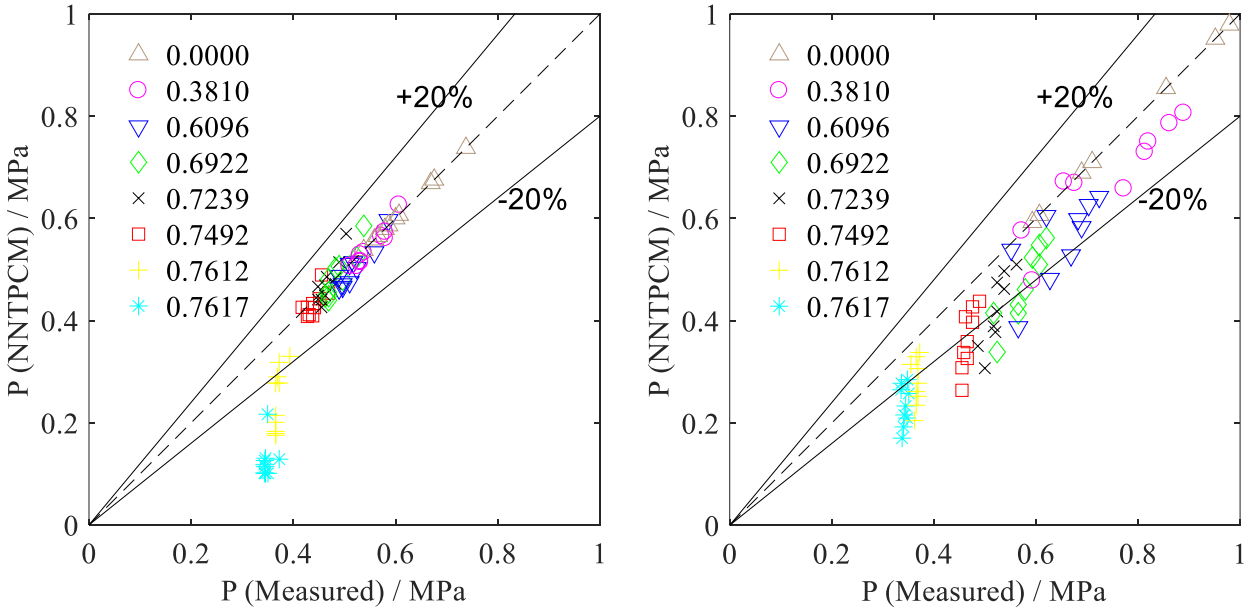

(a) Subcooled upstream conditions (b) Saturated upstream conditions

Figure 5.21: Predictions of pressure profiles using NNTPCM for Henry test

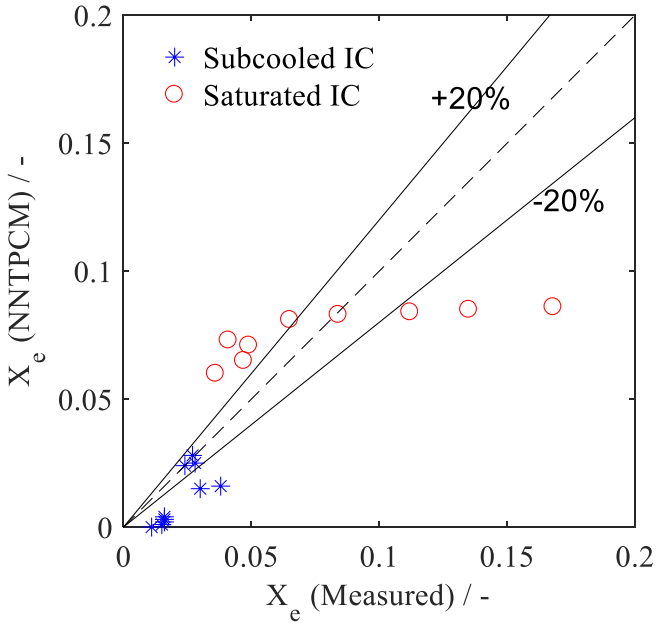

Figure 5.22: Predictions of choking qualities using NNTPCM for Henry test

Figure 5.22 shows the NNTPCM calculated exit qualities (choking qualities) of Henry experiment compared with the measured data. The qualities were smaller for subcooled upstream conditions and comparing with saturated condition since the flow regimes for subcooled condition did not develop fully along the pipe before choking points. Both the calculated and measured choking qualities for saturated upstream conditions have big uncertainties caused by sharp pressure deviation and interfacial interactions. Furthermore, the calculated values could be smaller or larger values comparing with test values.

5.5 In-depth analysis of critical flow process

Furthermore, this work focused on the behavior of the critical flow process, aspect with little payed attention in other previous studies from literature. The process behavior analysis was very helpful for a better understanding of the critical flow phenomenon.

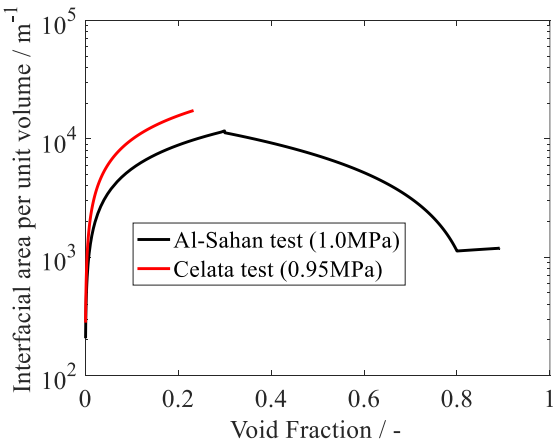

Figure 5.23: Interfacial area per unit volume v.s. VF for Al-Sahan and Celata tests

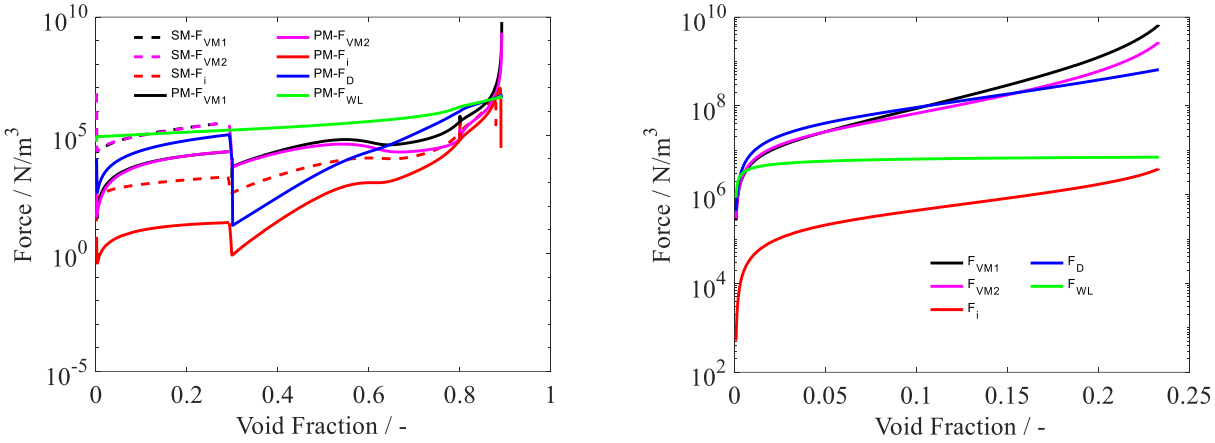

(a) Al-Sahan test at 1.00 MPa (b) Celata test at 0.95 MPa

Al-Sahan (PM-present model, SM-Schwellnus model) and Celata (present model, only)

Figure 5.24: Model forces versus void fraction for Al-Sahan and Celata tests

Since all of the non-equilibrium models are based on the six conservation equations of mass, momentum and energy for the liquid and vapor phases separately, the differences come out from the constitutive correlations. Therefore, the modeling of the choking process is strongly influenced by the built-in correlations. Since the constitutive correlations are selected by the different flow regimes, void fraction was chosen as the independent variable on the x-axis for graphical representations involving the constitutive parameters, as used (generated) in the present model.

As shown in Figure 5.23, in the range of the bubbly flow the interfacial area increases sharply since the bubbles grow up in this flow regime. But in annular flow the interface between the two phases was considered as a cylinder making the interfacial area much smaller then at the end of the bubbly flow regime and it nearly keeps constant. It has to be stressed here that there is no difference between my model and that of Schwellnus with respect to interfacial area.

In the two phase momentum conservation Eq. (5.9) and (5.10), the wall friction of liquid F_{WL}, the drag force F_D, the virtual mass force F_{VM} (F_{VM1} for vapor velocity change and F_{VM2} for liquid velocity change, $F_{VM} = F_{VM1} - F_{VM2}$) and the force for interfacial momentum transport F_i (since $\eta = 0.5$, $F_{Li} = F_{Gi}$=F_i) were considered. Their changing processes are displayed by Figure 5.24. Since the present work used different virtual mass force and different force for interfacial momentum transport compared with the Schwellnus model, the values of these forces in Schwellnus model are also displayed by Figure 5.24. For Schwellnus model, virtual mass force F_{VM} was only considered in bubbly flow. In other words, it did not impact the behavior at the choked point. For the present work, all forces have upward trends during discharge except for the flow regime transformation from bubble to slug/churn flow. The liquid wall friction and drag forces are the leading forces before the fluid is choked. The force for interfacial momentum transport F_i is several orders of magnitude smaller than the other forces. It decreases at the choked point (in annular flow) in Al-Sahan test since the quality derivative sinks there. The virtual mass forces F_{VM1} and F_{VM2} increase very sharply at the choked point, which makes their difference F_{VM} larger than other forces. As a result, the virtual mass force becomes the main force at the choked point, which is different from Schwellnus model.

The interfacial heat transfer between liquid and vapor is divided into two parts: sensitive and latent heat transfers. They increase along the discharge pipe before the choked point since the derivative of quality increases. As to be seen in Figure 5.25, the heat transfer is very small in Al-Sahan test (compared with heat transfer in Celata test) since the liquid approaches the saturated temperature. For

Celata test, the liquid is super-heated and the heat transfer becomes larger because of the sensitive heat transfer contribution. Consequently, the thermodynamic non-equilibrium becomes relevant in shorter tubes or orifices. We should remark here that our model and that of Schwellnus are almost identical in modelling the interfacial heat transfer.

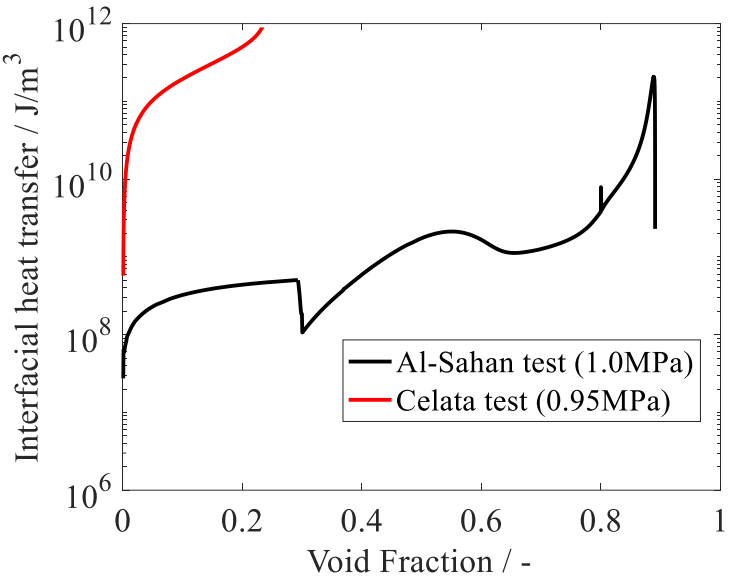

Figure 5.25: Present model interfacial heat transfers v.s. VF for Al-Sahan and Celata tests

5.6 Summary

After a literature review of ATHLET critical flow model and typical models in other STH codes, a new two-fluid model for the analysis of two-phase critical discharge was developed as a potential CFM in ATHLET. The model allows thermodynamic non-equilibrium and hydrodynamic non-homogeneity between the liquid and vapor phases. It is based on the solution of six conservation equations of mass, momentum and energy for separated phases. The model is able to simulate several flow regimes from subcooled to annular flows. Closure was achieved by a set of constitutive relations chosen based on extensive literature review. The main methodology has been introduced in this work in detail.

The experimental data from Al-Sahan tests (long pipe discharge), Celata test (nozzle discharge), Dobrans test (long pipe discharge), Sozzi–Wutherland tests (short pipe discharge) and Henry critical flow test (which comprised both 9 subcooled and 10 saturated upstream conditions) were chosen for validation. The comparison of results shows excellent agreement with measured critical mass fluxes (also pressure profiles in Al-Sahan tests and Henry tests). The calculation result is the best compared with other models from literature. The results of Henry tests show that NNTPCM could predict most of the mass fluxes in Henry tests within the error band ±20% not only for subcooled upstream conditions but also for saturated upstream conditions, better than other models in ATHLET. Furthermore, the calculated pressure profiles along the discharge pipes by NNTPCM are highly consistent with test measurements for subcooled upstream conditions except for the choking points. For saturated upstream conditions, the difference of pressure profiles between simulation and test measurement is larger but also acceptable since the pressure deviations and curves are similar. This study verifies the necessity of the critical flow model modification for STH code ATHLET.

A special attention was paid to the understanding of the choking process by analyzing the evolution of the main constitutive parameters, an aspect seldom considered in previous studies. According to this

analysis of the constitutive parameters, some interesting conclusions are extracted: the interfacial area becomes maximum at the transition point from bubbly flow to slug/churn flow; the virtual mass force becomes important and sometimes decisive for choked flow; for long pipe, the thermodynamic non-equilibrium plays negligible role because of the good heat transfer between the two phases but the hydrodynamic non-homogeneity has to be taken into account since the velocity difference is very large at the choked point; on the contrary, the hydrodynamic non-homogeneity may be neglected but the thermodynamic non-equilibrium considered for short pipe or orifice because of the superheated liquid and small velocity difference.

As an appendix of this chapter, appendix A discusses two different kinds of critical criteria (pressure gradient criterion and determinant criterion) in detail. Different tests were used to study the two criteria. The results obtained by using the two different criteria are consistent as long as the chosen pressure gradient value remains large enough. Simultaneously, according to our results, this value is larger for the case of orifice and short pipe discharges (compared with the long pipe discharge).

This study contributes to a detailed understanding of the critical flow phenomenon and to the development of related codes, especially STH code ATHLET for safety analysis of engineering systems. In the next chapter, the new developed 6-equation NNTPCM will be applied in ATHLET. Furthermore, a Marviken SET facility for critical flow transient will be used as example of application.

6 Implementation and application of the new CFM

In the practical application of STH code for nuclear safety analysis, the phenomena during accident scenarios are very complex, comprising a ‘‘full-range” thermal hydraulic process, from single-phase subcooled liquid to single-phase superheated steam [186]. Faced with such a complex system, it is very easy for code users, especially beginners, to choose the unsuitable models (including the choice of CFMs since several CFMs are normally supplied in a STH code). Furthermore, the capability of full-scope accident simulation - in both design basic accidents (DBAs) and beyond design basic accidents (BDBAs) - is the development direction for STH codes [187].

This situation may be improved by a full range CFM, which involves single-phase subcooled water region, bubbly flow, slug/churn flow, annular flow, dispersed droplet flow and the single-phase superheated steam region. Unfortunately, at present there is no general model or correlation for critical flow to be valid for a broad range of pipe lengths, pipe diameters, and upstream conditions, including subcooled liquids.

CDR1D model in ATHLET is a model that fulfills this requirement only in case of a mass flux greater than 3000 kg/m^2s. A pre-calculated critical flux table is prepared before the simulation of accident transient. The table should encompass completely the full range of conditions (critical fluxes at different pressures, void fractions and temperatures). During the transient simulation, the table is used in a lookup method. In other words, the critical flux at concerned point could be interpolated according to the table, based on the pressure, void fraction and temperature. As introduced before, it is based on 4 conservation equations (mixture mass conservation equation, two-phase momentum equations, and the mixture energy equation). Since it does not consider the velocity difference between the two phases, it normally underestimates the critical flow against the experimental critical flow data, in particular at a low mass flux.

Therefore, under the premise of inheriting the “full range” attribute of CDR1D, it is necessary to develop a model that is more accurate for critical flow prediction. One development method is based on the natural idea that since CDR1D model does not consider the velocity difference between two phases in some cases, a more accurate model may be achieved if the slip ratio of the two-phase flow is considered. This will lead to a 5-equation or 6-equation model instead of 4-equation CDR1D model. According to the validation of last chapter, a full range CFM based on NNTPCM should be a potential modification for ATHLET.

In this chapter, the NNTPCM will be plugged into ATHLET instead and be applied to several Marviken full scale critical flow tests. It should be noted that, while all validation results for

NNTPCM in last chapter were based on separated upstream condition, the application of NNTPCM in ATHLET is a transient application. A meticulous work should be done for the critical flux calculation of each possible upstream condition and for the plug-in of the new full range CFM table in ATHLET.

6.1 Methodology for new full-range CFM plug-in in ATHLET

During the transient simulation of ATHLET, the CFM table needs to be called. Consequently, it should be prepared in advance and plugged into the ATHLET input deck for the concerned accident scenario. The general idea of this chapter is to replace the previous CDR1D table in ATHLET, with the newly generated data by the NNTPCM calculation for each pre-set upstream condition (matrix of different pressures, void fractions and temperatures). Simultaneously, it is defaulted that the parameter ranges for CDR1D table are valid for concerned accident scenario. In other words, the newly generated ATHLET input deck with the full-range CFM table is based on the old ATHLET input deck with CDR1D table. The main difference is that the old CDR1D table is replaced with the CFM table based on NNTPCM. The specific process for the new full-range critical flux table generation is shown in Figure 6.1.

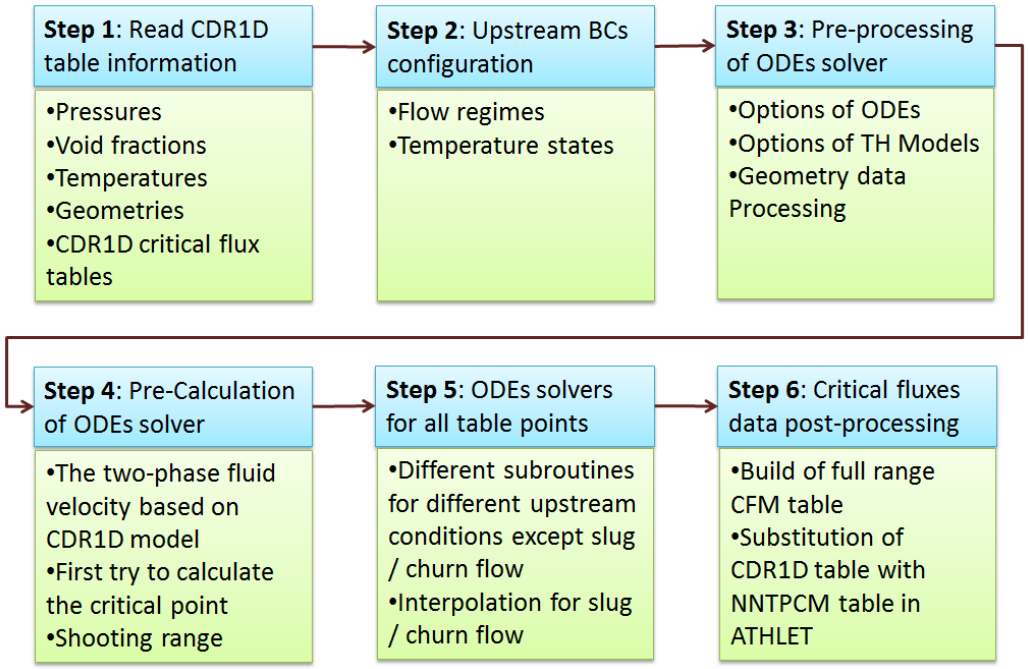

Figure 6.1: Flow chart for full-range CFM table generation

Step 1: Read CDR1D table information

According to the CDR1D table, the ranges of pressures, void fractions and temperatures of the concerned accident scenario could be known. At the same time, it is assumed that the geometry information (length, diameters and cross-section areas at the two ends and their variation along the pipe) of the discharge pipe for the new full range CFM is the same as CDR1D model since the results of both models are geometrically related, which are different from HEM and Moody model.

Furthermore, it is assumed that for a fixed upstream condition, there is no order of magnitude difference between the critical flux results of CDR1D model and the new full range CFM. As a result, the critical flux data in CDR1D table is also recorded since it is very useful for the setting the initial velocity of critical flow.

Step 2: Upstream BCs configuration

Based on the information from the CDR1D model, the flow regimes and temperature states of the upstream condition for critical flux calculation using the new NNTPCM could be classified into different situations, as shown in Figure 6.2. The flow regimes of upstream condition are divided into five conditions, based on the void fraction: single phase liquid, bubbly flow, slug/churn flow, annular flow and single-phase vapor. A droplet flow is never considered and an annular flow is always assumed instead. Concerning the liquid temperatures (the upstream vapor is assumed in saturated condition), the upstream conditions could be subcooled, saturated or superheated. It should be noted that, for a fixed pressure value in the full-range CFM table, any combination of flow regimes and temperature states is possible, and an essential part for the full-range table generation. Therefore, the new full range CFM should have the capability to deal with any of such upstream conditions for critical flux calculation. The classification is based on their different treatments when the ODEs are solved.

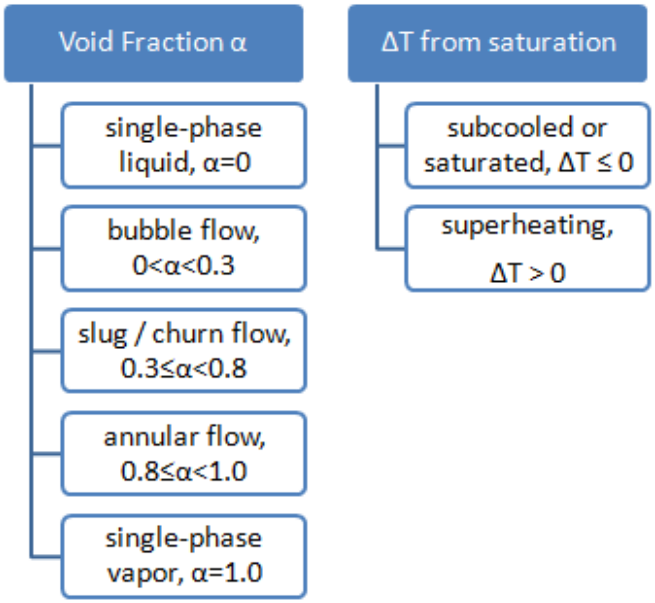

Figure 6.2: Module options for NNTPCM critical flux table generation

Step 3: Pre-processing of ODEs solver

Similar to any ODE solvers, some options, for instance the ODEs solution method, the convergence criterion, maximum and minimum steps etc. should be confirmed before the start of ODEs solving. Furthermore, different kinds of thermal-hydraulic models could also be selected for the new full range CFM calculation. For example, there are several correlations available for frictional pressure drop: Martinelli-Nelson correlation, Chisholm correlation, Friedel correlation etc. According to their domain of application and experience researchers, different models could be selected. Another example is the virtual mass force. There are also several options for this model, considered for the two-phase critical flow calculation [188] [189]. At the same time, the geometry information of the discharge pipe should be further interpolated along the pipe.

Step 4: Pre-Calculation of ODEs solver

As introduced above, the critical flux of each upstream condition is recorded at the first step. According to the critical flux, the fluid velocity of the upstream could be calculated. This velocity is

used for the first try for critical location prediction in shooting method. According to the shooting methodology, if a longer critical length (comparing with the length of discharge pipe) is achieved by the usage of this velocity as upstream condition, the upstream velocity should be enlarged to achieve a shorter critical length. On the contrary, if a shorter critical length is achieved, the upstream velocity should be decreased. Based on this logic, a reasonable range for the shooting method could be achieved.

Step 5: ODEs solvers for all table points

Based on the classification of the upstream BCs configuration (flow regimes and temperature states) in step 2, different treatments (corresponding to different calculation modules) will be carried out for them, as shown in Table 6.1. It should be emphasized that for the upstream condition of slug/churn flow, it could not be solved by a 6-equation ODEs model since it does not go through the flow regime of bubbly flow and, therefore, the constitutive parameters as BCs are unknown for the ODEs solution. The solution for this dilemma is to get the critical flux of slug/churn flow upstream condition based on the interpolation of the critical flux values of other flow regions at the same pressure and temperature.

Step 6: Critical fluxes data post-processing

After the critical flux for each upstream condition is calculated, the building of the new NNTPCM table could be achieved. The last operation of this methodology is substitution of CDR1D critical flux table with the newly generated NNTPCM table in ATHLET input deck, following the default format of CDR1D table.

Table 6.1: Setting for different module options

α \ ΔT	$\Delta T \leq 0$	$\Delta T > 0$
$\alpha=0$	• Start from single liquid (3-equation model) • Initial bubble diameter from minimum size	• Start from bubbly flow (7-equation model) • Initial bubble diameter from minimum size • Liquid density equals saturated value
$0<\alpha<0.3$	• Start from single liquid (3-equation model) • Initial bubble diameter based on void fraction	• Start from bubbly flow (7-equation model) • Initial bubble diameter based on void fraction • Liquid density equals saturated value
$0.3\leqslant\alpha<0.8$	• Interpolation based on the critical flux value of other flow region	• Interpolation based on the critical flux value of other flow region
$0.8\leqslant\alpha<1$	• Start from single liquid (3-equation model) • Flashing bubble diameter use minimum size • After flashing, transit to annular flow directly	• Start from annular flow (6-equation model) • Liquid density equals saturated value
$\alpha=1$	• Single phase 3-equation model	• Single phase 3-equation model

6.2 Simulation of Marviken (a SET facility) critical flow experiment

In 1965 Sweden began to build the Marviken nuclear power station on the east coast of Sweden, outside Norrköping. The reactor was planned to be a boiling water reactor fueled by Swedish natural uranium and using heavy water as coolant and moderator [190]. Because of the inherently unstable design of Marviken and the nuclear weapons non-proliferation treaty [191], the project of Marviken nuclear power station was abandoned. Left was a fully built reactor that never produced any nuclear power.

Marviken facility is the source of experimental data for various fields of nuclear safety research. Investigated phenomena include (but are not limited to) blowdown, containment leakage, aerosol transport and critical flow. Between 1977 and 1979 the Marviken Full critical flow tests (CFTs) were conducted at the Marviken power station. The reactor tank and containment was used to conduct the largest critical flow experiments. From the beginning of 1980s until now, much work has been done for critical flow model assessment which were based on Marviken test datasets [192][193]. Different STH codes (for example, RELAP5 and TRACE, TRACE and MELCOR) were also compared using Marviken test data [194][195].

6.2.1 Description of Marviken Facility

The vessel had a net volume of 425 m^3 and a maximum design temperature and pressure of 272 ℃ and 5.75 MPa, respectively. In each test, the vessel was filled with deionized water. The CFTs were the source of experimental data on choking flow for nozzles with different diameters and lengths, as shown in Table 6.2. The nine test nozzle geometries were of different lengths, ranging from 166 mm to 1809 mm, and had rounded entrances followed by a nominally 200, 300, 500 or 509 mm diameter cross-section followed by rupture disc. With these different pipe geometries and a wide range of initial conditions, a total of 27 CFTs were conducted and thoroughly documented [196]. The discharge pipe that connects the vessel to the nozzle is 6283 mm long and is geometrically complex. It is made up of several pieces: a nozzle, drift tube, globe valve, instrument rings etc.

Table 6.2: Marviken test nozzles

Nozzle No.	Diameter / mm	Length / mm	L/D	Used in test No.
1	200	590	3.0	13, **14**
2	300	290	1.0	6, 7
3	300	511	1.7	25, 26
4	300	895	3.0	1, 2, 12
5	300	1116	3.7	17, 18, 19
6	500	166	0.3	23, **24**
7	500	730	1.5	20, **21**, 22, 27
8	500	1809	3.6	**15**, 16
9	509	1589	3.1	3,4,5,8,9,10,11

The tests were conducted by discharging water and steam-water mixtures from a reactor vessel through a large diameter discharge pipe that supplied the flow to the test nozzle. Since the vessel was not designed for high pressures, the nominal pressure in the steam dome was set to 5 MPa for all tests except one which was set to 4 MPa. The initial sub-cooling ranged from 50 °C sub-cooling to low quality saturated water. Measurements of changes in the fluid state in the vessel and discharge pipe during blowdown were recorded using a pulse code modulation (PCM) system, from 180 s before test initiation until the experiment was terminated.

Tests were initiated by failing the discs contained in the rupture disc assembly. During the tests, the steam-water mixture was expected to choke because of the large pressure drop when it discharged from the nozzle to the containment area. The containment consisted of a drywell with a volume of 1934 m^3, a wet well with a volume of 2144 m^3 and the fuel transport hall with a volume of 303 m^3. In each test, the deionized water drained until the required elevation at room temperature was reached. The test is completed when either the ball valve in the discharge line is starting to close, or vapor flow is detected in the discharge pipe [197].

In order to validate NNTPCM comprehensively, CFT experiments 14, 15, 21 and 24, which have different discharge nozzle geometries, as shown in Figure 6.3, were selected as the reference cases for the ATHLET simulations with newly generated full-range NNTPCM model. The results should be convincing since the selected test cases have a large range of diameters, lengths and L/D ratios.

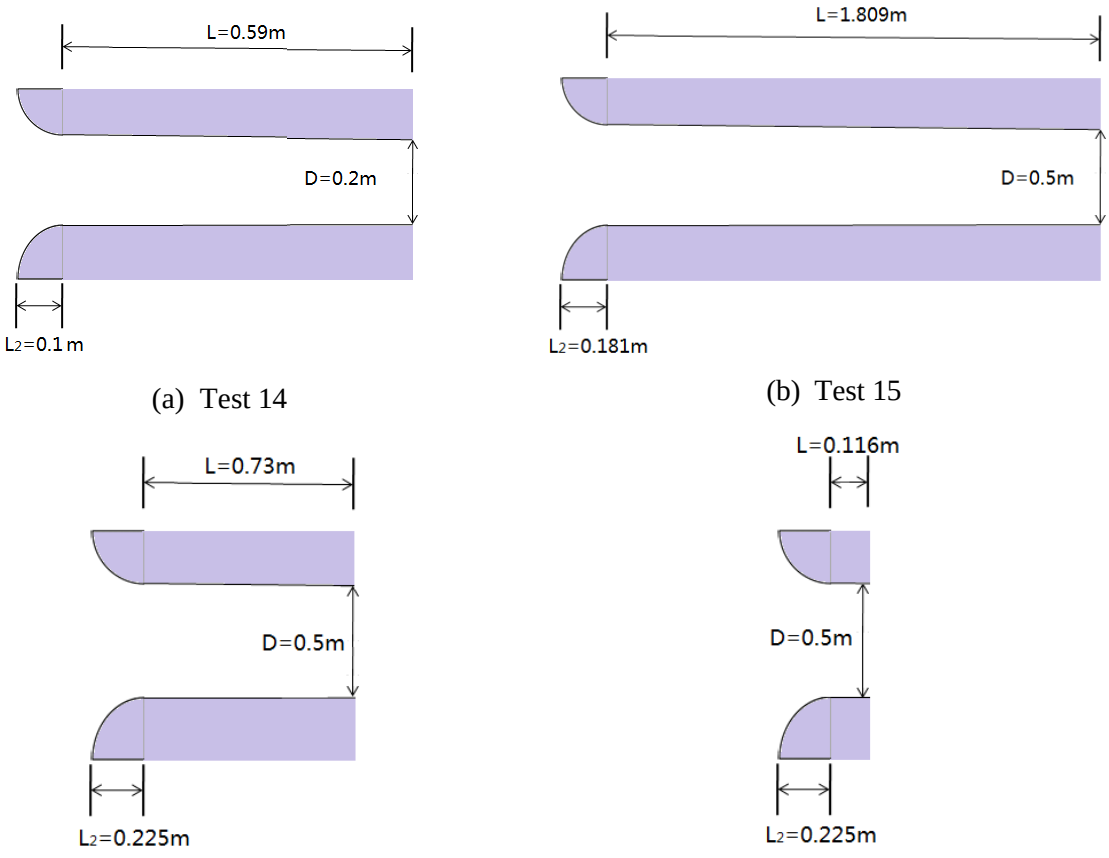

(a) Test 14

(b) Test 15

(c) Test 21

(d) Test 24

Figure 6.3: Module options for full-range critical flux table generation

6.2.2 ATHLET Modeling

This section focuses on the ATHLET input deck build for Marviken test. Although four tests were chosen for NNTPCM validation, their main differences are the discharge nozzle geometries (see Figure 6.3) and initial conditions and boundary conditions (ICs / BCs).

6.2.2.1 Nodalization

The detailed description available from the Marviken CFT means that a highly accurate geometrical model could be built for the simulations. As an example, the geometrical model and nodalization for test 14 is shown in Figure 6.4. A total of 44 cylindrical nodes were used. These nodes were divided into three parts, namely vessel, discharge pipe and discharge nozzle, as seen in Figure 6.4. The diameter at the top of the vessel is decreased a little bit so that the total volume of the reactor pressure vessel was equal to the real version since the volume of some internal structures should be excluded.

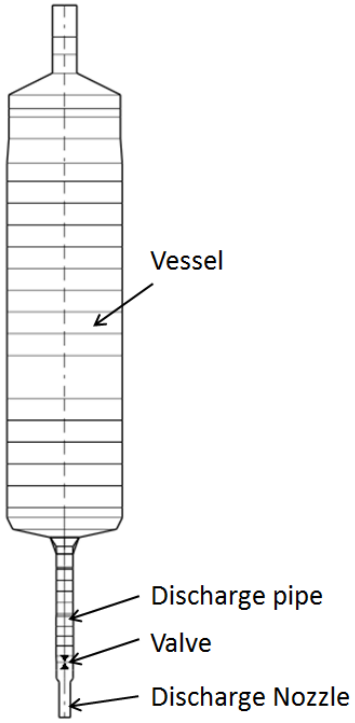

Figure 6.4: Geometry and Nodalization of Marviken test

6.2.2.2 Initial conditions and boundary conditions

Data necessary to determine initial conditions in the model were obtained from measurement.

The test matrix of Marviken CFT is classified as categories I, II and III, according to initial conditions in the vessel.

(1) Initial conditions category I test denotes that the test was conducted with water initially subcooled, 15 °C or more.
(2) Initial condition category II test denotes that the test was conducted with water initially subcooled, 30 °C or more.
(3) Initial condition category III test denotes that the test was conducted with water initially subcooled, less than 5 °C.

Test 14 belonged to category III with water initially subcooled less than 5 °C, and the other three chosen tests belonged to category II tests, conducted with modified vessel temperature profiles and

with water subcooled 30 °C or more, as shown in Figure 6.5. The elevation levels are negative value since the top of the vessel is chosen as the zero elevation position. The section part below the globe valve (the lower part of the discharge pipe and the nozzle) was filled with water.

The test conditions including the ATHLET input values as initial conditions are listed in Table 6.3[198].

Table 6.3: Initial conditions for test 14, 15, 21 and 24

Parameter	Test 14		Test 15		Test 21&24	
	Mea.	ATHLET	Mea.	ATHLET	Mea.	ATHLET
Vessel Dome Pressure / MPa	4.97	4.97	5.04	5.04	4.94	4.94
Saturation Temperature / °C	264	264	264	264	263	264
Degree of Nominal Subcooling in the Lower Vessel / °C	3	3	31	29	33	34
Minimum Fluid Temperature in the Vessel / °C	260	260	233	235	230	230
Initial Temperature at Nozzle Inlet / °C	170	176	177	179	184	186
Mass of Water and Steam (Incl. Discharge Pipe) / t	286	287	327	325	330	331
Mass of Steam / t	1.6	1.52	0.6	0.58	0.6	0.58
Initial Level in the Vessel / m	18.1	18.1	19.93	19.93	19.95	19.93

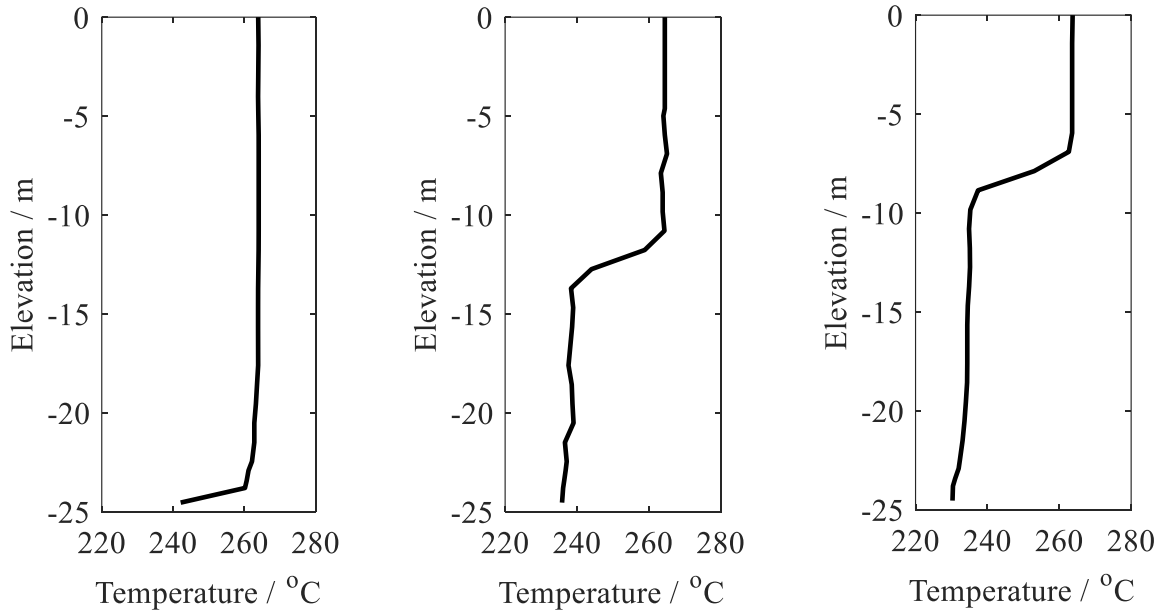

(a) Test 14 (b) Test 15 (c) Test 21&24

Figure 6.5: Initial temperature profiles for chosen Marviken CFTs

6.2.3 Simulation results

In order to validate the effectiveness of NNTPCM, the results of 4-equation CDR1D model are chosen for comparison against the test data. The comparison is divided into two steps:

(1) The full-range critical flux table
(2) The transient results of Marviken tests.

6.2.3.1 The full-range critical flux table for Marviken test

The trends for critical flux in different Marviken CFTs are similar in both CDR1D model and NNTPCM, although the values of the full-range critical flux tables for the chosen four test cases have big differences. As an example, the full-range critical flux tables for Marviken test 14 are shown in Figure 6.6.

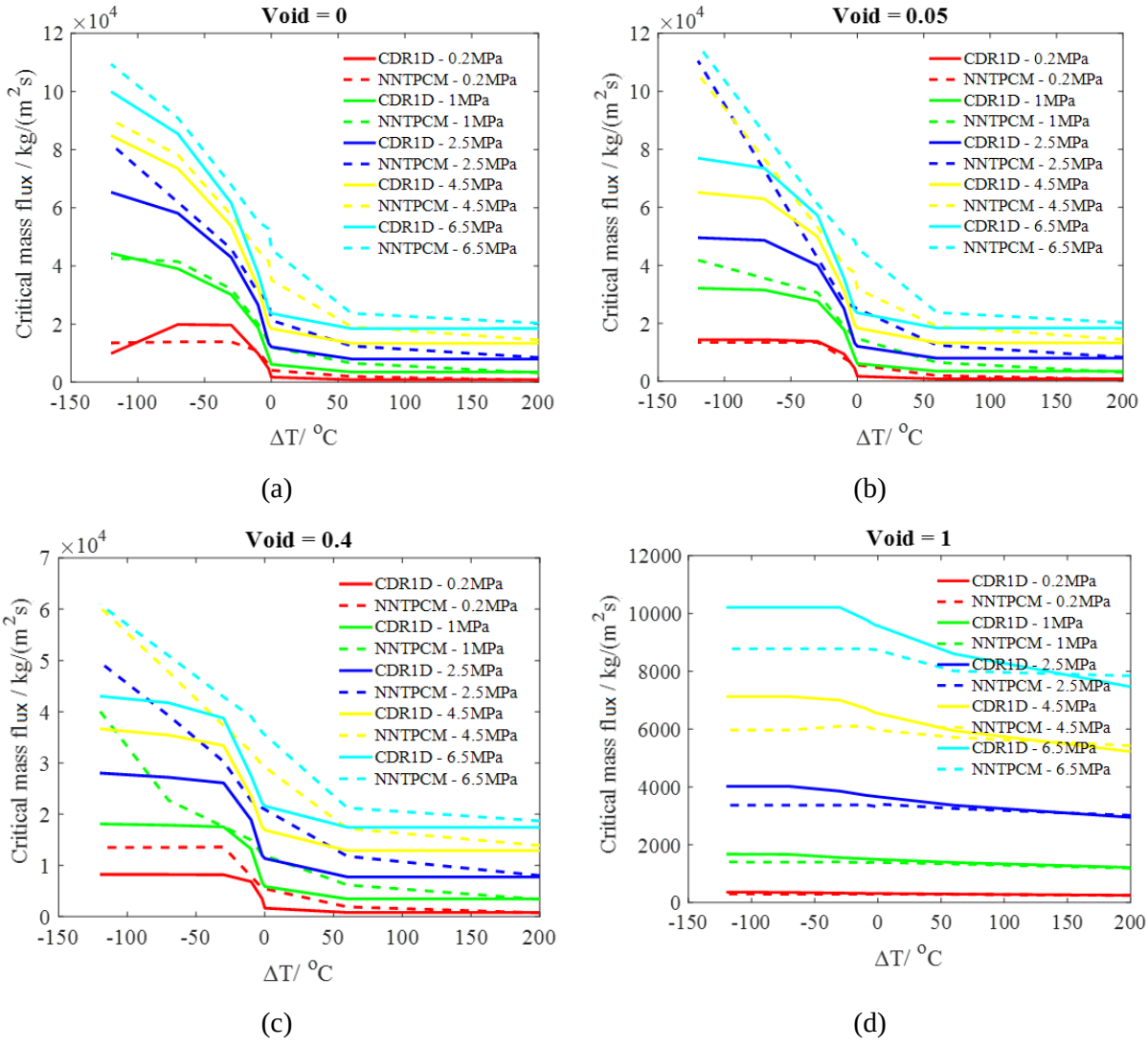

Figure 6.6: Full-range critical flux table for Marviken test 14

CDR1D model normally underestimates the critical flow against the experimental critical flow data since it does not consider the velocity difference between the two phases. According to Figure 6.6, for most upstream condition, NNTPCM could get a higher critical flux comparing with CDR1D model except the pure vapor conditions. But for the pure vapor conditions, their difference is within 15%. Actually, both CDR1D model and NNTPCM are degenerated to the same 3-equation model (mass, momentum and energy conservation equations of vapor). The difference of the results comes from the selection of the constitutive correlations.

For the superheated liquid upstream condition, the difference of NNTPCM and CDR1D model is not as large as that of the subcooled condition, especially for the upstream conditions with high superheating value. But the difference will be larger when the upstream pressure increases.

The main difference between these two models is in subcooled liquid upstream condition with different void fractions. As the upstream void fraction increases, this difference becomes more and more obvious.

6.2.3.2 Transient results

The parameters chosen to be analyzed in the transient results are limited to the pressure in the bottom of the vessel and the mass flow rate through the break. The NNTPCM results are compared with both ATHLET results using CDR1D model and the test data, as shown in Figure 6.7. The test period for test 14 was around 140 s and around 55 s for the other three tests.

In the Marviken test 14, with water in vessel initially subcooled less than 5 °C, the NNTPCM predicted the pressure very well but with the discharge mass flow higher during the subcooled discharge period (before 35 s) comparing with test data, as shown in Figure 6.7 (a) and Figure 6.7 (b). On the contrary, NNTPCM predicted the pressure lower than test but a comparable mass flow during the saturated discharge condition. Considering these two conditions together, it may come to a conclusion that NNTPCM overestimate the critical mass flow, although it got better results than CDR1D model, which obviously underestimate the critical flux. According to Figure 6.7 (c) and Figure 6.7 (d), NNTPCM predicted the subcooled discharge period very well for both transient pressure and mass flow rate. The discrepancy came from the transient when the upstream of the discharge had large void fraction in slug/churn flow and annular flow. Test 14 and Test 15 have one thing in common: the L/D ratios of the discharge nozzles were greater than or equal to 3.0.

According to the results from Figure 6.7 (e) to Figure 6.7 (h) for test 21 and 24, it seems that NNTPCM could get better critical flux prediction for subcooled upstream conditions and better pressure prediction for saturated upstream conditions comparing to the CDR1D model.

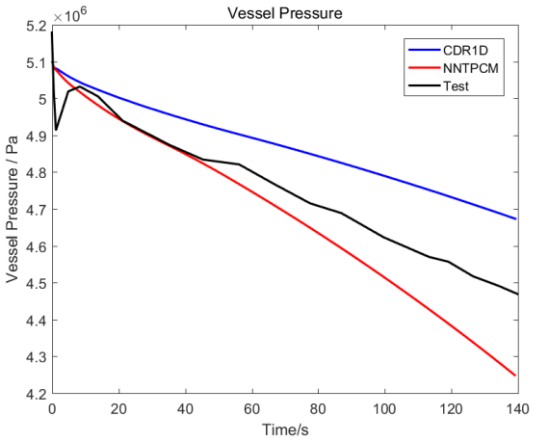

(a) Pressure of test 14

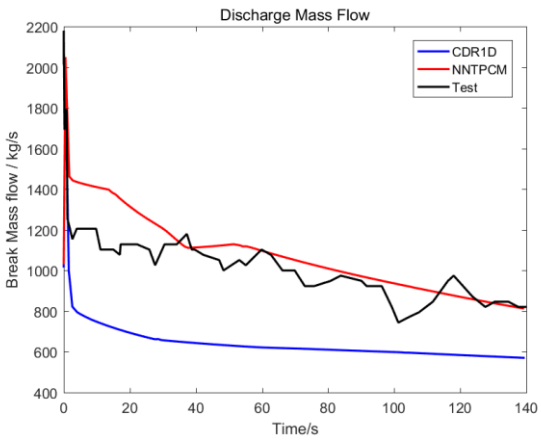

(b) Break mass flow of test 14

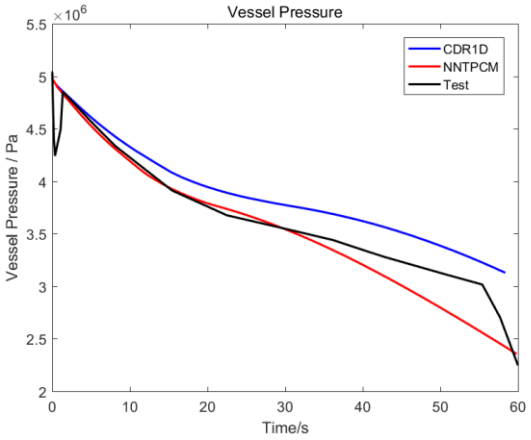

(c) Pressure of test 14

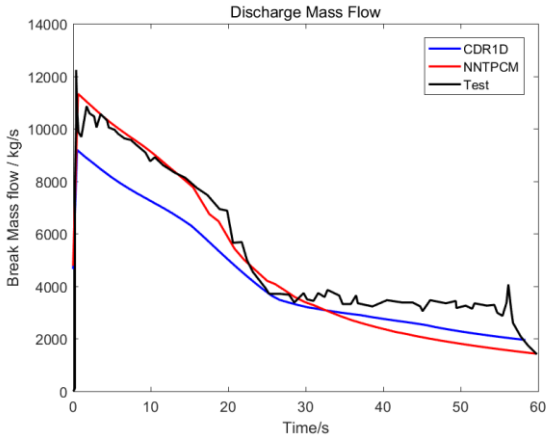

(d) Break mass flow of test 15

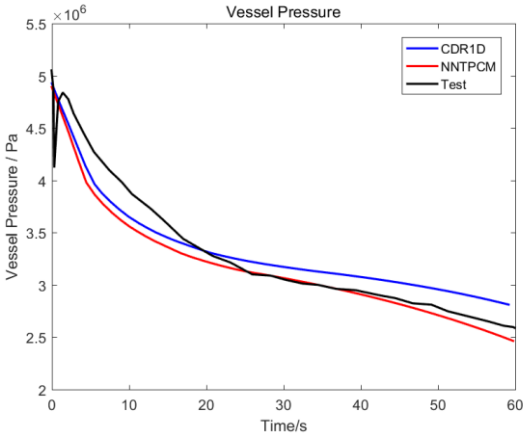

(e) Pressure of test 21

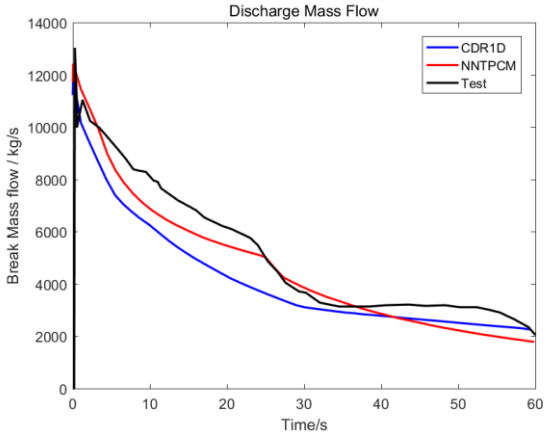

(f) Break mass flow of test 21

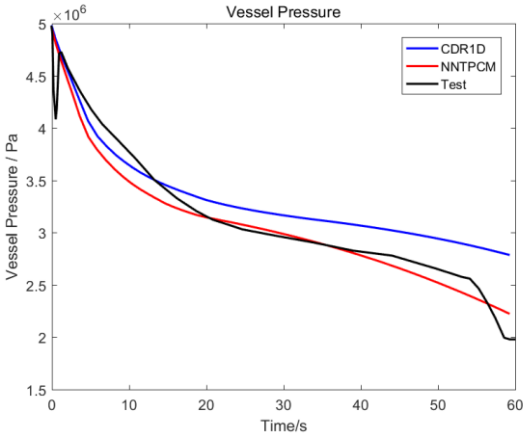

(g) Pressure of test 24

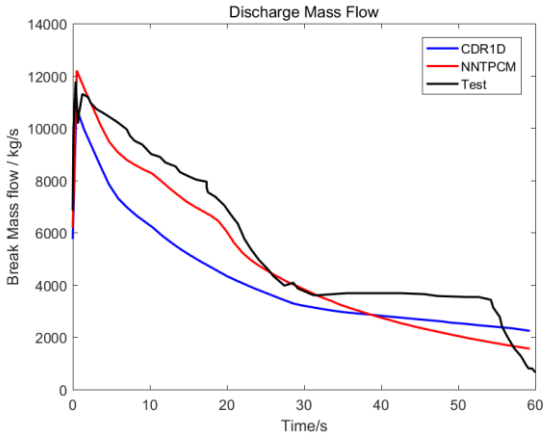

(h) Break mass flow of test 24

Figure 6.7: Transient results

After the comparison of the two models, it could come to a general conclusion that NNTPCM could get better or at least comparable results comparing with CDR1D model for the typical Marviken CFTs, especially at the beginning of the transient.

6.3 Simulation of PKL (ITF) I2.2 IBLOCA benchmark

According to the object of the dissertation, the new model will be applied to the PKL I2.2 IBLOCA benchmark simulation. It is obvious that the break mass flow depends strongly on the upstream parameters (pressures, temperatures and so on) which are calculated by the ATHLET. To avoid the strong impacts of other phenomena, the following simulation only considers the first 350s before the ACC injections start. Furthermore, the main phenomena in the IBLOCA benchmark already took place in this period. The most important parameters which are concentrated on in the PKL I2.2 IBLOCA benchmark are showed next.

The mass flow of the break pipe is shown in Figure 6.8. It shows that the simulation with the new CFM – NNTPCM – could get results with a higher precision comparing with CDR1D model:

1) At the beginning of the blowdown period, the coolant in the primary loop was in the subcooled condition. In this condition, a higher mass flux was achieved by the use of NNTPCM, closer to the test measurement.
2) After the blowdown period, the coolant was in saturated condition, and the break mass flux decreased sharply. The results using NNTPCM were more reasonable than those using CDR1D model.

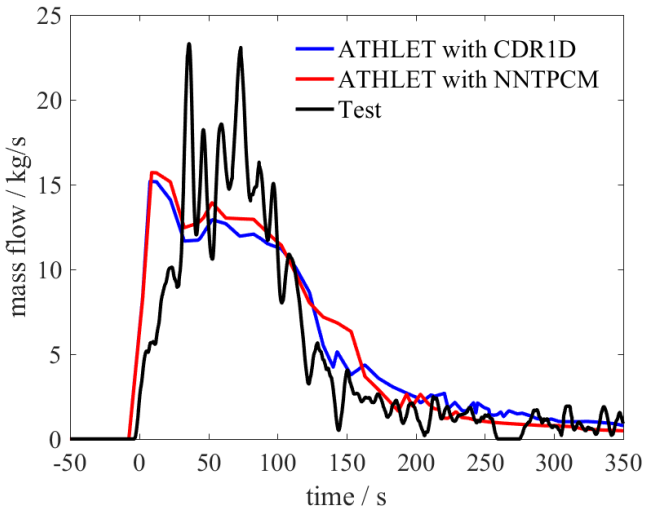

Figure 6.8: Break mass flow

Figure 6.9 shows the peak cladding temperature with different models. According to the overall trend of the transient, the results with the NNTPCM were closer to the measurements. Although both of the two models did not reproduce the heat-up process with accuracy (their heat-up phenomena happened a little bit later than the test, with lower PCT values), the results with NNTPCM were closer to the time when the heat-up phenomenon took place in the test.

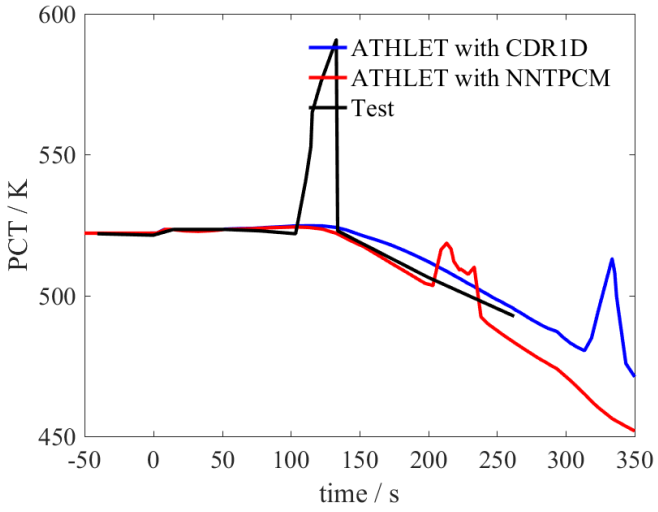

Figure 6.9: Peak cladding temperature

According to the results, the simulation with NNTPCM could get better results comparing with those using CDR1D model, especially in the blowdown period with subcooled coolant in the primary loop. But with the development of the scenario, the calculation with NNTPCM could not show more reasonable results since the phenomena in the primary loop became more and more complex and interdependent.

6.4 Summary

A full-range CFM based on NNTPCM was introduced in this chapter. As a potential substitute for CDR1D model for ATHLET, the methodology for the plugin in ATHLET has been described in details. To validate the effectiveness of the model and to verify its ability to replace the CDR1D model, several Marviken full scale critical flow tests and PKL I2.2 IBLOCA benchmark were chosen for the model validation, by comparing with both test data and CDR1D results. According to the comparison results of the two models, it could come to a general conclusion that NNTPCM could get better or at least comparable results (compared to CDR1D model) for the typical Marviken CFTs and IBLOCA benchmark.

7 Conclusions and Outlook

Nuclear safety analysis is always the fundamental technical item for nuclear development. During the safety analysis, the most important aspect is the thermal hydraulic analysis of operation conditions and accident (including DBA and BDBA). Some of the thermal hydraulic parameters directly reflect the safety conditions of NPP, e.g. departure from nuclear boiling ratio (DNBR), PCT etc. After development of around half a century, the concerned issue in thermal hydraulic safety issue has switched from IBLOCA and SBLOCA to IBLOCA scenario in the recent decade. IBLOCA scenario was focused by ROSA/LSTF, ATLAS facility and, most recently, by PKL facility for experimental studies. Based on the IBLOCA test scenario of LSTF facility, an important issue has been found: the phenomena of core heat-up and PCT are very sensitive to the break size and the operation of safety injections. Unfortunately, most of the STH codes could not reproduce these processes in different IBLOCA scenarios. In order to confirm and solve this problem, PKL I2.2 IBLOCA benchmark was resorted to, as a counterpart test similar to the IBLOCA scenario in LSTF, and some typical STH codes should be evaluated by the test data of PKL I2.2 IBLOCA benchmark.

This dissertation is based on the above-mentioned background. ATHLET was chosen as the objective STH for the simulation of the benchmark at KIT. Consequently, this study was focused on calculation and model assessment of ATHLET in PKL I2.2 IBLOCA benchmark. After the confirmation of the most sensitive model for the IBLOCA scenario, leading to the discrepancy between the simulation and test data, the improvement of the CFM model in ATHLET has been achieved. The detailed model description was given in this work and the general process of V&V of STH model development has been followed to evaluate the new model. Finally, this model was plugged into ATHLET and applied to Marviken (which is a full scale critical flow SET facility) test, and PKL I2.2 IBLOCA benchmark again.

As a summary, here are the most important original contributions:

1) Development of a new two-layer method, which is based on FFTBM and MSM, to evaluate the simulation results of STH and find the most sensitive model
2) Development of a new 6-equation model called NNTPCM for critical flow simulation
3) Discussion on the detailed process of choking and choking criteria
4) Implementation of the new full range CFM based on NNTPCM into ATHLET and its application to accident scenario analysis

The most important conclusions and the outlook for this work are given further.

7.1 Conclusions

The main steps for ATHLET input deck preparation for PKL I2.2 IBLOCA benchmark simulation, the simulation results - including steady state and transient - were described in detail in this work. In order

to make the results convincing, the related state-of-art methodology was used in each step. Firstly, the geometries of the PKL facility and (as reproduced by) ATHLET were quantitatively compared. The difference between them was acceptable based on the volume criterion. Subsequently, a primary nodalization for ATHLET simulation was made. In the steady state calculation, the primary nodalization was confirmed since the PKL ICs/BCs and the significant measured parameters of the stable condition before SOT were reproduced during this period. A detailed transient nodalization qualification method was used and described. After this procedure, it has been proved that the KIT ATHLET final nodalization was convergent, with necessary fidelity of geometrical and involved phenomena reproducibility. A well-known method – FFTBM, which compared the simulation results and test data in frequency field - was introduced. Based on the analysis of the transient results and the FFTBM results, it could come to a conclusion that most of the variables in PKL I2.2 IBLOCA benchmark were predicted very well by ATHLET, which confirmed its effectiveness on IBLOCA simulation.

Furthermore, the PCT was not reproduced in the simulation. According to the AA values in FFTBM method, it is most likely related with the break mass flow simulation. In order to confirm the most sensitive model for PKL simulation, a sensitivity study for the thermal hydraulic models was resorted to and a new generalized two-layer methodology of sensitivity analysis has been developed, based on two classical methods: FFTBM and MSM. According to the trend analysis, FFTBM quantitative assessment and MSM sensitivity analysis, CFM is not simulated well enough in PKL I2.2 IBLOCA benchmark test and it has high impact on the simulation. Consequently, it is with high probability responsible for that and it was the candidate model for modification.

After a literature review of ATHLET critical flow model and typical models in other STH codes, a new two-fluid model for the analysis of two-phase critical discharge was developed as a potential CFM in ATHLET. The model allows thermodynamic non-equilibrium and hydrodynamic non-homogeneity between the liquid and vapor phases. It is based on the solution of six conservation equations of mass, momentum and energy for separated phases (the present ATHLET CFM CDR1D being a 4-equation model). The model is able to simulate several flow regimes from subcooled to annular flows. Closure was achieved by a set of constitutive relations chosen based on extensive literature review.

Two kinds of choking criteria (determinant and pressure gradient) were discussed and their strict derivations for single-phase flow were recalled in this study. For the determinant criterion, a compatibility condition should be considered for the system of ODEs describing the two-phase flow to have a solution at choking point. A deeper look into the compatibility condition is offered in this study by algebraic consideration. The criteria may be also extended for two-phase flow. In order to confirm that, the two criteria were numerically investigated for long pipe, short pipe and orifice discharge tests. The results obtained by using the two different criteria are consistent as long as the chosen pressure gradient value remains large enough. Simultaneously, according to our results, this value is larger for the case of orifice and short pipe discharges (compared with the long pipe discharge).

The model was validated based on a procedure of V&V. The experimental data from Al-Sahan tests (long pipe discharge), Celata test (nozzle discharge), Dobran test (long pipe discharge), Sozzi–Wutherland tests (short pipe discharge) and Henry tests (which are comprised of both 9 subcooled and 10 saturated upstream conditions) were chosen for validation. The comparison of results showed excellent agreement with measured critical mass fluxes (also pressure profiles in Al-Sahan tests and Henry tests). The calculation results were the best compared with other models from literature. Other

model parameters, such as fluid temperature, liquid and vapor velocities, and void fraction were compared with those predicted by other models.

A special attention was paid to the understanding of the choking process by analyzing the evolution of the main constitutive parameters, aspect seldom considered in previous studies. According to this analysis of the constitutive parameters, some interesting conclusions were extracted: the interfacial area becomes maximum at the transition point from bubbly flow to slug/churn flow; the virtual mass force becomes important and sometimes decisive for choked flow; for long pipe, the thermodynamic non-equilibrium plays negligible role because of the good heat transfer between the two phases but the hydrodynamic non-homogeneity has to be taken into account since the velocity difference is very large at the choked point; on the contrary, the hydrodynamic non-homogeneity may be neglected but the thermodynamic non-equilibrium considered for short pipe or orifice because of the superheated liquid and small velocity difference.

As application, a full-range CFM table based on NNTPCM was introduced by this work. As a potential substitute for CDR1D model for ATHLET, the methodology for the plugin in ATHLET has been described in details. To validate the effectiveness of the model and to verify its ability to replace the CDR1D model, several Marviken full scale critical flow tests and PKL I2.2 IBLOCA benchmark were chosen for the model validation, comparing with both test data and CDR1D results. According to the comparison of the results of the two models, it could come to a general conclusion that NNTPCM could get better or at least comparable results comparing with CDR1D model for the simulation of thermal-hydraulic scenarios in PWRs.

7.2 Outlook

Though some achievements have been made in the present work on the aspects of both model evaluation methodology for STH code model and the theoretical modeling of critical flow, some deficiencies still remain to be clarified in future work:

- Further detailed simulation of the bundles of core and their interactions in PKL since different behaviors have been observed in the IBLOCA benchmark but the present work did not consider these details
- Uncertainty study on the PKL I2.2 IBLOCA benchmark scenario to evaluate the safety issue comprehensively based on the frame of BEPU methodology
- Further V&V for the new developed CFM considering the impact of discharge duct shapes (long pipe, short pipe, nozzle, orifice, crack and slit) on the results
- Further discussion on the influence of different constitutive relationships on CFM results and the S&U study on the constitutive relationships
- Further study on the phenomena of bubble formation and growth during the process of critical flow, especially the impact of flashing phenomenon and the existence of non-condensable gas on critical flow

Appendix: Choking Criterion

There are two choking criteria in literature: the determinant criterion and the pressure gradient criterion. But so far, the relationships between them, their convergence processes and the thresholds values for the pressure gradient are not very well understood. This section focused on choking criteria for both single phase and two-phase flows, seldom studied before especially in the case of the two-phase flow before the discussion of 6-equation model validation in the next section. The mathematical derivation of the two choking criteria for single phase will be also recalled since single phase and two-phase flows should be consistent with respect to the choking criterion based on the acoustic propagation of fluid. Furthermore, the determinant criterion includes a compatibility condition; an important proposition — not yet proven in literature — of the compatibility condition will be also mentioned and a proof of it will be offered. Afterwards, the choking process was studied in detail with respect to different parameters (calculation step size, determinant of ODEs, pressure and its gradient, temperature, void fraction etc.). Finally, the results obtained with the two different choking criteria will be discussed in detail.

A.1 Derivation in Single Phase

A.1.1 Determinant criterion

The mass, momentum and energy conservation equations of single phase flow could be combined and written in matrix form as (analog to Eq. (5.48)):

$$[\boldsymbol{A}]\frac{d}{dz}[\boldsymbol{X}] = [\boldsymbol{b}] \tag{A.1}$$

The vector $[\boldsymbol{X}]$ means $[P, T_F, u_F]^T$, which represents the unknown parameters during discharge line. The matrix $[\boldsymbol{A}]$ and vector $[\boldsymbol{b}]$ have the following expressions:

$$[\boldsymbol{A}] = \begin{bmatrix} u_F(\partial\rho_F/\partial P)_s & 0 & \rho_F \\ 1 & 0 & \rho_F u_F \\ 0 & C_P & u_F \end{bmatrix} \tag{A.2}$$

$$[\boldsymbol{b}] = \begin{bmatrix} -\rho_F u_F/A \cdot dA/dz \\ -F_{WF} - \rho_F g\, sin(\theta) \\ -g\, sin(\theta) \end{bmatrix} \tag{A.3}$$

Based on the definition of critical flow and assuming an isentropic process, $a = \sqrt{(\partial P/\partial\, \rho_F)_s}$; it may be easily obtain that for critical flow:

$$|\boldsymbol{A}| = 0 \tag{A.4}$$

This means that the determinant choking criterion given by Eq. (A.4) is equivalent to the definition of the critical flow / sound speed.

A.1.2 Pressure gradient criterion

Since the mass flux $G = \rho_F u_F$ keeps constant along the discharge line, the first item on the left side of the momentum conservation may be expressed as following:

$$\rho_F u_F \frac{du_F}{dz} = G \frac{d}{dz}\left(\frac{G}{\rho_F}\right) = \frac{d}{dz}\left(\frac{G^2}{\rho_F}\right) \tag{A.5}$$

Consequently, the momentum conservation may be rewritten as:

$$\frac{d}{dz}\left(\frac{G^2}{\rho_F}\right) + \frac{dP}{dz} = -F_{WF} - \rho_F g\, sin(\theta) \tag{A.6}$$

Since the first item on the left side of Eq. (A.6) is a differential related with ρ_F, it may be written:

$$\frac{d}{dz}\left(\frac{G^2}{\rho_F}\right) = -\frac{G^2}{\rho_F^2}\frac{d\rho_F}{dP}\frac{dP}{dz} = -\frac{u_F^2\rho_F^2}{a^2\rho_F^2}\frac{dP}{dz} = -\frac{u_F^2}{a^2}\frac{dP}{dz} \tag{A.7}$$

Here the definition of sound speed was used.

Based on Eq. (A.6) and Eq. (A.7), the following relation is obtained:

$$\frac{dP}{dz} = -\frac{F_{WF} + \rho_F g\, sin(\theta)}{1 - \frac{u_F^2}{a^2}} \tag{A.8}$$

When the single phase fluid velocity u_F increases along discharge pipe and approaches the sound speed a, the denominator of the right side of Eq. (A.8) approaches 0 and, consequently, the pressure gradient dP/dz on the left side approaches negative infinity. In other words, the pressure gradient criterion may be written as:

$$\lim_{u_F \to a} \frac{dP}{dz} = -\infty \tag{A.9}$$

Since infinity does not exist in numerical calculation, a large value (e.g. 10^{12} Pa/m) is chosen for the pressure gradient criterion.

A.2 Discussion on ODEs Solution

Actually, the two choking criteria may be derived from each other. According to the matrix form of ODEs in Eq. (5.48) for two-phase flow and Eq. (A.1) for single phase flow, the solution may be obtained using the Cramer's rule[199]:

$$\frac{d}{dz}[\boldsymbol{X_i}] = [\boldsymbol{A}]^{-1}[\boldsymbol{b}] = \frac{|\boldsymbol{A_i}|}{|\boldsymbol{A}|} \tag{A.10}$$

where $[\boldsymbol{A_i}]$ is the matrix where the vector $[\boldsymbol{b}]$ replaces the ith column of matrix $[\boldsymbol{A}]$. The existence of solutions needs to be discussed for different situations.

i) As long as $|\boldsymbol{A}| < 0$ for z until its end L (which means discharge duct length), a singularity occurs in the process and the outlet conditions are uniquely determined as Eq. (A.10) by the prescribed inlet conditions [200]. For this situation the flow is subcritical.

ii) In the situation of $|\boldsymbol{A}| = 0$, the formulas of Cramer's rule Eq. (A.10) are undefined. In this case, the system could be either dependent or inconsistent depending on the values of $|\boldsymbol{A_i}|$.

ii.1) If $|\boldsymbol{A}| = 0$ and also all of $|\boldsymbol{A_i}| = 0$ the system is dependent which means the solution is in indeterminate form $0/0$ [201]. Normally, there are infinitely many solutions (if it is over an infinite field) for an indeterminate linear equations system, since the solutions can be expressed in terms of one or more parameters that can take arbitrary values, except for some special examples (e.g. the 3×3 incompatible system: x+y+z=1, x+y+z=2, x+y+z=3). Since the conservation equations are based on different mechanisms and the critical flow exists authentically, one may think that the system of ODEs for critical flow is compatible. Furthermore, the existence and uniqueness of the solution for the upstream of the critical point makes the critical flow rate existing and unique. We call the equation $|\mathrm{A_i}| = 0$ as the compatibility condition for the choking criterion $|\mathrm{A}| = 0$, which has to be satisfied simultaneously along the discharge line.

ii.2) When $|\mathrm{A}| = 0$ and either $|\mathrm{A_i}|$ is nonzero, then the system is inconsistent or incompatible. In other words, the flow is impossible. This means the given inlet conditions are unrealistic (e.g. the assumed flow rate is too high).

According to the Eq. (A.10), the pressure gradient could be written as in Eq. (A.11) below. The two choking criteria $|\boldsymbol{A}| = 0$ and $dP/dz \to -\infty$ mean that $|\boldsymbol{A_P}|$ is an infinitesimal of lower order than $|\boldsymbol{A}|$.

$$\frac{dP}{dz} = \frac{|\boldsymbol{A_P}|}{|\boldsymbol{A}|} \tag{A.11}$$

A.3 Compatibility Condition

The compatibility condition for choked (critical) flow may be expressed: the determinant $|\boldsymbol{A}|$ and all of $|\boldsymbol{A_i}|$ should equal 0. Many researchers have pointed out the compatibility condition during their critical flow studies[202][203][204][205][206][207]. It is also thought that the proposition:

$$|\boldsymbol{A}| = \boldsymbol{0},\ |\boldsymbol{A_i}| = \boldsymbol{0} \Rightarrow |\boldsymbol{A_j}| = \boldsymbol{0} \tag{A.12}$$

is tenable.

But there is no proof in the literature for the proposition Eq. (A.12). Therefore, we introduced a proof of it. The proof is based on the hypothesis that the system of linear equations (LEs)

$$\boldsymbol{Ax} = \boldsymbol{b} \tag{A.13}$$

has solution, no matter the Cramer's rule can be used or not. Otherwise, one may find counter-examples easily. For example, $\boldsymbol{A} = \begin{pmatrix} 1 & 0 \\ 0 & 0 \end{pmatrix}$, $\boldsymbol{b} = \begin{pmatrix} 0 \\ 1 \end{pmatrix}$, then it is easy to verify that $|\boldsymbol{A}| = 0$, $|\boldsymbol{A}_1| = 0$, $|\boldsymbol{A}_2| = 1 \neq 0$.

The proof makes use of the dependence analysis of the column vectors of matrix $\boldsymbol{A}$, $\boldsymbol{A_i}$ and $\boldsymbol{A_j}$. Without losing generality, we will show that:

$$|\boldsymbol{A}| = \boldsymbol{0},\ |\boldsymbol{A_1}| = \boldsymbol{0} \Rightarrow |\boldsymbol{A_2}| = \boldsymbol{0} \tag{A.14}$$

The matrices may be referred as forms of column vectors: $\boldsymbol{A} = (a_1, a_2, a_3, \cdots, a_n)$, $\boldsymbol{A_1} = (b, a_2, a_3, \cdots, a_n)$, $\boldsymbol{A_2} = (a_1, b, a_3, \cdots, a_n)$, where a_i $(i = 1, 2, \cdots, n)$ are column vector, n is the order of the matrix and b is the vector on the right side of the linear equations.

$|\boldsymbol{A}| = 0$ means $\mathrm{Rank}(A) = m < n$ and the column vectors $(a_1, a_2, \cdots, a_n)$ are linearly dependent. Then different situations are considered as follows.

a) If $m \leq n-2$, $\text{Rank}(\boldsymbol{A_2}) = \text{Rank}(a_1, b, a_3, \cdots, a_n) \leq n-1$, then obviously $|\boldsymbol{A_2}| = 0$.

b) If $m = n-1$, n-1 vectors of $\boldsymbol{A} = (a_1, a_2, a_3, \cdots, a_n)$ form the base vectors. And the remained one is a linear combination of the base vectors.

1) If a_1, a_2 are both base vectors, this means $\text{Rank}(a_3, \cdots, a_n) = n-3$. Consequently, $\text{Rank}(\boldsymbol{A_2}) = \text{Rank}(a_1, b, a_3, \cdots, a_n) \leq n-1$, then $|\boldsymbol{A_2}| = 0$.
2) If a_1 is not base vector but a_2 is base vector, then $\text{Rank}(a_1, a_3, \cdots, a_n) = n-2$. Therefore, $\text{Rank}(\boldsymbol{A_2}) = \text{Rank}(a_1, b, a_3, \cdots, a_n) \leq n-1$ and $|\boldsymbol{A_2}| = 0$.
3) If a_1 is base vector but a_2 is not base vector, then a_2 could be a linear combination of the base vectors $(a_1, a_3, , \cdots, a_n)$. Consequently, $\text{Rank}(\boldsymbol{A_1}) = \text{Rank}(b, a_2, a_3, \cdots, a_n) = \text{Rank}(b, (a_1, a_3, \cdots, a_n), a_3, \cdots, a_n) = \text{Rank}(a_1, b, a_3, \cdots, a_n) = \text{Rank}(\boldsymbol{A_2})$. Since the ranks of $\boldsymbol{A_1}$ and $\boldsymbol{A_2}$ are equal and $|\boldsymbol{A_1}| = \boldsymbol{0}$, then $|\boldsymbol{A_2}| = \boldsymbol{0}$

Bibliography

[1] Ichikawa Hiroshi, 2016. Obninsk, 1955: The World's First Nuclear Power Plant and 'The Atomic Diplomacy' by Soviet Scientists, Historia Scientiarum, 26(1), p. 25–41.

[2] Abram, T., and Ion, S., 2008. Generation-IV nuclear power: A review of the state of the science. Energy Policy, 36(12), p. 4323–4330.

[3] IAEA, 2019. World Nuclear Performance Report 2019. Technical report, No. 2019/007, IAEA.

[4] IAEA, 2003. Guidance for the Evaluation of Innovative Nuclear Reactors and Fuel Cycles, Report of Phase 1A of INPRO, IAEATOCDEC-1362, Vienna.

[5] Rachamin, R., Fridman, E. and Galperin, A., 2015. Feasibility assessment of the once-through thorium fuel cycle for the PTVM LWR concept. Annals of Nuclear Energy, 85, p. 1119-1130.

[6] Polmar, N., Moore, K., 2004. Cold War Submarines. Dulles, VA: Potomac Books.

[7] Kessler, G. et al., 2014. The Risks of Nuclear Energy Technology. Technical Reports, Springer-Verlag Berlin Heidelberg.

[8] Misak, J., 2009. Selection of a new nuclear unit for Slovakia: possibilities and key technical issues, International Conference, Secure Energy Supply, September 23-25, Bratislava, p. 1-29.

[9] Aksan, N., 2019. An overview on thermal-hydraulic phenomena for water cooled nuclear reactors; part I: SETs, and ITFs of PWRs, BWRs, VVERs, Nuclear Engineering and Design 354, 110212.

[10] USAEC, 1971. Interim Acceptance Criteria (IAC) for ECCS. USAEC, Washington (DC), USA.

[11] Hashmi, J.A., Rahman, M.S., Mallick, S.A., 2006. Effective nuclear regulatory systems: Facing safety and security challenges. Proceedings of an international conference, Moscow, Feb. 27 - Mar. 3, p. 79-80.

[12] Makai,M., Végh, J., 2017. Reactor Core Monitoring, Lecture Notes in Energy 58. Springer International Publishing AG, Cham, Switzerland.

[13] IAEA, 2006. Fundamental safety principles, safety fundamentals. IAEA Safety Standards No. SF-1, Vienna, Austria.

[14] Berg, H.P., 2015. Development of a framework of safety goals for nuclear installations and its application in Germany. Journal of Polish Safety and Reliability Association, 6(1), p.15-22.

[15] Di Maio, F., Zio, E., Smith C., Rychkov, V., 2015. Integrated deterministic and probabilistic safety analysis for safety assessment of nuclear power plants. Science and Technology of Nuclear Installations, Volume 2015, Article ID 136940, p. 1-2.

[16] Coscarelli, E., 2013. An integrated approach to accident analysis in PWR, Dissertation, University of Pisa, Pisa, Italy.

[17] USNRC, 1988. 10 CFR 50.46 - Acceptance Criteria for Emergency Core Cooling Systems for Light Water Nuclear Power Reactors. Technical report, U.S. Nuclear Regulatory Commission.

[18] Liang, T.K.S., et al., 2002. Development and Assessment of the Appendix K Version of RELAP5-3D for LOCA Licensing Analysis. Nuclear technology, 139(3), p. 233-252.

[19] IAEA, 2010. Deterministic Safety Analysis for Nuclear Power. SSG-2, IAEA, Vienna, Austria.

[20] D'Auria, F., 2017. Best-Estimate Plus Uncertainty (BEPU) approach for accident analysis. Thermal-Hydraulics of Water Cooled Nuclear Reactors, 905–950, Woodhead Publishing, Pisa, Italy.

[21] Kovtonyuk, A., Petruzzi, A., and D'Auria, F., 2012. A Procedure for Characterizing the Range of input Uncertainty Parameters by the Use of the FFTBM, Proceedings of ICONE-20 conference, p. 9-19.

[22] Glaeser, H., 2008. GRS method for uncertainty and sensitivity evaluation of code results and applications, Science and Technology of Nuclear Installations, Volume 2008, ID: 798901.

[23] D'Auria, F., Giannotti, W., 2000. Development of code with capability of internal assessment of uncertainty. Nuclear Technology, 131 (1), 159–196.

[24] Ahn, S.H., Aksan, N., Austregesilo, H., Bestion, D., 2015. FONESYS: The FOrum & NEtwork of SYStem Thermal-Hydraulic Codes in Nuclear Reactor Thermal-Hydraulics. Nuclear Engineering and Design 281, 103–113.

[25] Wolfert K., Frisch W., 1983. Proposal for the Formulation of a Validation Matrix. Technical report, OECD/NEA-CSNI-SINDOC (83) 117, Paris (F), OECD/NEA.

[26] Annunziato, A., Glaeser, H., Lillington, J., Marsili, P., Renault, C., Sjöberg, A., 1996, CSNI Integral Test Facility Validation Matrix for the Assessment of Thermal-Hydraulic Codes for LWR LOCA and Transients, Technical report, NEA/CSNI/R(96)17, OECD/NEA.

[27] Bestion, D., D'Auria, F., Lien, P., Nakamura,H., 2017, A state-of-the-art report on scaling in system thermal-hydraulics applications to nuclear reactor safety and design, Technical report, NEA/CSNI/R(2016)14, OECD/NEA.

[28] Bajs, T., Debrecin, N., Krajnc, B., 1998, Development of the Qualified Plant Nodalization for Safety and Operational Transient Analysis, International Conference of Croatian Nuclear Society: Nuclear Option in Countries with Small and Medium Electricity Grid, Dubrovnik, Croatia, p. 219-226.

[29] Huber, K., 2017, A multiscale method for mixed convective systems. Coupled calculations with ATHLET and OpenFOAM of the PHENIX NCT, Dissertation, Karlsruhe Institite of Technology, Karlsruhe, Germany.

[30] Addabbo, C. and Annunziato, A., 2000. CERTA-TN: Consolidation of Integral System Experimental Databases for Reactor Thermal-Hydraulic Safety Analysis (European Thematic Network Final Report), EUROPEAN COMMISSION Euratom Framework Programme 5 (1998-2002), Contract No.: FIR1-CT-2000-20052.

[31] OECD, 2018. Solving Thermal Hydraulic Safety Issues for Current and New Pressurised Water Reactor Design Concepts, Technical report, NEA/CSNI/R(2017)6, OECD/NEA.

[32] D'Auria, F., Bousbia-Salah, A., Petruzzi, A., Nevo, A., 2006. State of the Art in Using Best Estimate Calculation Tools in Nuclear Technology, Nuclear Engineering and Technology, 38, p. 11–32.

[33] Angelucci, M., Martelli, D., Barone, G., Di Piazza, I., and Forgione, N., 2017. STH-CFD Codes Coupled Calculations Applied to HLM Loop and Pool Systems. Science and Technology of Nuclear Installations, 1–13.

[34] Maljovec, D., Liu, S., Wang, B., Mandelli, D., Bremer, P.-T., Pascucci, V., and Smith, C. (2016). Analyzing simulation-based PRA data through traditional and topological clustering: A BWR station blackout case study. Reliability Engineering and System Safety, 145, p. 262-276.

[35] Zschaeck, G., Frank, T., and Burns, A. D., 2014. CFD modelling and validation of wall condensation in the presence of non-condensable gases. Nuclear Engineering and Design, 279, p. 137-146.

[36] Umminger, K., Kastner, W., Liebert, J., and Mull, T., 2001. Thermal hydraulics of PWRS with respect to boron dilution phenomena. Experimental results from the test facilities PKL and UPTF. Nuclear Engineering and Design, 204(1-3), p. 191-203.

[37] USNRC, 2007, Reactor Concepts Manual: Pressurized Water Reactor (PWR) Systems, USNRC Regulatory Commission Technical Training Center, Washington DC, Educational Teaching Material 0603.

[38] Laaksonen, L, 2011. How can we assure nuclear safety: is the risk of big technology controllable, Institute of Applied Energy Symposium, Tokyo, 17 December, p. 1-56.

[39] Takeda, T., Ohtsu, I, 2018. Uncertainty analysis of ROSA/LSTF test by RELAP5 code and PKL counterpart test concerning PWR hot leg break LOCAs, Nuclear Engineering and Technology, 50 , p. 829-841.

[40] Tregoning, R.L., Abramson, L.R., Scott, P.M., Chokshi, N, 2007. LOCA frequency evaluation using expert elicitation. Nuclear Engineering and Design. 237, p. 1429-1436.

[41] USNRC, 2005. 10 CFR part 50 risk-informed changes to loss-of-coolant accident technical requirements; proposed rule. Fed. Reg. 70 (214), p. 6.

[42] CHOI, K.Y., 2018. Summary Report of the NEA-Advanced Thermal-Hydraulic Test Loop for Accident Simulation Joint Project. Technical report, NEA-CSNI-R(2017)9, OECD/NEA.

[43] J. Vagner, D. Guichard, 1985. Influence of cladding and shape of defect on the critical crack size at a PWR vessel beltline during an intermediate LOCA. Transactions of the 8th International Conference on Structural Mechanics in Reactor Technology, Brussels G4/1.

[44] Vojtek, I., 1986. Heat transfer processes during intermediate and large break loss of-coolant accidents (LOCAs). Technical report, NUREG/IA0002, U.S. Nuclear Regulatory Commission.

[45] Kmetyk, LN., 1986. TRAC-PF1/MOD1 independent assessment Semiscale Mod-2A intermediate break test S-IB-3. Technical report, NUREG/CR-4465, U.S. Nuclear Regulatory Commission.

[46] Boyack, B.E., Lime, J.F., 1995. Intermediate-break LOCA analyses for the AP600 design. Technical report, LA-UR-95-1785, Los Alamos national laboratory.

[47] Bajorek, S. M., Petkov, N., Ohkawa, K., et al., 2001, realistic Small and Intermediate Break Loss of Coolant Accident Analysis Using WCOBRA/TRAC. Nuclear Technology, 136(1), p. 50-62.

[48] Tahir, M., Chughtai, I.R., Aslam, M., 2008. Response of proposed passive safety injection system for an intermediate size break LOCA on CHASNUPP-1. Annals of Nuclear Energy 35, p. 1986-1993.

[49] Gurgacz, S., Pawluczyk, M., Mazgaj, P., et al., 2015. EPR Medium Break LOCA Benchmarking Exercise Using RELAP5 and CATHARE. Technical report, NUREG/IA-0459, U.S. Nuclear Regulatory Commission.

[50] Mazgaj, P., Vacher, J.-L., and Carnevali, S., 2016. Comparison of CATHARE results with the experimental results of cold leg intermediate break LOCA obtained during ROSA-2/LSTF test 7. EPJ Nuclear Sciences and Technologies, 2(1), p. 1-8.

[51] Takeda, T., 2018. ROSA/LSTF test and RELAP5 code analyses on PWR hot leg small-break LOCA with accident management measure based on core exit temperature and PKL counterpart test. Annals of Nuclear Energy, 121, p. 594-606.

[52] Abe, S., Satou, A., Takeda, T., and Nakamura, H., 2014. RELAP5 analyses on the influence of multi-dimensional flow in the core on core cooling during LSTF cold-leg intermediate break LOCA experiments in the OECD/NEA ROSA-2 Project. Journal of Nuclear Science and Technology, 51(10), p. 1164-1176.

[53] Freixa, J., Kim, T.W., Manera, A., 2013. Post-test thermal-hydraulic analysis of two intermediate LOCA tests at the ROSA facility including uncertainty evaluation. Nuclear Engineering and Design, 264, p. 153-160.

[54] Nalezny, C.L., 1983. Summary of nuclear regulatory commission's LOFT program experiments. Technical report, NUREG/CR-3214, EGG-2248, U.S. Nuclear Regulatory Commission.

[55] Addabbo, C., Annunziato, A., 2012. The LOBI integral system test facility experimental programme. Science and Technology of Nuclear Installations, Volume 2012, Article ID 238019, p. 1-16.

[56] Koizumi, Y, Tasaka, K, 1986. Investigation of Break Location Effects on Thermal-Hydraulics during Intermediate Break Loss-of-Coolant Accident Experiments at ROSA-III Journal of Nuclear Science and Technology, 23(11), p. 1008-1019.

[57] Group of Experts of the NEA/CSNI, 2001. Validation matrix for the assessment of thermal-hydraulic codes for VVER LOCA and transients, NEA/CSNI/R(2001)4, OECD/NEA.

[58] Del Nevo, A., Adorni, M., D'Auria, F., 2012. Validation of advanced computer codes for VVER technology: LB-LOCA transient in PSB-VVER facility. Science and Technology of Nuclear Installations, Volume 2012, Article ID 480948, p. 1-15.

[59] Melikhov, I., Elkin, I.V., Lipatov, I.A., et al., 2005. Post-test full experimental data report (test 4). Technical report, OECD PSB-VVER Project Report PSB-26, EREC, Electrogorsk, Russia.

[60] Nakamura, H., Takeda, T., Satou, A., Ishigaki, M., Abe, S., Irwanto, D., 2013. Major outcomes from OECD/NEA ROSA and ROSA-2 Projects. In: Proceedings of the 15th International Topical Meeting on Nuclear Reactor Thermal Hydraulics (NURETH-15), Pisa, Italy, p. 1-21.

[61] The ROSA-V Group, 2003. ROSA-V large scale test facility (LSTF) system description for the third and fourth simulated fuel assemblies JAERI-Tech 2003-037. Technical report, Japan Atomic Energy Research Institute, Ibaraki, Japan.

[62] NEA, 2017, Final Integration Report of the Rig-of-Safety Assessment (ROSA-2) Project (2009-2012). Technical report, NEA/CSNI/R(2016)10, OECD/NEA.

[63] Schollenberger, S.P., 2017. OECD/PKL phase 4 PKL IIIi2.2 Cold-leg IB-LOCA Quick-Look Report. Technical report, D02-ARV-01-112-795 Rev. A, Erlangen, December.

[64] Kang, K.H., 2013. Thermal-Hydraulic Integral Effect Test with ATLAS for an Intermediate Break Loss of Coolant Accident at a Pressurizer Surge Line. Transactions of the Korean Nuclear Society Autumn Meeting, Gyeongju, Korea, October 24-25, p. 1-2.

[65] Umminger, K., et al., 2012. Integral Test Facility PKL: Experimental PWR Accident Investigation, Science and Technology of Nuclear Installations, Volume 2012, Article ID 891056.

[66] Umminger, K., et al., 2009. Integral Effect Tests in the PKL Facility with International Participation. Nuclear engineering and technology, 41(6), p. 765-774.

[67] Umminger, K., Mull, T., Schoen, B., 2003. Experiments on Boron Dilution in the Integral Test Facility PKL. NURETH 10, Seoul, Korea, October 5-9, p. 1-17.

[68] Bucalossi, A., 2005. Validation of Thermal-Hydraulic Codes for Boron Dilution Transients in the Context of the OECD/SETH Project. Eurosafe 2005, November, Brussels, p. 1-11.

[69] Munoz-Cobo, J.L., Chiva, S., Escrivá, A., 2013. International Agreement Report: Analysis with TRACE Code of PKL-III Test F 1.2. Technical report, NUREG/IA-0423, U.S. Nuclear Regulatory Commission.

[70] Mandl, R., Brand, B., and Watzinger, H., 1985. PKL reflood tests including end-of-blowdown. Proceedings of the 13th Water Reactor Safety Research Information Meeting, Gaithersburg, Md, USA, October, p. 173-196

[71] Gordon, D., 2017. AREVA Technical Center Scientific Thermal Hydraulic Testing Capabilities. NSUF-GAIN Nuclear Thermal-Hydraulics Workshop, Idaho, July 13, p. 1-14.

[72] Freixa, J., Martinez-Quiroga, V. and Reventos, F., 2019, Validation of a BEPU methodology through a blind benchmark activity at the PKL test facility, NURETH-18, Portland, Oregon, USA, August 18-22, p. 366-379.

[73] Austregesilo, H., Bals, C., Hora, A., Lerchl, G. et al., 2016. ATHLET 3.1A Models and Methods. Technical report, Gesellschaft für Anlagen- und Reaktorsicherheit gGmbH, Garching, Germany.

[74] Hollands, T., Buchholz, S., Wielenberg, A., 2019. Validation of the AC2 Codes ATHLET and ATHLET-CD. Kerntechnik, 84(5), p. 397-405.

[75] Lerchl, G. et al., 2016. ATHLET Validation. Technical report, GRS-P-1/Vol. 3 Rev. 4, Gesellschaft für Anlagen- und Reaktorsicherheit gGmbH, Garching, Germany, March.

[76] Diaz Pescador, E., Schäfer, F., and Kliem, S., 2019. Thermal-hydraulic insights during a main steam line break in a generic PWR KONVOI reactor with ATHLET 3.1A. Kerntechnik, 84(5), p. 367-374.

[77] Pochard R., Porracchia A., 1986. Assessment closure proposal. OECD/CSNI SACTE Task Group Meeting, Paris, December.
[78] Riebold W., 1987. Minutes of the OECD/CSNI SACTE Task Group Meeting, Paris, December.
[79] Ambrosini W., Bovalini R., D'Auria F., 1990. Evaluation of accuracy of thermal hydraulic code calculations, Energia Nucleare, 7(2), p. 5-16.
[80] D'Auria, F., Galassi, G.M., 1997. Accuracy Quantificationby the FFT method in FARO L-14 (ISP 39) open calculations. University of Pisa, Nuclear technology (NT), 309(97).
[81] Prošek, A., D'Auria, F., Mavko, B, 2002. Review of Quantitative accuracy assessment with Fast Fourier Transform Based Method. Nuclear Engineering and Design 217,1&2, p. 179-206.
[82] Prošek, A., D'Auria, F., Richards, D.J., Mavko, B., 2006. Quantitative assessment of thermal–hydraulic codes used for heavy water reactor calculations, Nuclear Engineering and Design, 236(3), p. 295-308.
[83] Saghafi, M., 2019. A sensitivity study on cut frequency of FFTBM for quantitative assessment of thermal-hydraulic modeling by MELCOR code. Progress in Nuclear Energy, 115, p. 62–73.
[84] Prošek, A., Kvizda, B., Mavko, B., and Kliment, T., 2004. Quantitative assessment of MCP trip transient in a VVER. Nuclear Engineering and Design, 227, p. 85-96.
[85] D'Auria, F., 2019. Best Estimate Plus Uncertainty (BEPU) Status and perspectives. Nuclear Engineering and Design, 352, 110190.
[86] D'Auria, F., Lanfredini, M., 2018. Introducing V&V&C in nuclear thermal-hydraulics. Proceedings of the ASME 2018 Verification and Validation Symposium (VVS2018), May 16-18, 2018, Minneapolis, MN, USA, p. 1-13.
[87] D'Auria, F., Lanfredini, M., 2019. V&V&C in nuclear reactor thermal-hydraulics. Nuclear Engineering and Design, 354, 110162.
[88] Šegon, V., Bajs, T., Debrecin, N., Čavlina, N., 2001. BETHSY nodalization study during MID-LOOP operation. Nuclear Energy in Central Europe 2001, Portorož, Slovenia, September 10-13, Nuclear Society of Slovenia, p. 1-8.
[89] Bajs, T., Debrecin, N., Šegon, V., Kahn, L., Mahmood, A., 2000. Assessment of Discretization Approach for RELAP5/MOD3 Computer Code. Nuclear Energy in Central Europe 2000, Bled, Slovenia, September 11-14, Nuclear Society of Slovenia, p. 1-8.
[90] Martinez-Quiroga, V., Reventos, F., Freixa, J., 2014. Applying UPC Scaling-Up Methodology to the LSTF-PKL Counterpart Test. Science and Technology of Nuclear Installations, volume 2014, p. 1-18.
[91] Bonuccelli, M., D'Auria, F., Debrecin, N., Galassi, G.M., 1993. A methodology for the qualification of thermal-hydraulic codes nodalizations. International meeting on Nuclear Reactor Thermal-Hydraulics (NURETH-6), Grenoble, France, Oct. 5-8, p. 1-10.
[92] Petruzzi, A., Cherubini, M., and D'Auria, F., 2016. Thirty Years' Experience in RELAP5 Applications at GRNSPG and NINE. Nuclear Technology, 193(1), p. 47-87.
[93] De Luca, D., Petruzzi, A., Cherubini, M., and Parrinello, V., 2016. RELAP5-3D Analysis of EBR-II Shutdown Heat Removal Test SHRT-17. Proceedings of the 2016 24th International Conference on Nuclear Engineering (ICONE24), vol. 3. American Society of Mechanical Engineers and Japan Society of Mechanical Engineers, June 26-30, Charlotte, North Carolina, p. 1-7.
[94] Saghafi, M., Ghofrani, M.B., D'Auria, F., 2016. Development and qualification of a thermal-hydraulic nodalization for modeling station blackout accident in PSB-VVER test facility. Nuclear Engineering and Design, 303, p. 109-121.
[95] Saltelli, A., Chan, K., Scott, E.M. 2000. Sensitivity Analysis. Wiley Series in Probability and Statistics. Wiley, New York.
[96] Dellino G, Meloni C, 2015. Uncertainty management in simulation-optimization of complex systems: algorithms and applications. Springer, New York.
[97] Morris, M. D., 1991. Factorial Sampling Plans for Preliminary Computational Experiments. Technometrics, 33, p. 161-174.

[98] Sharifan, R.A., Roshan, A., Aflatoni, M. et al., 2010. Uncertainty and sensitivity analysis of SWMM model in computation of manhole water depth and subcatchment peak flood. Procedia - Social and Behavioral Sciences, 2(6), p. 7739-7740.
[99] Feng, K., Lu, Z., Yang, C., 2019. Enhanced Morris method for global sensitivity analysis: good proxy of Sobol' index. Structural and Multidisciplinary Optimization, 59, p. 373-387.
[100] Kong, X., He, W., Qin, N., He, Q.,et al., 2012. Simulation of the fate and seasonal variations of alpha-hexachlorocyclohexane in Lake Chaohu using a dynamic fugacity model. Scientific World Journal, volume 2012, 691539.
[101] Li, J., Zhang, B., Mu, C., Chen, L., 2018. Simulation of the hydrological and environmental effects of a sponge city based on MIKE FLOOD. Environmental Earth Sciences, 77(2), p. 32.
[102] Schollenberger, S.P., 2016a. Description of the PKL III test Facility. Technical Report, NTCTP-G_2007_en_0010 rev.B, AREVA NP GmbH, Erlangen, Germany, May.
[103] Schollenberger, S.P., 2016b. Determination of Masses in the PKL Test Facility. Technical Report, FANP NT31_01_e34 rev. D, AREVA NP GmbH, Erlangen, Germany, May.
[104] Güneysu, R., 2017. Determination of Individual Volumes and of Total Volume in the PKL Test Facility (PKL III A - IIIi). Technical Report, DTICTP-G_2017_en_0002 rev.A, AREVA NP GmbH, Erlangen, Germany, March.
[105] Schollenberger, S.P., 2006. Determination of heat Losses in the PKL III Test Facility. Technical Report, NTT1-G_2006_en_0067 rev. A, AREVA NP GmbH, Erlangen, Germany, December.
[106] Wolfert, K., 1977. A New Method to Evaluate Critical Discharge Rates in Blowdown Codes that are based on the Lumped ‐ Parameter Technique. Thermal Reactor Safety Meeting, Sun Valley, USA.
[107] Yadigaroglu, G., Andreani, M., Aksan, S.N., Analytis, G.Th., Lubbesmeyer, D., Olek, S., 1990. Modelling of Thermohydraulic Emergency Core Cooling Phenomena. Technical report, Labor für Thermohydraulik, Paul Scherrer Institut, PSI Report No. 27, Wurenlingen (CH).
[108] Austregesilo, H., Bals, C., Hora, A., Lerchl, G. et al., 2012. ATHLET 3.0 Cycle A Models and Methods. Technical report, Gesellschaft für Anlagen- und Reaktorsicherheit gGmbH, Garching, Germany.
[109] Schollenberger, S.P., 2006. Determination of the Pressure Losses in the PKL III Test Facility, Technical Report, NTT1-G/2006/en/0066 AREVA NP GmbH, Erlangen, Germany, December.
[110] Huang, T., 2018. Simulation of the i2.2 run 3 test (IB LOCA) of PKL4 facility. Joint PKL-ATLAS Workshop on Analytical Activities related to OECD/PKL4 and OECD/ATLAS2 Projects, Barcelona, Spain, November 7-9, p. 1-24.
[111] UPC, 2019. Benchmark activity within the OECD/NEA PKL-4 project, related to the simulation of Test i2.2. Technical Report, Universitat Politècnica de Catalunya.
[112] D'Auria, F., Eramo, A., Frogheri, M., Galassi, G.M., 1996. Accuracy quantification in SPE-1 to SPE-4 organised by IAEA, Proceedings of the 4th International Conference on Nuclear Engineering (ICONE-4), vol. 3. American Society of Mechanical Engineers and Japan Society of Mechanical Engineers, p. 461-469.
[113] Xu, H., Badea, A.F., Cheng, X., 2020. ATHLET simulation of PKL IBLOCA I2.2 benchmark test and quantitative assessment. ATH'2020, Palaiseau, France, March 31-April 3, p. 1-14.
[114] Freixa, J., de Alfonso, E., Reventós, F., 2016. Testing methodologies for quantifying physical models uncertainties. A comparative exercise using CIRCE and IPREM (FFTBM), Nuclear Engineering and Design, 305, p. 653-665.
[115] Kozmenkov, Y., Jobst, M., Kliem, S., Schaefer, F. and Wilhelm, P., 2017. Statistical analysis of the early phase of SBO accidents for PWR. Nuclear Engineering and Design, 314(1), p. 131-141.
[116] Aksan, N., D'Auria, F., Glaeser, H., Pochard, R., Richards, C., Sjoberg, A., 1993. Separate Effects Test Matrix for Thermal-Hydraulic Code Validation. Committee on the Safety of Nuclear Installations. Technical Report, NEA/CSNI/R(93)14, OECD/NEA.
[117] Ihle, P., Rust, K., 1984. FEBA Flooding Experiments with Blocked Arrays. Technical Report, KFK Karlsruhe, KFK-3657.

[118] Kim, Y.S., 2015. A proposed correlation for critical flow rate of water flow. Nuclear Engineering and Technology, 47(1), p. 135-138.
[119] Feburie, V., Giot, M., Granger, S., Seynhaeve, J.M., 1993. A model for choked flow through cracks with inlet subcooling. International Journal of Multiphase Flow, 19, p. 541-562.
[120] Kestin, J., Zaremba, S.K., 1953. One-dimensional high-speed flows: Flow Patterns Derived for the Flow of Gases Through Nozzles, Including Compressibility and Viscosity Effects. Aircraft Engineering and Aerospace Technology, 25(6), p. 172-179.
[121] Michaelides, E. E., and K. L. Zissis, 1983. Velocity of sound in two-phase mixtures. International Journal of Heat and Fluid Flow, 4(2), p. 79-84.
[122] Wein, M., 2002. Simulation von kritischen und nahkritischen Zweiphasenströmungen mit thermischen und fluiddynamischen Nichtgleichgewichtseffekten. Dissertation, Technische Universität Dresden.
[123] D'Auria, F., Vigni, P., 1980. Two-phase critical flow models - a technical addendum to CSNI state-of-the-art report on critical flow modelling. Technical Report, CSNI Report No. 49. Instituto di Impianti Nucleare, Universita di Pisa.
[124] Elias, E., Lelluche, G. S. 1994. Two-phase critical flow. Int. J. Multiphase Flow 20, Suppl. 91-168.
[125] Wallis, G. B., 1969. One-Dimensional Two-Phase Flow, McGraw Hill, New York.
[126] Pana, P, 1976. Berechnung der stationären Massenstromdichte von Wasserdampfgemischen und der auftretenden Rückstoßkräfte. Technical Report, IRS-W24, Institut für Reaktorsicherheit, Köln.
[127] Levy, S., Abdollahian, D., 1982. Homogeneous non-equilibrium critical flow model. Int. J. Heat Mass Transfer, 25, p. 759-770.
[128] Elias, E., Chambré, P. L., 1993. Flashing inception in water during rapid decompression. Transactions - ASME Journal of Heat Transfer, 115, p. 231-238.
[129] Levy, S., 1960. Steam slip - theoretical prediction from momentum model. Transactions - ASME Journal of Heat Transfer, 82, p. 113-124.
[130] Moody, F. J., 1966. Maximum Two-Phase Vessel Blowdown from Pipes. Transactions - ASME Journal of Heat Transfer, 88, p. 285-293.
[131] Ishii, M., 1977. One-Dimensional Drift-Flux Model and Constitutive Equations for Relative Motion Between Phases in Various Two-Phase Flow Regimes. Technical Report, ANL 77-47, Argonne National Laboratory.
[132] Richter, H. J., 1983. Separated Two-Phase Flow Model: Application to Critical Two-Phase Flow. International Journal of Multiphase Flow, 9, p. 511–530.
[133] Dobran, F., 1987, Nonequilibrium Modeling of Two-Phase Critical Flows in Tubes. Transactions - ASME Journal of Heat Transfer, 109, p. 731-738.
[134] Burnell, J. A, 1947. Flow of boiling water through nozzles, orifices and pipes. Engineering, p 572-576.
[135] Relap5 Code Development Team, 1995. RELAP5/MOD3 Code Manual: Vol. 4, Models and Correlations. Technical Report, NUREG0CR-5535, INEL-9500174, Idaho National Engineering Laboratory.
[136] Paulsen, M.P., et al., 2014. RETRAN-3D – A program for transient thermal-hydraulic analysis of complex fluid flow systems, Volume 3: User's Manual. Technical Report, NP-7450, Electric Power Research Institute.
[137] Relap5 Code Development Team, 2001. SCDAP/RELAP5/MOD 3.3 Code Manual. Technical Report, NUREG/CR-6150-Rev 1, Vol III, U.S. Nuclear Regulatory Commission.
[138] Roth, G.A., Aydogan, F., 2014. Theory and implementation of nuclear safety codes –Part I: conservation equations, flow regimes, numerics and significant assumptions. Progress in Nuclear Energy, 76, p. 160-182.
[139] Chung, M.K., Chang, S.K., 1992. The study of two-phase critical flow characteristics in nuclear reactor coolant system. Technical Report, KAERI/AR-360/92, Korea Atomic Energy Research Institute.

[140] Oussoren A., Riznic J., Revankar S.T., 2015. Assessment of Critical Subcooled Flow through Cracks in Large and Small Pipes using TRACE and RELAP5. Technical Report, NUREG/IA-0457, U.S. Nuclear Regulatory Commission.
[141] Wallis, G.B., 1980. Critical two-phase flow. International Journal of Multiphase Flow, 6, p. 97-112
[142] Todreas, N.E., Kazimi, M.S., 1993. Nuclear Systems I, Thermal Hydraulic Fundamentals. Taylor & Francis, Levittown.
[143] Ranson. Y. H., et al., 1982. RELAP5/MOD1 Code Manual, Vols. 1 & 2, Technical Report, NUREG/CR-1826, EGG-2070, U.S. Nuclear Regulatory Commission.
[144] Schwellnus, C. F., Shoukri, M., 1991. A Two-Fluid Model for Non-Equilibrium Two-Phase Critical Discharge. The Canadian Journal of Chemical Engineering, 69, p. 188-197.
[145] Dagan, R., Elias, E., Wacholder, E. und Olek, S., 1993, A Two-Fluid Model for Critical Flashing Flows in Pipes. International Journal of Multiphase Flow, 19, p. 15-25.
[146] Martinelli, R.C. and Nelson, D.B., 1948. Prediction of Pressure Drop during Forced-Circulation of Boiling Water. Transactions of the American Society of Mechanical Engineers, 70, p. 695.
[147] Chisholm, D., 1973. Pressure Gradients Due to Friction During the Flow of Evaporating Two-Phase Mixtures in Smooth Tubes and Channels. International Journal of Heat and Mass Transfer, 16, p. 347-348.
[148] Friedel, L., 1979. Improved Friction Pressure Drop Correlations for Horizontal and Vertical Two-Phase Pipe Flow. 3R international, 18, p. 485-491.
[149] Ishii, M., T. Hibiki, 2010. Thermo-Fluid Dynamics of Two-Phase Flow. Springer Link: Book. Springer New York.
[150] Dave, Akshay J., 2016. Interfacial Area Transport Equation Models and Validation against High Resolution Experimental Data for Small and Large Diameter Vertical Pipes. Dissertation, University of Michigan.
[151] Schwellnus, C. F., 1988. A Study of a General One-Dimensional Two-Fluid Critical Flow Model. Master's Thesis, Mechanical Engineering, McMaster University, Toronto.
[152] Clift, R., Grace, J.R., and Weber, M.E., 1978. Bubbles, Drops, and Particles. New York: Academic.
[153] Ishii, M., 1990. Two-fluid model for two-phase flow. Multiphase Sci. Technol. 5, p. 1-65.
[154] Pudasaini, S. P., 2019. A fully analytical model for virtual mass force in mixture flows. International Journal of Multiphase Flow, 113, p. 142-152.
[155] No, H.C., Kazimi, M.S., 1981. The effect of virtual mass on the characteristics and the numerical stability in two-phase flows. Technical Report, Report No MIT-EL 81-023. MIT Energy Laboratory.
[156] Maliska, C.R., Paladino, E.E., 2006. The role of virtual mass, lift and wall lubrication forces in accelerated bubbly flows. Production, Distribution and Conservation – Milan, p. 953-962.
[157] Ishii, M., Chawla, T. C., 1979. Local Drag Laws in Dispersed Two-phase Flow. Technical report, ANL-79-105, Argonne National Lab.
[158] Xu, J.L, Wong, T.N and Huang, X.Y, 2006. Two-fluid modelling for low-pressure subcooled flow boiling. Int. J. Heat Mass Transfer. 49, p. 377-386.
[159] Rohsenow, W. M. and Choi, H., 1961. Heat, Mass and Momentum Transfer, Prentice-Hall, Englewood Cliffs, N.J.
[160] Ghiaasiaan, S. M., Muller, J. R., Sadowski, D. L., Abdel-khalik, S. I., 1997. Critical Flow of Initially Highly Subcooled Water Through a Short Capillary. Nuclear Science and Engineering, 126, p. 229.
[161] Collier, J. G., 1981. Convective Boiling and Condensations, McGraw-Hill, New York.
[162] Emagbetere, E., Oluwole, O., Salau, T.A.O., 2017. Comparative study of Matlab ODE solvers for the Korakianitis and Shi model. Bulletin of Mathematical Sciences and Applications, 19, p. 31-44.
[163] Quarteroni, A, Saleri, F., 2006. Scientific Computing with MATLAB and Octave (Texts in Computational Science and Engineering). Milan: Springer - Verlag.

[164] Lemmon, E. W., Huber, M. L., and McLinden, M. O., 2010. NIST Standard Reference Database 23: Reference Fluid Thermodynamic and Transport Properties-REFPROP. National Institute of Standards and Technology, Gaithersburg.
[165] Ardron, K.H., Furness, R.A., 1976. A study of the critical flow models used in reactor blowdown analysis. Nuclear Engineering and Design, 39, p. 257-266.
[166] Kabanikhin, S.I., 2008. Definitions and examples of inverse and ill-posed problems. Journal of Inverse and Ill-posed Problems, 16(4), p. 317-357.
[167] Burtt, J.D., 1984. International Standard Problem 13 (LOFT Experiment L2-5) Final Comparison Report. Technical report, NUREG/CR-4115 EGG-2369, U.S. Nuclear Regulatory Commission.
[168] Britain, I. et al., 1982. Critical flow modeling in nuclear safety: a state-of-the-art report. Technical report, ISBN: 9264123660, OECD/NEA.
[169] Ilic, V., et al. 1986. A qualified data base for critical flow of water. Technical report, EPRI NP 4556, Electric Power Research Institute.
[170] Isbin, H.S., Moy, J.E., and DaCruz, A.J.R., 1957. Two-Phase, Steam-Water Critical Flow. American Institute of Chemical Engineers Journal, 3(3), p. 361-365.
[171] Zaloudek, F.R., 1961. The low pressure critical discharge of steam-water mixtures from pipes. Technical Report, HW-68934 (REV), General Electric Co. Hanford Atomic Products Operation, Richland, Wash.
[172] Henry, R.E., Fauske, H.K., and McComas, S T., 1970. Two Phase Critical Flow at Low Qualities Part I: Experimental, Nuclear Science and Engineering, 41, p. 79-91.
[173] Fauske, H.K., 1962. Contribution to the Theory of Two Phase One Component Critical Flow. Technical Report, ANL-6633, Argonne National Laboratory.
[174] Celata, G. P., Cumo, M., Farello, G. E., Incalterra, G. C. and Naviglio, A., 1983. Thermodynamic Disequilibrium in the Critical Flow of Subcooled Liquids. Nuclear Technology, 60, p. 137-142.
[175] Cruver, J.E., 1963. Metastable Critical Flow of Steam-Water Mixtures. Dissertation, University of Washington.
[176] Sozzi, G.L., Wutherland, W.A., 1975. Critical flow of saturated and subcooled water at high pressure. Technical Report NEDO-13418, General Electric Co.
[177] Ardron, K.H., and Ackerman, M.C., 1978. Studies of the Critical Flow of Subcooled Water in a Pipe. Technical Report, No. RD/B/N 4299, Berkeley Nuclear Laboratories.
[178] Al-Sahan, M.A., 1980. Experimental Study of Two-Phase Critical Flow of Initially Subcooled Water in Long Tubes. Master's Thesis, University of Toronto.
[179] Abdollahiari, D., Healzer, J., Janssen, E., and Amos, C., 1982. Critical Flow Data Review and Analysis. Technical Report, EPRI NP-2192, Electric Power Research Institute.
[180] Al-Sahan, M.A., 1988. On the Development of the Flow Regimes and the Formulation of a Mechanistic Non-Equilibrium Model for Critical Two-Phase Flow, Ph.D. Thesis, University of Toronto.
[181] Henry, R.E., 1968. A study of one- and two-component, two-phase critical flows at low qualities. Technical report, ANL-7430, Argonne National Laboratory.
[182] Ardron, K.H., 1978. A two-fluid model for critical vapor-liquid flow. International Journal of Multiphase Flow, 4, p. 323-337.
[183] Ewan, B.C.R., Moodie, K., Harper, P.J., 1988. A study of two-phase critical pipe flow models for superheated liquid releases. Journal of Hazardous Materials, 20, p. 273-286.
[184] Javidmand, P., Hoffmann, K.A., 2015. Comprehensive two fluid model simulation of critical two-phase flow through short tube orifices. Proceedings of the ASME 2015 International Technical Conference and Exhibition on Packaging and Integration of Electronic and Photonic Microsystems and ASME 2015 12th International Conference on Nanochannels, Microchannels, and Minichannels, July 6-9, 2015, San Francisco, California, USA, p. 1-13.
[185] Lv, Y. Zhao, F., Li, W., 2018. A Choking Model with Thermal Non-Equilibrium for Initially Subcooled Water. The 26th International Conference on Nuclear Engineering (ICONE26), London, England, July 22-26, p. 1-7.

[186] Shi, J., Sun, B., Yu, X., Zhang, P., and Song, F., 2017. Modeling the full-range thermal-hydraulic characteristics and post-dryout deviation from thermodynamic equilibrium in once-through steam generators. International Journal of Heat and Mass Transfer, 109, p. 266–277.
[187] Carlson, D.E., and Ball, S.J., 2016. Perspectives on understanding and verifying the safety terrain of modular high temperature gas-cooled reactors. Nuclear Engineering and Design, 306, p. 117–123.
[188] Zuber, N., 1964. On the Dispersed Two-Phase Flow in the Laminar Flow Regime. Chem. Eng. Sci. 19, p. 897.
[189] Van Wijngaarden, L., 1976. Hodrodynamic interaction between gas bubbles in liquid. J. Fluid Mech. 77, p. 27–44.
[190] Wäng, J., 2015. Valdiation of the Critical Flow Models in POLCA-T. Master's Thesis, KTH Royal Institute of Technology.
[191] Jonter, T., Statens kärnkraftsinspektion, 2001. Försvarets Forskningsanstalt och Planerna på Svenska Kärnvapen. SKI 01(5) p. 1104-1374.
[192] Moore, R.L., Sloan, S.M., Schultz, R.R., Wilson, G.E.,1996, RELAP5/MOD3 code manual: Summaries and reviews of independent code assessment reports. NUREG/CR-5535, INEI-95/0174, Vol. 7, Rev. 1, U.S. Nuclear Regulatory Commission.
[193] Lee, I.S., Bang, Y.S., Oh, D.Y., Kim, B.S., et al., 2017. Uncertainty Estimation of Henry-Fauske Critical Flow Model Considering Thermal-nonequilibrium Constant and Discharge Coefficient in MARS-KS. Transactions of the Korean Nuclear Society Spring Meeting, Jeju, Korea, May 17-19, p. 1-3.
[194] Sokolowski, L., Kozlowski, T., 2012. Assessment of Two-Phase Critical Flow Models Performance in RELAP5 and TRACE Against Marviken Critical Flow Tests. NUREG/IA-0401, U.S. Nuclear Regulatory Commission.
[195] Domitr, P., Darnowski, P., et al., 2019. The assessment of critical flow models of MELCOR2.2 and TRACE v5.0 patch 5 against Marviken critical flow tests. 18th International Topical Meeting on Nuclear Reactor Thermal Hydraulics – NURETH, Portland, Oregon, USA, p.1-13.
[196] USNRC, 1982. The Marviken Full Scale Critical Flow Tests, Summary Report (Joint Reactor Safety Experiments in the Marviken Power Station, Sweden). Technical report, NUREG/CR2671, U.S. Nuclear Regulatory Commission.
[197] OECD/NEA, 1979. The Marviekn Full Scale Critical Flow Tests Report, Marviken Project. Technical Report, OECD/NEA.
[198] Kim, K., Kim, H.J., 1992. Assessment of RELAP5/MOD2 critical flow model using Marviken Test Data 15 and 24. Technical Report, NUREG/IA-0086, U.S. Nuclear Regulatory Commission.
[199] Werner, H.J., 1984. On extension of Cramer's rule for solution of restricted linear systems. Linear Multilinear Algebra, 15, p. 319-330.
[200] Cheng, L., Lahey, R.T. und Drew, D. A., 1983. The Effect of Virtual Mass on the Prediction of Critical Flow. Specialist meeting on transient two-phase flow, Pasadena, CA (USA), 23-25 March, 1981.
[201] Gustafson, D., 1996. Intermediate Algebra. Pacific Grove, CA: Brooks/Cole Pub.
[202] Katto, Y., 1968. Dynamics of compressible saturated two-phase flow (critical flow). Bulletin of JSME, 11 (48), p. 1135-1144.
[203] Ogasawara, H., 1969. A theoretical approach to two-phase critical flow (3rd Report, the critical condition including interphase slip). Bulletin of JSME, 12 (52), p. 827-836.
[204] Bouré, J.A., 1974. Critical two-phase flows, Lecture Series, von Karman Institute for Fluid Dynamics, Centre d'Etudes Nucléaires de Grenoble, France, December 9-13.
[205] Bouré J.A., Fritte, A.A., Giot, M.M., Réocreux, M.L., 1976. Highlights of two-phase critical flow: on the links between maximum flow rates, sonic velocities, propagation and transfer phenomena in single and two-phase flows. International Journal of Multiphase Flow, 3, p. 1-22.
[206] Bartosiewicz, Y., Seynhaeve, J.-M., 2013. Delayed Equilibrium Model (DEM) of Flashing Flows Relevant to LOCA. Multiphase Science and Technology, 25 (2-4), p. 117-131.

[207] Yin, S., Wang, H., Xu, B., Yang, C., Gu, H, 2020. Critical flow leakage of a vapour-liquid mixture from sub-cooled water: Nucleation boiling study. International Journal of Heat and Mass Transfer, 146, 118807.